ISBN: 978-972-8692-53-7

International Workshop on Biological Processes & Petri Nets (BioPPN)

–

A satellite event of Petri Nets 2010

Braga, Portugal, June 21 2010

Introductory note

Integrative biology aims at deciphering essential biological processes that are driven by complex mechanisms, involving miscellaneous interacting molecular compounds. In this context, the need for appropriate mathematical and computational modelling tools is widely advocated. Petri nets have proved their usefulness for the modelling, analysis, and simulation of a diversity of biological networks, covering qualitative, stochastic, continuous and hybrid models. The deployment of Petri nets to study biological applications has not only generated original models, but has also motivated fundamental research.

This workshop gathers researchers interested in the application of Petri nets for biological applications. Its main goal is to demonstrate that this field of application raises new challenges and that Petri nets can be effective to tackle such challenges.

We received two types of contributions: research and work-in-progress papers. All have been reviewed by four to five referees. Demonstrating the inter-disciplinary nature of the topic, the present document encloses theoretical contributions as well as biological applications.

Additionally, there is one invited talk given by Jorge Carneiro, who is a principle investigator at the Oeiras Associate Laboratory and the leader of the Quantitative Organism Biology lab at the Gulbenkian Institute of Science. Jorge Carneiro has an interdisciplinary background, being experienced in laboratory work and in biomathematics. In his talk he will discuss some challenges for the Petri net community.

Claudine Chaouiya
Instituto Gulbenkian de Ciência, IGC
Oeiras, Portugal
chaouiya@igc.gulbenkian.pt

Monika Heiner
Brandenburg University of Technology at Cottbus
Computer Science Institute, Germany
monika.heiner@informatik.tu-cottbus.de

Program Committee:

David Angeli, I, UK
Gianfranco Balbo, I
Rainer Breitling, NL
David Gilbert, UK
Simon Hardy, CA
Ralf Hofestdt, D
Peter Kemper, US
Hanna Klaudel, F
Kurt Lautenbach, D
Wolfgang Marwan, D
Eduardo Mendoza, Philippines, D
Satoru Miyano, JP
P.S. Thiagarajan, SG

Table of Contents

* Research paper
** "Work in progress" paper

Why aren't Petri nets widely used in biological research?

Jorge Carneiro

Instituto Gulbenkian de Ciência, Portugal
http://qobweb.igc.gulbenkian.pt

Abstract. Many cellular and supra-cellular processes are stochastic and combinatorial in nature. Binding of transcriptional factors to gene promoters or enhancers, context-dependent multistep epigenetic modifications of gene loci, regulation of ion channel gating, and multicellular interactions controlling cell differentiation and cycle are examples of fundamental stochastic processes that involve multiple intertwined concurrent events. Designing and analysing models of such systems is a challenging and painstaking task, since the number of variables and potential events increases exponentially with the number of relevant components one is willing to include in the model. Like in any modelling exercise these systems involve a trade-off between simplicity and realism, but, here, inadvertent omissions or oversimplifications in early model design are paid a too high price when redesign is necessary. The stochastic Petri nets (SPN) formalism is almost ideal to deal with these modelling difficulties, since it offers an intuitive and straightforward representation of interactions and concurrent events, and provides a solid theoretical framework to analyse the model structure and dynamics. Furthermore, several SPN software tools are available that allow a modeller to rapidly draw, modify, and analyse model variants. This "rapid prototyping" of a model facilitates the tasks of pruning away unnecessary components and identifying missing ones. Considering these advantages of the use of SPN it is almost surprising that this formalism is not widely applied in modelling biological systems. Based on two examples of SPN application, namely to modelling somatic recombination of immune receptor genes and ion channel gating in sea urchin spermatozoa, I will argue that SPN software tools are well-suited for engineering artificial systems, but do not yet offer all the functionalities one would wish to have at hand when modelling a natural biological system.

Cycle structure in SR and DSR graphs: implications for multiple equilibria and stable oscillation in chemical reaction networks

Murad Banaji

Department of Medical Physics and Bioengineering, University College London, Gower Street, London WC1E 6BT, UK.

Abstract. Associated with a chemical reaction network is a natural labelled bipartite multigraph termed an SR graph, and its directed version, the DSR graph. These objects are closely related to Petri nets. The construction of SR and DSR graphs for chemical reaction networks is presented. Conclusions about asymptotic behaviour of the associated dynamical systems which can be drawn easily from the graphs are discussed. In particular, theorems on ruling out the possibility of multiple equilibria or stable oscillation in chemical reaction networks based on computations on SR/DSR graphs are presented. These include both published and new results. The power and limitations of such results are illustrated via several examples.

1 Chemical reaction networks: structure and kinetics

Models of chemical reaction networks (CRNs) are able to display a rich variety of dynamical behaviours [1]. In this paper, a spatially homogeneous setting is assumed, so that CRNs involving n chemicals give rise to local semiflows on $\mathbb{R}^n_{\geq 0}$, the nonnegative orthant in $\mathbb{R}^n$. These local semiflows are fully determined if we know 1) the CRN *structure*, that is, which chemicals react with each other and in what proportions, and 2) the CRN *kinetics*, that is, how the reaction rates depend on the chemical concentrations. An important question is what CRN behaviours are determined primarily by reaction network structure, with limited assumptions about the kinetics.

A variety of representations of CRN structure are possible, for example via matrices or generalised graphs. Of these, a signed, labelled, bipartite multigraph, termed an *SR graph*, and its directed version, the *DSR graph*, are formally similar to Petri nets. This relationship is discussed further below.

It is now well established that graphical representations can tell us a great deal about asymptotic behaviours in the associated dynamical systems. Pioneering early work on CRNs with mass-action kinetics ([2, 3] for example), had a graph-theoretic component (using graphs somewhat different from those to be presented here). More recently, graph-theoretic approaches have been used to draw conclusions about multistationarity and oscillation in CRNs with restricted classes of kinetics [4, 5].

The applicability of such work, particularly in biological contexts, is greatly increased if only weak assumptions are made about kinetics. Consequently, there is a growing body of recent work on CRNs with essentially arbitrary kinetics. It has been shown that examination of Petri nets associated with a CRN allows conclusions about persistence, that is, whether ω-limit sets of interior points of $\mathbb{R}^n_{\geq 0}$ can intersect the boundary of $\mathbb{R}^n_{\geq 0}$ [6]. Work on multistationarity has been extended beyond the mass-action setting [7, 8]: some conclusions of this work will be outlined below. Finally, recent work applying the theory of monotone dynamical systems [9, 10] in innovative ways to CRNs [11] has close links with some of the new material presented below.

Outline. After some preliminaries, the construction of SR and DSR graphs is presented, and their relationship to Petri nets is discussed. Some recent results about multistationarity based on cycle structure in these objects are described. Subsequently, a new result on monotonicity in CRNs is proved. This result, Proposition 4, is a graph-theoretic corollary of results in [12]. It bears an interesting relationship to results in [11], which provide stronger conclusions about convergence, but make different assumptions, and a somewhat different claim. Finally, several examples, some raising interesting open questions, are presented. At various points, in order to simplify the exposition, the results are presented in less generality than possible, with more technical results being referenced.

2 Preliminaries

2.1 A motivating example

Consider the following simple family of CRNs treated in [13, 14]:

SYS 1	**SYS** 2	$\cdots$	**SYS** n
$A_1 + A_2 \rightleftharpoons B_1$	$A_1 + A_2 \rightleftharpoons B_1$		$A_i + A_{i+1} \rightleftharpoons B_i,$
$A_2 + A_3 \rightleftharpoons B_2$	$A_2 + A_3 \rightleftharpoons B_2$	$\cdots$	$i = 1, \ldots, n+1$
$A_3 \rightleftharpoons 2A_1$	$A_3 + A_4 \rightleftharpoons B_3$		$A_{n+2} \rightleftharpoons 2A_1$
	$A_4 \rightleftharpoons 2A_1$		

(1)

The reader may wish to look ahead to Figure 2 to see representations of the SR graphs associated with the first three CRNs in this family. This family will be revisited in Section 7, and the theory to be presented will imply the following conclusions (to be made precise below): when n is even, **SYS** n does not allow multiple nondegenerate equilibria; when n is odd, **SYS** n cannot have a nontrivial periodic attractor. Both conclusions require only minimal assumptions about the kinetics.

2.2 Dynamical systems associated with CRNs

In a spatially homogeneous setting, a chemical reaction system in which n reactants participate in m reactions has dynamics governed by the ordinary differential equation

$$\dot{x} = \Gamma v(x). \tag{2}$$

$x = [x_1, \ldots, x_n]^T$ is the nonnegative vector of reactant concentrations, and $v = [v_1, \ldots, v_m]^T$ is the vector of reaction rates, assumed to be C^1. A reaction rate is the rate at which a reaction proceeds *to the right* and may take any real value. Γ is the (constant) $n \times m$ **stoichiometric matrix** of the reaction system. Since reactant concentrations cannot be negative, it is always reasonable to assume invariance of $\mathbb{R}^n_{\geq 0}$, i.e. $x_i = 0 \Rightarrow \dot{x}_i \geq 0$.

The jth column of Γ, termed Γ_j, is the **reaction vector** for the jth reaction, and a stoichiometric matrix is defined only up to an arbitrary signing of its columns. In other words, given any $m \times m$ signature matrix D (i.e. any diagonal matrix with diagonal entries ± 1), one could replace Γ with ΓD and $v(x)$ with $Dv(x)$. Obviously the dynamical system is left unchanged. The subspace $\mathrm{Im}(\Gamma)$ of $\mathbb{R}^n$ spanned by the reaction vectors is called the **stoichiometric subspace**. The intersection of any coset of the $\mathrm{Im}(\Gamma)$ with $\mathbb{R}^n_{\geq 0}$ is called a **stoichiometry class**.

Two generalisations of (2) which include explicit inflow and outflow of substrates are worth considering. The first of these is a so-called CFSTR

$$\dot{x} = q(x_{in} - x) + \Gamma v(x). \tag{3}$$

$q \in \mathbb{R}$, the flow rate, is generally assumed to be positive, but we allow $q = 0$ so that (2) becomes a special case of (3). $x_{in} \in \mathbb{R}^n$ is a constant nonnegative vector representing the "feed" (i.e., inflow) concentrations. The second class of systems is:

$$\dot{x} = x_{in} + \Gamma v(x) - Q(x). \tag{4}$$

Here $Q(x) = [q_1(x_1), \ldots, q_n(x_n)]^T$, with each $q_i(x_i)$ assumed to be a C^1 function satisfying $\frac{\partial q_i}{\partial x_i} > 0$, and all other quantities defined as before. Systems (4) include systems (3) with $q \neq 0$, while systems (2) lie in the closure of systems (4).

Define the $m \times n$ matrix $V = [V_{ji}]$ where $V_{ji} = \frac{\partial v_j}{\partial x_i}$. A very reasonable, but weak, assumption about many reaction systems is that reaction rates are monotonic functions of substrate concentrations as assumed in [14–16] amongst other places. We use the following definition from [14] (there called NAC):

> A reaction system is **N1C** if i) $\Gamma_{ij} V_{ji} \leq 0$ for all i and j, and ii) $\Gamma_{ij} = 0 \Rightarrow V_{ji} = 0$.

As discussed in [14], the relationship between signs of entries in Γ and V encoded in the N1C criterion is fulfilled by all reasonable reaction kinetics (including mass action and Michaelis-Menten kinetics for example), provided that reactants never occur on both sides of a reaction.

3 Introduction to SR and DSR graphs

3.1 Construction and relation to Petri nets

SR graphs are signed, bipartite multigraphs with two vertex sets V_S (termed "S-vertices") and V_R (termed "R-vertices"). The edges E form a multiset, consisting

of unordered pairs of vertices, one from V_S and one from V_R. Each edge is signed and labelled either with a positive real number or the formal label ∞. In other words, there are functions $\mathrm{sgn} : E \to \{-1, 1\}$, and $\mathrm{lbl} : E \to (0, \infty) \cup \{\infty\}$. The quintuple $(V_S, V_R, E, \mathrm{sgn}, \mathrm{lbl})$ defines an SR graph.

DSR graphs are similar, but have an additional "orientation function" on their edges, $\mathcal{O} : E \to \{-1, 0, 1\}$. The sextuple $(V_S, V_R, E, \mathrm{sgn}, \mathrm{lbl}, \mathcal{O})$ defines a DSR graph. If $\mathcal{O}(e) = -1$ we will say that the edge e has "S-to-R direction", if $\mathcal{O}(e) = 1$, then e has "R-to-S direction", and if $\mathcal{O}(e) = 0$, then e is "undirected". An undirected edge can be regarded as an edge with both S-to-R and R-to-S direction, and indeed, several results below are unchanged if an undirected edge is treated as a pair of antiparallel edges of the same sign. SR graphs can be regarded as the subset of DSR graphs where all edges are undirected.

Both the underlying meanings, and the formal structures, of Petri nets and SR/DSR graphs have some similarity. If we replace each undirected edge in a DSR graph with a pair of antiparallel edges, a DSR graph is simply a Petri net graph, i.e. a bipartite, multidigraph. Similarly, an SR graph is a bipartite multigraph. S-vertices correspond to variables, while R-vertices correspond to processes which govern their interaction. The notions of variable and process are similar to the notions of "place" and "transition" for a Petri net. Edges in SR/DSR graphs tell us which variables participate in each process, with additional qualitative information on the nature of this participation in the form of signs, labels, and directions; edges in Petri nets inform on which objects are changed by a transition, again with additional information in the form of labels (multiplicities) and directions. Thus both Petri net graphs and SR/DSR graphs encode partial information about associated dynamical systems, while neither includes an explicit notion of time.

There are some important differences, however. Where SR/DSR graphs generally represent the structures of continuous-state, continuous-time dynamical systems, Petri nets most often correspond to discrete-state, discrete-time systems, although the translation to a continuous-state and continuous-time context is possible [17]. Although in both cases additional structures give partial information about these dynamical systems, there are differences of meaning and emphasis. Signs on edges in a DSR graph, crucial to much of the associated theory, are analogous to directions on edges in a Petri net: for example for an irreversible chemical reaction, an arc from a substrate to reaction vertex in the Petri net would correspond to a negative, undirected, edge in the SR/DSR graph. Unlike SR/DSR graphs, markings (i.e. vertex-labellings representing the current state) are often considered an intrinsic component of Petri nets.

Apart from formal variations between Petri nets and SR/DSR graphs, differences in the notions of state and time lead naturally to differences in the questions asked. Most current work using SR/DSR graphs aims to inform on the existence, nature, and stability of limit sets of the associated local semiflows. Analogous questions are certainly possible with Petri nets, for example questions about the existence of stationary probability distributions for stochastic Petri nets [18]. However, much study, for example about reachability, safeness and

boundedness, concerns the structure of the state space itself, and has no obvious analogy in the SR/DSR case. This explains to some extent the importance of markings in the study of Petri nets; in the case of SR/DSR graphs, the underlying space is generally assumed to have a simple structure, and the aim is to draw conclusions which are largely independent of initial conditions.

3.2 SR and DSR graphs associated with CRNs

SR and DSR graphs can be associated with arbitrary CRNs and more general dynamical systems [7, 8]. For example, the construction extends to situations where there are modulators of reactions which do not themselves participate in reactions, and where substrates occur on both sides of a reaction. Here, for simplicity, the construction is presented for an N1C reaction system with stoichiometric matrix Γ. Assume that there is a set of substrates $V_S = \{S_1, \ldots, S_n\}$, having concentrations $x_1, \ldots, x_n$, and reactions $V_R = \{R_1, \ldots, R_m\}$ occurring at rates $v_1, \ldots, v_m$. The labels in V_S and V_R will be used to refer both to the substrate/reaction, and the associated substrate/reaction vertices.

- If $\Gamma_{ij} \neq 0$ (i.e. there is net production or consumption of S_i reaction j), and also $\frac{\partial v_j}{\partial x_i}$ is not identically zero, i.e. the concentration of substrate i affects the rate of reaction j, then there is an undirected edge $\{S_i, R_j\}$.
- If $\Gamma_{ij} \neq 0$, but $\frac{\partial v_j}{\partial x_i} \equiv 0$, then the edge $\{S_i, R_j\}$ has only R-to-S direction.

The edge $\{S_i, R_j\}$ has the sign of Γ_{ij} and label $|\Gamma_{ij}|$. Thus the labels on edges are just stoichiometries, while the signs on edges encode information on which substrates occur together on each side of a reaction. A more complete discussion of the meanings of edge-signs in terms of "activation" and "inhibition" is presented in [8]. Note that in the context of N1C reaction systems, the following features (which are reasonably common in the more general setting) do not occur: edges with only R-to-S direction; multiple edges between a vertex pair; and edges with edge-label ∞.

SR/DSR graphs can be uniquely associated with (2), (3), or (4): in the case of (3) and (4), the inflows and outflows are ignored, and the SR/DSR graph is just that derived from the associated system (2). The construction is most easily visualised via an example. Consider, first, the simple system of two reactions:

$$A + B \rightleftharpoons C, \qquad A \rightleftharpoons B \tag{5}$$

This has SR graph, shown in Figure 1, *left*. If all substrates affect the rates of reactions in which they participate then this is also the DSR graph for the reaction. If, now, the second reaction is irreversible, i.e. one can write

$$A + B \rightleftharpoons C, \qquad A \to B, \tag{6}$$

and consequently the concentration of B does not affect the rate of the second reaction[1], then the SR graph remains the same, losing information about irreversibility, but the DSR graph now appears as in Figure 1 *right*.

[1] Note that this is usually, but not always, implied by irreversibility: it is possible for the product of an irreversible reaction to influence a reaction rate.

Fig. 1. *Left.* The SR (and DSR graph) for reaction system (5). Negative edges are depicted as dashed lines, while positive edges are bold lines. This convention will be followed throughout. *Right.* The DSR graph for reaction system (6), that is, when B is assumed not to affect the rate of the second reaction.

4 Paths and cycles in SR and DSR graphs

In the usual way, **cycles** in SR (DSR) graphs are minimal undirected (directed) paths from some vertex to itself. All paths have a sign, defined as the product of signs of edges in the path. Given any subgraph E, its size (or length, if it is a path) $|E|$ is the number of edges in E. Paths of length two will be called **short** paths. Any path E of even length also has a **parity**

$$P(E) = (-1)^{|E|/2}\text{sign}(E).$$

A cycle C is an **e-cycle** if $P(C) = 1$, and an **o-cycle** otherwise. Given a cycle C containing edges $e_1, e_2, \ldots, e_{2r}$ such that e_i and $e_{(i \bmod 2r)+1}$ are adjacent for each $i = 1, \ldots, 2r$, define:

$$\text{stoich}(C) = \left| \prod_{i=1}^{r} \text{lbl}(e_{2i-1}) - \prod_{i=1}^{r} \text{lbl}(e_{2i}) \right| .$$

Note that this definition is independent of the starting point chosen on the cycle. A cycle with $\text{stoich}(C) = 0$ is termed an **s-cycle**.

An **S-to-R path** in an SR graph is a non-self-intersecting path between an S-vertex and an R-vertex. **R-to-R paths** and **S-to-S paths** are similarly defined, though in these cases the initial and terminal vertices may coincide. Any cycle is both an R-to-R path and an S-to-S path. Two cycles have **S-to-R intersection** if each component of their intersection is an S-to-R path. This definition can be generalised to DSR graphs in a natural way, but to avoid technicalities regarding cycle orientation, the reader is referred to [8] for the details. Further notation will be presented as needed.

Returning to the family of CRNs in (1), these give SR graphs shown in Figure 2. If all reactants can influence the rates of reactions in which they participate, then these are also their DSR graphs (otherwise some edges may become directed). Each SR graph contains a single cycle, which is an e-cycle (resp. o-cycle) if n is odd (resp. even). These cycles all fail to be s-cycles because of the unique edge-label of 2.

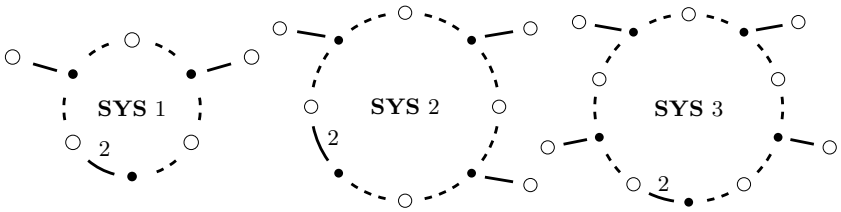

Fig. 2. The structure of the SR graphs for **SYS** 1, 2 and 3 in (1). For simplicity vertices are unlabelled, but filled circles are S-vertices while open circles are R-vertices. Unlabelled edges have edge-label 1.

5 Existing results on CRNs, injectivity and monotonicity

5.1 Injectivity and multiple equilibria

A function $f : X \to \mathbb{R}^n$ is **injective** if for any $x, y \in X$, $f(x) = f(y)$ implies $x = y$. Injectivity of a vector field on some domain is sufficient to guarantee that there can be no more than one equilibrium on this domain. Define the following easily computable condition on an SR or DSR graph:

Condition $(*)$: All e-cycles are s-cycles, and no two e-cycles have S-to-R intersection.

Note that if an SR/DSR graph has no e-cycles, then Condition $(*)$ is trivially fulfilled. A key result in [7] was:

Proposition 1. *An N1C reaction system of the form (4) with SR graph satisfying Condition $(*)$ is injective.*

Proof. See Theorem 1 in [7].

In [8] this result was strengthened considerably and extended beyond CRNs. In the context of CRNs with N1C kinetics it specialises to:

Proposition 2. *An N1C reaction system of the form (4) with DSR graph satisfying Condition $(*)$ is injective.*

Proof. See Corollary 4.2 in [8].

Proposition 2 is stronger than Proposition 1 because irreversibility is taken into account. In the case without outflows (2), attention must be restricted to some fixed stoichiometric class. The results then state that no stoichiometry class can contain more than one nondegenerate equilibrium in the interior of the positive orthant [8, 19]. (In this context, a degenerate equilibrium is defined to be an equilibrium with a zero eigenvalue and corresponding eigenvector lying in the stoichiometric subspace.) The case with partial outflows was also treated.

5.2 Monotonicity

A closed, convex, solid, pointed cone $K \subset \mathbb{R}^n$ is termed a **proper cone** [20]. The reader is referred to [20] for basic definitions related to cones. Any proper cone defines a partial order on $\mathbb{R}^n$ as follows: given two points $x, y \in \mathbb{R}^n$:

1. $x \geq y \Leftrightarrow x - y \in K$;
2. $x > y \Leftrightarrow x \geq y$ and $x \neq y$;
3. $x \gg y \Leftrightarrow x - y \in \operatorname{int} K$.

An extremal ray is a one dimensional face of a cone. A proper cone with exactly n extremal rays is termed **simplicial**. Simplicial cones have the feature that unit vectors on the extremal rays can be chosen as basis vectors for a new coordinate system. Consider some linear subspace $\mathcal{A} \subset \mathbb{R}^n$. Then any closed, convex, pointed cone $K \subset \mathcal{A}$ with nonempty interior in $\mathcal{A}$ is termed $\mathcal{A}$-proper. If, further, K has exactly $\dim(\mathcal{A})$ extremal rays, then K is termed $\mathcal{A}$-simplicial.

Consider some local semiflow ϕ defined on $X \subset \mathbb{R}^n$. Assume that there is some linear subspace $\mathcal{A} \subset \mathbb{R}^n$ with a coset $\mathcal{A}'$ with nonempty intersection with X, and such that ϕ leaves $\mathcal{A}' \cap X$ invariant. Suppose further that there is an $\mathcal{A}$-proper cone K such that for all $x, y \in \mathcal{A}' \cap X$, $x > y \Rightarrow \phi_t(x) > \phi_t(y)$ for all values of $t \geq 0$ such that $\phi_t(x)$ and $\phi_t(y)$ are defined. Then we say that $\phi|_{\mathcal{A}' \cap X}$ **preserves** K, and that $\phi|_{\mathcal{A}' \cap X}$ is **monotone**. If, further, $x > y \Rightarrow \phi_t(x) \gg \phi_t(y)$ for all values of $t > 0$ such that $\phi_t(x)$ and $\phi_t(y)$ are defined, then $\phi|_{\mathcal{A}' \cap X}$ is **strongly monotone**. A local semiflow is monotone with respect to the nonnegative orthant if and only if the Jacobian of the vector field has nonnegative off-diagonal elements, in which case the vector field is termed **cooperative**.

Returning to (3), in the case $q = 0$, all stoichiometry classes are invariant, while if $q > 0$, there is a globally attracting stoichiometry class. Conditions for monotonicity of ϕ restricted to invariant subspaces of $\mathbb{R}^n$ were discussed extensively in [12]. Here the immediate aim is to develop graph-theoretic corollaries of one of these results, and to raise some interesting open questions.

Given a vector $y \in \mathbb{R}^n$, define

$$\mathcal{Q}_1(y) \equiv \{v \in \mathbb{R}^n \mid v_i y_i \geq 0\}.$$

A matrix Γ is **R-sorted** (resp. **S-sorted**) if any two distinct columns (resp. rows) Γ_i and Γ_j of Γ satisfy $\Gamma_i \in \mathcal{Q}_1(-\Gamma_j)$. A matrix Γ' is **R-sortable** (resp. **S-sortable**) if there exists a signature matrix D such that $\Gamma \equiv \Gamma' D$ (resp. $\Gamma \equiv D\Gamma'$) is well-defined, and is R-sorted (resp. S-sorted).

Proposition 3. *Consider a system of N1C reactions of the form (3) whose stoichiometric matrix Γ is R-sortable, and whose reaction vectors $\{\Gamma_k\}$ are linearly independent. Let $\mathcal{S} = \operatorname{Im}(\Gamma)$. Then there is an $\mathcal{S}$-simplicial cone K preserved by the system restricted to any invariant stoichiometry class, such that each reaction vector is collinear with an extremal ray of K.*

Proof. This is a specialisation of Corollary A7 in [12].

Systems fulfilling the assumptions of Proposition 3, cannot have periodic orbits intersecting the interior of the positive orthant which are stable on their stoichiometry class. In fact, mild additional assumptions ensure strong monotonicity guaranteeing generic convergence of bounded trajectories to equilibria [9, 10].

6 Graph-theoretic implications of Proposition 3

Some more notation is needed for the results to follow. The **S-degree** (**R-degree**) of an SR graph G is the maximum degree of its S-vertices (R-vertices). Analogous to the terminology for matrices, a subgraph E is **R-sorted** (**S-sorted**) if each R-to-R (S-to-S) path E_k in E satisfies $P(E_k) = 1$. Note that E is R-sorted if and only if each R-to-R path E_k of length 2 in E satisfies $P(E_k) = 1$.

An **R-flip** on a SR/DSR graph G is an operation which changes the signs on all edges incident on some R-vertex in G. (This is equivalent to exchanging left and right for the chemical reaction associated with the R-vertex). An **R-resigning** is a sequence of R-flips. An **S-flip** and **S-resigning** can be defined similarly. Given a set of R-vertices $\{R_k\}$ in G, the closed neighbourhood of $\{R_k\}$ will be denoted $G_{\{R_k\}}$, i.e., $G_{\{R_k\}}$ is the subgraph consisting of $\{R_k\}$ along with all edges incident on vertices of $\{R_k\}$, and all S-vertices adjacent to those in $\{R_k\}$.

Proposition 4. *Consider a system of N1C reactions of the form (3) with stoichiometric matrix Γ, and whose reaction vectors $\{\Gamma_k\}$ are linearly independent. Define $\mathcal{S} = \mathrm{Im}(Gamma)$. Associate with the system the SR graph G. Suppose that*

1. *G has S-degree ≤ 2.*
2. *All cycles in G are e-cycles.*

Then there is an $\mathcal{S}$-simplicial cone K preserved by the system restricted to any invariant stoichiometry class, such that each reaction vector is collinear with an extremal ray of K.

The key idea of the proof is simple: if the system satisfies the conditions of Proposition 4, then the conditions of Proposition 3 are also met. In this case, the extremal vectors of the cone K define a local coordinate system on each stoichiometry class, such that the (restricted) system is cooperative in this coordinate system. This interpretation in terms of recoordinatisation is best illustrated with an example.

Consider **SYS** 1 from (1) with SR graph shown in Figure 2 *left*, which can easily be confirmed to satisfy the conditions of Proposition 4. Define the following matrices:

$$\Gamma = \begin{pmatrix} -1 & 0 & 2 \\ -1 & -1 & 0 \\ 0 & -1 & -1 \\ 1 & 0 & 0 \\ 0 & 1 & 0 \end{pmatrix}, \qquad T = \begin{pmatrix} -1 & 0 & 2 \\ -1 & 1 & 0 \\ 0 & 1 & -1 \\ 1 & 0 & 0 \\ 0 & -1 & 0 \end{pmatrix}, \qquad T' = \begin{pmatrix} 1 & -2 & 2 & 0 & 0 \\ 1 & -1 & 2 & 0 & 0 \\ 1 & -1 & 1 & 0 & 0 \end{pmatrix}$$

Γ, the stoichiometric matrix, has rank 3, and so Proposition 4 applies. Let $x_1, \ldots, x_5$ be the concentrations of the five substrates involved, v_1, v_2, v_3 be the rates of the three reactions, and $v_{ij} \equiv \frac{\partial v_i}{\partial x_j}$. Assuming that the system is N1C means that $V \equiv [v_{ij}]$ has sign structure

$$\mathrm{sgn}(V) = \begin{pmatrix} + & + & 0 & - & 0 \\ 0 & + & + & 0 & - \\ - & 0 & + & 0 & 0 \end{pmatrix}$$

where $+$ denotes a nonnegative quantity, and $-$ denotes a nonpositive quantity. Consider now any coordinates y satisfying $x = Ty$. Note that T is a re-signed version of Γ. Choosing some left inverse for T, say $T^{'}$, gives $y_1 = x_1 - 2x_2 + 2x_3$, $y_2 = x_1 - x_2 + 2x_3$ and $y_3 = x_1 - x_2 + x_3$. (The choice of $T^{'}$ is not unique, but this does not affect the argument.) Calculation gives that $J = T^{'}\Gamma V T$ has sign structure

$$\mathrm{sgn}(J) = \begin{pmatrix} - & + & + \\ + & - & + \\ + & + & - \end{pmatrix},$$

i.e., restricting to any invariant stoichiometry class, the dynamical system for the evolution of the quantities y_1, y_2, y_3 is cooperative. Further, the evolution of $\{x_i\}$ is uniquely determined by the evolution of $\{y_i\}$ via the equation $x = Ty$.

It is time to return to the steps leading to the proof of Proposition 4. In Lemmas 1 and 2 below, G is an SR graph with S-degree ≤ 2. This implies the following: consider R-vertices v, $v^{'}$ and $v^{''}$ such that $v \neq v^{'}$ and $v \neq v^{''}$ ($v^{'} = v^{''}$ is possible). Assume there exist two distinct short paths in G, one from v to $v^{'}$ and one from v to $v^{''}$. These paths must be edge disjoint, for otherwise there must be an S-vertex lying on both A and B, and hence having degree ≥ 3.

Lemma 1. *Suppose G is a connected SR graph with S-degree ≤ 2, and has some connected, R-sorted, subgraph E containing R-vertices $v^{'}$ and $v^{''}$. Assume that there is a path C_1 of length 4 between $v^{'}$ and $v^{''}$ containing an R-vertex not in E. Then either C_1 is even or G contains an o-cycle.*

Proof. If $v^{'} = v^{''}$, then C_1 is not even, then it is itself and e-cycle. Otherwise consider any path C_2 connecting $v^{'}$ and $v^{''}$ and lying entirely in E. C_2 exists since E is connected, and $P(C_2) = 1$ since E is R-sorted. Since G has S-degree ≤ 2, and $|C_1| = 4$, C_1 and C_2 share only endpoints, $v^{'}$ and $v^{''}$, and hence together they form a cycle C. If $P(C_1) = -1$, then $P(C) = P(C_2)P(C_1) = -1$, and so C is an o-cycle. □

Lemma 2. *Suppose G is a connected SR graph with S-degree ≤ 2 which does not contain an o-cycle. Then it can be R-sorted.*

Proof. The result is trivial if G contains a single R-vertex, as it contains no short R-to-R paths. Suppose the result is true for graphs containing k R-vertices. Then it must be true for graphs containing $k+1$ R-vertices. Suppose G contains

$k+1$ R-vertices. Enumerate these R-vertices as $R_1, \ldots, R_{k+1}$ in such a way that $G_- \equiv G_{\{R_1,\ldots,R_k\}}$ is connected. This is possible since G is connected.

By the induction hypothesis, G_- can be R-sorted. Having R-sorted G_-, consider R_{k+1}. If all short paths between R_{k+1} and R-vertices in G_- have the same parity, then either they are all even and G is R-sorted; or they are all odd, and a single R-flip on R_{k+1} R-sorts G. (Note that an R-flip on R_{k+1} does not affect the parity of any R-to-R paths in G_-.) Otherwise there must be two distinct short paths of opposite sign, between R_{k+1} and R-vertices $v', v'' \in G_-$ ($v' = v''$ is possible). Since G has S-degree ≤ 2, these paths must be edge-disjoint, and together form an odd path of length 4 from v' to R_{k+1} to v''. By Lemma 1, G contains an o-cycle. □

PROOF of Proposition 4. From Lemma 2, if no connected component of G contains an o-cycle then each connected component of G (and hence G itself) can be R-sorted. The fact that G can be R-sorted corresponds to choosing a signing of the stoichiometric matrix Γ such that any two columns Γ_i and Γ_j satisfy $\Gamma_i \in \mathcal{Q}_1(-\Gamma_j)$. Thus the conditions of Proposition 3 are satisfied. □

7 Examples illustrating the result and its limitations

Example 1: SYS n from Section 1. It is easy to confirm that the reactions in **SYS** n have linearly independent reaction vectors for all n . Moreover, as illustrated by Figure 2, the corresponding SR graphs contain a single cycle, which, for odd (even) n is an e-cycle (o-cycle). Thus for even n, Proposition 1 and subsequent remarks apply, ruling out the possibility of more than one positive nondegenerate equilibrium for (2) on each stoichiometry class, or in the case with outflows (4), ruling out multiple equilibria altogether; meanwhile, while for odd n, Proposition 4 can be applied to (2) or (3), implying that restricted to any invariant stoichiometry class the system is monotone, and the restricted dynamical system cannot have an attracting periodic orbit intersecting the interior of the nonnegative orthant.

Example 2: Generalised interconversion networks. Consider the following system of chemical reactions:

$$A \rightleftharpoons B, \quad A \rightleftharpoons C, \quad A \rightleftharpoons D, \quad B \rightleftharpoons C \tag{7}$$

with SR graph shown in Figure 3. Formally, such systems have R-degree ≤ 2 and have SR graphs which are S-sorted. Although Proposition 4 cannot be applied, such "interconversion networks", with the N1C assumption, in fact give rise to cooperative dynamical systems [12], and a variety of different techniques give strong convergence results, both with and without outflows [16, 11, 21].

This example highlights that there is an immediate dual to Lemma 2, and hence Proposition 4. The following lemma can be regarded as a restatement of well-known results on systems preserving orthant cones (see [10], for example, and the discussion for CRNs in [11]). Its proof is omitted as it follows closely that of Lemma 2.

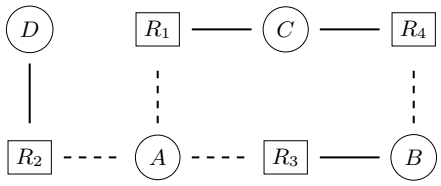

Fig. 3. The SR graph for reaction system 7. All edge labels are 1 and have been omitted. The system preserves the nonnegative orthant.

Lemma 3. *Let G be an SR graph with R-degree ≤ 2 and containing no o-cycles. Then, via an S-resigning, G can be S-sorted.*

Although the S-sorting process is formally similar to the R-sorting one, the interpretation of the result is quite different: changing the sign of the ith row of Γ and the ith column of V is equivalent to a recoordinatisation replacing concentration x_i with $-x_i$. Such recoordinatisations give rise to a cooperative system if and only if the original system is monotone with respect to an orthant cone.

Example 3: Linearly independent reaction vectors are not necessary for monotonicity. Consider the system of three reactions involving four substrates

$$A \rightleftharpoons B + C, \qquad B \rightleftharpoons D, \qquad C + D \rightleftharpoons A \tag{8}$$

with stoichiometric matrix Γ and SR graph shown in Figure 4.

$$\Gamma = \begin{pmatrix} -1 & 0 & 1 \\ 1 & -1 & 0 \\ 1 & 0 & -1 \\ 0 & 1 & -1 \end{pmatrix}$$

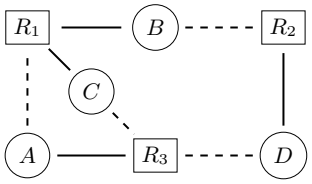

Fig. 4. The stoichiometric matrix and SR graph for reaction system 8. All edge labels are 1 and have been omitted.

Note that Γ is R-sorted, but has rank 2 as all row-sums are zero. As before, let x_i be the concentrations of the four substrates involved. Now, choose new coordinates y satisfying $x = Ty$, where

$$T = \begin{pmatrix} 1 & 0 & 0 \\ 0 & 1 & 0 \\ -1 & 0 & 0 \\ 0 & 0 & 1 \end{pmatrix}.$$

Note: i) T has rank 3, ii) $\mathrm{Im}(\Gamma) \subset \mathrm{Im}(T)$, and iii) regarding the columns of T as extremal vectors of a cone K, K has trivial intersection with $\mathrm{Im}(\Gamma)$. One can proceed to choose some left inverse $T^{'}$ of T, and calculate that the Jacobian $J = T^{'}\Gamma V T$ has nonnegative off-diagonal entries. In other words the y-variables define a cooperative dynamical system. The relationship between T and Γ is further discussed in the concluding section.

Note that although K has empty interior in $\mathbb{R}^4$, both K and $\mathrm{Im}(\Gamma)$ lie in the hyperplane $H = \mathrm{Im}(T)$ defined by $x_1 + x_3 = 0$. As K is H-proper, attention can be restricted to invariant cosets of H. With mild additional assumptions on the kinetics, the theory in [21] can be applied to get strong convergence results, but this is not pursued here.

Example 4a: The absence of o-cycles is not necessary for monotonicity. Consider the following system of 4 chemical reactions on 5 substrates:

$$A \rightleftharpoons B + C, \qquad B \rightleftharpoons D, \qquad C + D \rightleftharpoons A \qquad C + E \rightleftharpoons A \tag{9}$$

Define

$$\Gamma = \begin{pmatrix} -1 & 0 & 1 & 1 \\ 1 & -1 & 0 & 0 \\ 1 & 0 & -1 & -1 \\ 0 & 1 & -1 & 0 \\ 0 & 0 & 0 & -1 \end{pmatrix} \qquad \text{and} \qquad T = \begin{pmatrix} 1 & 0 & 0 & 0 \\ 0 & 1 & 0 & 0 \\ -1 & 0 & 0 & 0 \\ 0 & 0 & 1 & 0 \\ 0 & 0 & 0 & 1 \end{pmatrix}.$$

Γ, the stoichiometric matrix, has rank 3, and the system has SR graph containing both e- and o-cycles (Figure 5). Further, there are substrates participating in 3 reactions, and reactions involving 3 substrates (and so it is neither R-sortable nor S-sortable). Thus, all the conditions for the results quoted so far in this paper, and for theorems in [11], are immediately violated. However, applying theory in [12], the system is order preserving. In particular, $\mathrm{Im}(T)$ is a 4D subspace of $\mathbb{R}^5$ containing $\mathrm{Im}(\Gamma)$ (the stoichiometric subspace), and T defines a cone K which is preserved by the system restricted to cosets of $\mathrm{Im}(T)$.

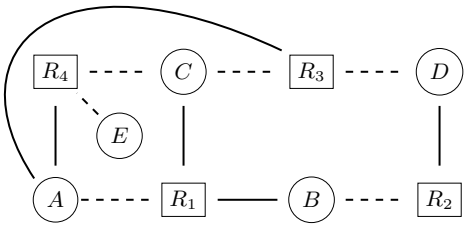

Fig. 5. The SR graph for reaction system 9. All edge labels are 1 and have been omitted.

Example 4b: The absence of o-cycles is not necessary for monotonicity. Returning to the system of reactions in (5), the system has SR graph

containing an o-cycle (Figure 1, *left*). Nevertheless, the system was shown in [12] to preserve a *nonsimplicial* cone for all N1C kinetics. In fact, the further analysis in [21] showed that with mild additional assumptions this system is strongly monotone and all orbits on each stoichiometry class converge to an equilibrium which is unique on that stoichiometry class. It is worth mentioning that this example is fundamentally different from Example 4a, and that it is currently unclear how commonly reaction systems preserve orders generated by nonsimplicial cones.

8 Discussion and open questions

The results presented here provide only a glimpse of the possibilities for analysis of limit sets of CRNs using graph-theoretic – and more generally combinatorial – approaches. The literature in this area is growing rapidly, and new techniques are constantly being brought into play. Working with the weakest possible kinetic assumptions often gives rise to approaches quite different from those used in the previous study of mass-action systems. Conversely, it is possible that such approaches can be used to provide explicit restrictions on the kinetics for which a system displays some particular behaviour.

The paper highlights an interesting duality between questions of multistationarity and questions of stable periodic behaviour, a duality already implicit in discussions of interaction graphs [22–25]. Loosely, the absence of e-cycles (positive cycles) is associated with injectivity for systems described by SR graphs (I graphs); and the absence of o-cycles (negative cycles) is associated with absence of periodic attractors for systems described by SR graphs (I graphs). The connections between apparently unrelated SR and I graph results on injectivity have been clarified in [26], but there is still considerable work to be done to clarify the results on monotonicity.

One open question regards the relationship between the theory and examples presented here on monotonicity, and previous results, particularly Theorem 1 in [11], on monotonicity in "reaction coordinates". Note that by Proposition 4.5 in [11] the "positive loop property" described there is precisely Conditions 1 and 2 in Proposition 4 here. At the same time, the requirement that the stoichiometric matrix has full rank, is not needed for monotonicity in reaction coordinates. In some cases (e.g. Example 3 above), it can be shown that this requirement is unnecessary for monotonicity too, but it is currently unclear whether this is always the case. On the other hand, as illustrated by Examples 4a and 4b, the positive loop property is not needed for monotonicity.

Consider again Examples 3 and 4a. The key fact is that their stoichiometric matrices admit factorisations $\Gamma = T_1 T_2$, taking the particular forms

$$\begin{pmatrix} -1 & 0 & 1 \\ 1 & -1 & 0 \\ 1 & 0 & -1 \\ 0 & 1 & -1 \end{pmatrix} = \begin{pmatrix} 1 & 0 & 0 \\ 0 & 1 & 0 \\ -1 & 0 & 0 \\ 0 & 0 & 1 \end{pmatrix} \begin{pmatrix} -1 & 0 & 1 \\ 1 & -1 & 0 \\ 0 & 1 & -1 \end{pmatrix} \qquad \text{(Example 3), and}$$

$$\begin{pmatrix} -1 & 0 & 1 & 1 \\ 1 & -1 & 0 & 0 \\ 1 & 0 & -1 & -1 \\ 0 & 1 & -1 & 0 \\ 0 & 0 & 0 & -1 \end{pmatrix} = \begin{pmatrix} 1 & 0 & 0 & 0 \\ 0 & 1 & 0 & 0 \\ -1 & 0 & 0 & 0 \\ 0 & 0 & 1 & 0 \\ 0 & 0 & 0 & 1 \end{pmatrix} \begin{pmatrix} -1 & 0 & 1 & 1 \\ 1 & -1 & 0 & 0 \\ 0 & 1 & -1 & 0 \\ 0 & 0 & 0 & -1 \end{pmatrix} \qquad \text{(Example 4a).}$$

In each case, the first factor, T_1, is R-sorted and has linearly independent columns. On the other hand, the second factor, T_2, is S-sorted. The theory in [12] ensures that these conditions are sufficient to guarantee that the system restricted to some coset of $\mathrm{Im}(T_1)$, is monotone with respect to the order defined by T_1. The dynamical implications of this rather surprising factorisation result will be elaborated on in future work.

A broad open question concerns the extent to which the techniques presented here extend to systems with discrete-time, and perhaps also discrete-state space. In [6], there were shown to be close relationships, but also subtle differences, between results on persistence in the continuous-time, continuous-state context, and results on liveness in the discrete-time, discrete-state context. Even discretising only time can lead to difficulties: while the interpretation of injectivity results in the context of discrete-time, continuous-state, systems is straightforward, the dynamical implications of monotonicity can differ from the continuous-time case. For example, strongly monotone disrete-time dynamical systems may have stable k-cycles for $k \geq 2$ [27]. When the state space is discrete, an additional difficulty which may arise concerns differentiability of the associated functions, an essential requirement for the results presented here.

Finally, the work on monotonicity here has an interesting relationship with examples presented by Kunze and Siegel, for example in [28]. This connection remains to be explored and clarified.

References

1. I. R. Epstein and J. A. Pojman, editors. *An Introduction to Nonlinear Chemical Dynamics: Oscillations, Waves, Patterns, and Chaos*. Oxford University Press, New York, 1998.
2. M. Feinberg. Complex balancing in general kinetic systems. *Arch Ration Mech Anal*, 49(3):187–194, 1972.
3. M. Feinberg. Chemical reaction network structure and the stability of complex isothermal reactors - I. The deficiency zero and deficiency one theorems. *Chem Eng Sci*, 42(10):2229–2268, 1987.
4. G. Craciun and M. Feinberg. Multiple equilibria in complex chemical reaction networks: II. The species-reaction graph. *SIAM J Appl Math*, 66(4):1321–1338, 2006.
5. M. Mincheva and M. R. Roussel. Graph-theoretic methods for the analysis of chemical and biochemical networks, I. multistability and oscillations in ordinary differential equation models. *J Math Biol*, 55:61–86, 2007.
6. D. Angeli, P. De Leenheer, and E. D. Sontag. A Petri net approach to the study of persistence in chemical reaction networks. *Math Biosci*, 210:598–618, 2007.

7. M. Banaji and G. Craciun. Graph-theoretic criteria for injectivity and unique equilibria in general chemical reaction systems. *Adv in Appl Math*, 44:168–184, 2010.
8. M. Banaji and G. Craciun. Graph-theoretic approaches to injectivity and multiple equilibria in systems of interacting elements. *Commun Math Sci*, 7(4):867–900, 2009.
9. M.W. Hirsch and H. Smith. *Handbook of Differential Equations: Ordinary Differential Equations, Vol II*, chapter Monotone Dynamical Systems, pages 239–357. Elsevier B. V., Amsterdam, 2005.
10. H. Smith. *Monotone Dynamical Systems: An introduction to the theory of competitive and cooperative systems*. American Mathematical Society, 1995.
11. D. Angeli, P. De Leenheer, and E. D. Sontag. Graph-theoretic characterizations of monotonicity of chemical reaction networks in reaction coordinates. *J Math Biol*, DOI 10.1007/s00285-009-0309-0, 2009.
12. M. Banaji. Monotonicity in chemical reaction systems. *Dyn Syst*, 24(1):1–30, 2009.
13. G. Craciun and M. Feinberg. Multiple equilibria in complex chemical reaction networks: I. The injectivity property. *SIAM J Appl Math*, 65(5):1526–1546, 2005.
14. M. Banaji, P. Donnell, and S. Baigent. P matrix properties, injectivity and stability in chemical reaction systems. *SIAM J Appl Math*, 67(6):1523–1547, 2007.
15. P. De Leenheer, D. Angeli, and E.D. Sontag. Monotone chemical reaction networks. *J Math Chem*, 41(3):295–314, 2007.
16. M. Banaji and S. Baigent. Electron transfer networks. *J Math Chem*, 43(4), 2008.
17. R. David and H. Alla. Autonomous and timed continous Petri nets. In *Papers from the 12th International Conference on Applications and Theory of Petri Nets: Advances in Petri Nets 1993*, volume 674 of *Lecture Notes In Computer Science*, pages 71–90. 1991.
18. F. Bause and P. S. Kritzinger. *Stochastic Petri nets*. Vieweg, 2nd edition, 2002.
19. G. Craciun and M. Feinberg. Multiple equilibria in complex chemical reaction networks: Extensions to entrapped species models. *IEEE Proc Syst Biol*, 153(4):179–186, 2006.
20. A. Berman and R. Plemmons. *Nonnegative matrices in the mathematical sciences*. Academic Press, New York, 1979.
21. M. Banaji and D. Angeli. Convergence in strongly monotone systems with an increasing first integral. *SIAM J Math Anal*, 42(1):334–353, 2010.
22. J.-L. Gouzé. Positive and negative circuits in dynamical systems. *J Biol Sys*, 6:11–15, 1998.
23. C. Soulé. Graphic requirements for multistationarity. *Complexus*, 1:123–133, 2003.
24. M. Kaufman, C. Soulé, and R. Thomas. A new necessary condition on interaction graphs for multistationarity. *J Theor Biol*, 248(4):675–685, 2007.
25. D. Angeli, M. W. Hirsch, and E. Sontag. Attractors in coherent systems of differential equations. *J Diff Eq*, 246:3058–3076, 2009.
26. M. Banaji. Graph-theoretic conditions for injectivity of functions on rectangular domains. *J Math Anal Appl*, 370:302–311, 2010.
27. J. F. Jiang and S. X. Yu. Stable cycles for attractors of strongly monotone discrete-time dynamical systems. *J Math Anal Appl*, 202:349–362, 1996.
28. H. Kunze and D. Siegel. A graph theoretic approach to strong monotonicity with respect to polyhedral cones. *Positivity*, 6:95–113, 2002.

Comparison of approximate kinetics for unireactant enzymes: Michaelis-Menten against the equivalent server

Alessio Angius[1], Gianfranco Balbo[1], Francesca Cordero[1,2], András Horváth[1], and Daniele Manini[1]

[1] Department of Computer Science, University of Torino, Torino, Italy
[2] Department of Clinical and Biological Sciences, University of Torino, Torino, Italy

Abstract. Mathematical models are widely used to create complex biochemical models. Model reduction in order to limit the complexity of a system is an important topic in the analysis of the model. A way to lower the complexity is to identify simple and recurrent sets of reactions and to substitute them with one or more reactions in such a way that the important properties are preserved but the analysis is easier.
In this paper we consider the typical recurrent reaction scheme $E + S \rightleftharpoons ES \longrightarrow E + P$ which describes the mechanism that an enzyme, E, binds a substrate, S, and the resulting substrate-bound enzyme, ES, gives rise to the generation of the product, P. If the initial quantities and the reaction rates are known, the temporal behaviour of all the quantities involved in the above reactions can be described exactly by a set of differential equations. It is often the case however that, as not all necessary information is available, only approximate analysis can be carried out. The most well-known approximate approach for the enzyme mechanism is provided by the kinetics of Michaelis-Menten. We propose, based on the concept of the flow-equivalent server which is used in Petri nets to model reduction, an alternative approximate kinetics for the analysis of enzymatic reactions. We evaluate the goodness of the proposed approximation with respect to both the exact analysis and the approximate kinetics of Michaelis and Menten. We show that the proposed new approximate kinetics can be used and gives satisfactory approximation not only in the standard deterministic setting but also in the case when the behaviour is modeled by a stochastic process.

1 Introduction

Mathematical models are widely used to describe biological pathways because, as it is phrased in [1], they "offer great advantages for integrating and evaluating information, generating prediction and focusing experimental directions". In the last few years, high-throughput techniques have increased steadily, leading to

Cordero is the recipient of a research fellowship supported by grants from Regione Piemonte, University of Torino and MIUR. Horváth is supported by MIUR PRIN 2008.

the production of a huge volume of data used to derive the complex texture behind the biological/biochemical mechanisms, and creating in this way the structure needed for mathematical modelling. Indeed, many models based on the combination and the integration of various elements in order to investigate their relationships and behaviour have been devised which become more complex with the growth of available data. The complexity is reflected in the number of dynamic state variables and parameters, as well as in the form of the kinetic rate expressions.

Such complexity leads to difficulties both from the point of view of defining the model as the parametrisation becomes unfeasible and for what concerns the analysis of the model. It is often the case hence that in order to have a model which is feasilble for the analysis simplifications must be performed.

In this paper we focus our attention on the simplified, approximate treatment of a set of reactions that very often appears as building blocks of complex models. We consider the reactions

$$E + S \underset{k_{-1}}{\overset{k_1}{\rightleftarrows}} ES \xrightarrow{k_2} E + P \tag{1}$$

describing that the enzyme, E, attaches reversibly to the substrate, S, forming the substrate-bound enzyme ES which gives rise then to the product P releasing the enzyme. This and similar enzymatic reactions are widely studied in biology. The most common approximate approach to deal with them is provided by the Michaelis-Menten (MM) kinetics (called also Michaelis-Menten-Henri kinetics) which, based on quasi-steady-state assumptions, connects the speed of producing P directly to the concentration of E and P, omitting the explicit modeling of ES.

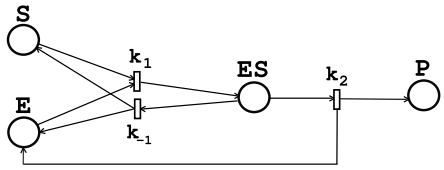

Fig. 1. Petri net representation of the reactions given in (1)

System of enzymatic reactions can be described by Petri nets [2] (Figure 1 shows the Petri net corresponding to the reactions given in (1)) and then analysed by methods developed for this formalism. We propose for the reactions in (1) an alternative to the approximate Michaelis-Menten kinetics. This new approximate kinetics is based on a concept widely used in the analysis of Petri nets and models described by other formalisms like queueing networks and process algebras. This concept is called the flow equivalent server [3]. The application of this concept, similarly to the Michaelis-Menten kinetics, leads to a simplified set

of reactions in which the intermediate complex ES is not modeled explicitly. The difference is, however, that, since the application of the flow equivalent server (FES) is based on assumptions that are different and less strict than those used by the Michaelis-Menten kinetics, the resulting approximation is more robust.

The concept of flow equivalent server has already been used in [4] where a complex signal transduction model was considered. In that paper we have shown that this concept can be applied not only to the small set of reactions given in (1) but also to bigger submodels. This leads to a simplified model which has less parameters and whose analysis is not as heavy as that of the complete one. For the model presented in [4] it was shown that the quantitative temporal behaviour of the simplified model coincides satisfactorily with that of the complete model and that important qualitative properties are maintained as well. In this paper our goal is to study in detail the goodness of the FES based approximation for the reactions in (1) and to compare it to the widely-used approximate kinetics of Michaelis, Menten and Henri.

The paper is organised as follows. Section 2 provides the necessary background, Section 3 describes the concept of the flow equivalent server and Section 4 presents the results of the comparison between the approximation approaches. We conclude with a discussion and an outlook on future works in Section 5.

2 Background

In 1901 Henri [5] proposed a partly reversible reaction scheme to describe the enzymatic process. According to this scheme the enzyme E and the substrate S form, through a reversible reaction, the enzyme-substrate complex ES. This complex can then give rise to the product P through an irreversible reaction during which the enzyme is freed and can bind again to other molecules of the substrate. This scheme is summarised in (1) where k_1 is the rate of the binding of E and S, k_{-1} is the rate of the unbinding of ES into E and S and k_2 is the rate at which ES decays to the product P freeing the enzyme E.

There are two typical approaches to associate a quantitative temporal behaviour to the reactions in (1). The first results in a deterministic representation while the other in a stochastic one. In the following we give a brief idea of both approaches. For a detailed description see, for example, [6, 7].

The deterministic approach describes the temporal behaviour of a reaction with a set of ordinary differential equations (ODE). For the reactions in (1) we have

$$\begin{aligned}
\frac{d[E]}{dt} &= -k_1[E][S] + (k_{-1} + k_2)[ES] \\
\frac{d[S]}{dt} &= -k_1[E][S] + k_{-1}[ES] \\
\frac{d[ES]}{dt} &= k_1[E][S] - (k_{-1} + k_2)[ES] \\
\frac{d[P]}{dt} &= k_2[ES]
\end{aligned} \tag{2}$$

where $[X]$ is the concentration of molecule X at time t. These equations state that the rate at which the concentration of a given molecule changes equals the difference between the rate at which it is formed and the rate at which it is utilised. The four equations can be solved numerically to yield the concentration of E, S, ES and P at any time t if both the initial concentration levels ($[S]_0$, $[E]_0$, $[ES]_0$, $[P]_0$) and the reaction rates (k_1, k_{-1}, k_2) are known. In the deterministic approach the concentrations of the molecules are described by continuous quantities.

In the stochastic approach a continuous time Markov chain (CTMC) is used to describe the process. Each state of the chain is described by a vector of integers in which the entries give the quantities of the molecules, which, accordingly, assume discrete values. These discrete values are resulting either directly from molecule count or from discretization of continuous values. Reactions are modeled by transitions between the states. For example, from state $|x_1, x_2, x_3, x_4|$ where x_1, x_2, x_3 and x_4 are the quantities of the molecules E, S, ES and P, respectively, there is a transition to state $|x_1 - 1, x_2 - 1, x_3 + 1, x_4|$ with rate $k_1 x_1 x_2$ which corresponds to the binding of one molecule E with one molecule S to form one molecule of ES. It is easy to see that even for small models the corresponding CTMC can have a huge state space whose transition rate structure is non-homogeneous. Exact analytical treatment of these chains is often unfeasible and in most cases simulation is the only method that can be used for their analysis.

2.1 Michaelis-Menten approximate kinetics

Under some assumptions, the temporal, quantitative dynamics of the mechanism described by the reactions in (1) can be summarised as follows. Initially we have a certain amount of substrate, denoted by $[S]_0$, and enzyme, denoted by $[E]_0$, and no complex ES ($[ES]_0 = 0$). Assuming that k_2 is significantly smaller than k_1 and k_{-1}, a brief transient period occurs during which the amount of the complex ES quickly increases up to a "plateau" level where it remains stable for a long period of time. As the ratio of $[S]_0/[E]_0$ increases, the time needed to reach the condition $d[ES]/dt \approx 0$ decreases and the period during which $d[ES]/dt \approx 0$ increases. In this period we have approximately

$$\frac{d[ES]}{dt} = k_1[E][S] - [ES](k_{-1} + k_2) = 0$$

from which, considering that the total amount of enzyme is conserved, i.e. $[E] + [ES] = [E]_0$, the quantity of ES can be expressed as

$$[ES] = \frac{[E]_0[S]}{\frac{k_{-1}+k_2}{k_1} + [S]} = \frac{[E]_0[S]}{k_M + [S]} \tag{3}$$

where the term $k_M = \frac{k_{-1}+k_2}{k_1}$ is called the Michaelis-Menten constant. Applying (3), the speed of the production of P can be approximated by

$$v_{MM} = \frac{k_2[E]_0[S]}{[S] + k_M} \tag{4}$$

Accordingly, after the "plateau" level of ES is reached, the kinetic parameters k_1, k_{-1} and k_2 together with $[S]$ and the initial total quantity of the enzyme, $[E]_0$, determine the overall rate of the production of P.

Applying the approximate kinetics of Michaelis and Menten, the differential equations describing the reactions become

$$\begin{aligned} \frac{d[E]}{dt} &= 0 \\ \frac{d[S]}{dt} &= -\frac{k_2[E][S]}{[S]+k_M} \\ \frac{d[P]}{dt} &= \frac{k_2[E][S]}{[S]+k_M} \end{aligned} \tag{5}$$

3 Approximate kinetics by flow equivalent server

In this section we derive an alternative approximate kinetics for the analysis of enzymatic reactions, based on the concept of the flow equivalent server. This technique was originally proposed in the context of the steady-state solution of queueing networks [3, 8, 9] and can be adapted to our purposes with a proper interpretation of the assumptions on which it is based. The idea behind this concept is to consider the reactions given in (1) as a fragment of a large biological system in which substrate S is produced by an "up-stream" portion of the system and product P is used "down-stream" within the same system. The goal of the flow equivalent method is to consider the flow of moles that move from the substrate to the product, in the presence of an enzyme that catalyse this phenomenon, and to evaluate its intensity in order to define the overall speed of a "composite" reaction that captures this situation in an abstract manner.

Figure 2 depicts the Petri net corresponding to the reactions of (1) organised in order to make explicit the relationship between the substrate S and the product P, via the enzyme E, enclosing in a dashed box the elements of the system whose dynamics we want to mimic with the composite transition. This

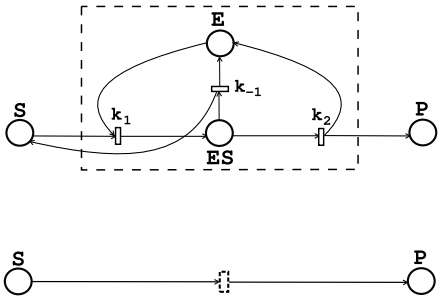

Fig. 2. Petri net of the reactions in (1) organised for computation of the flow equivalent-transition (above) and its approximation (below)

picture makes evident the fact that the speed of the composite transition must depend not only on the speeds of the transitions included in the box but also on the quantities present in the box, namely, the total amount of enzyme. Assuming to know the kinetic constants of the reactions inside the box and the quantity of the enzyme, the speed of the composite transition also depends on the amount $[S]$ that participates in the reactions and that may change during the evolution of the whole system. Following this point of view, it is possible to conceive a characterisation of the speed of the composite transition that is conditioned on the quantity of S. The flow equivalent approach accounts for this observation by computing the intensity of the flow of moles that reaches place P assuming that the total amount of S remains constant. Technically, this is obtained by short-circuiting the output and input places of the sub-net (introducing an immediate transition [10] that connects place P with place S) and by computing the throughput along the short-circuit which will be conditioned on the initial amount of S and that will thus be computed for all the possible values of S. In general, this amounts to the construction of a table that looks like that depicted in Figure 3, where S_1, S_2, ..., S_n represent different values of the amount of substrate S for which the speeds of the composite reaction $v_{FES}(S_1)$, $v_{FES}(S_2)$, ..., $v_{FES}(S_n)$ are computed, given that k_1, k_{-1}, k_2, and $\#E$ are assumed to be the values of the kinetics constant of the reactions in the box and of the amount of enzyme E.

In practice, this corresponds to the construction and to the (steady state) solution of the continuous time Markov chain (CTMC) that corresponds to the sub-model in isolation. Providing the speed of the composite transition in the tabular form highlighted by Figure 3 is convenient for cases where the domain of the function is "small", but may be impractical in many common situations. Despite the computational complexity of the approach, we must notice that the equilibrium assumption of the flow equivalent method is used only to obtain an approximate characterisation of the throughput for different sets of initial conditions and does not mean that the equivalent speed can only be used for steady state analysis.

The concept of flow equivalent server described above is used traditionally in a stochastic setting. However, it can be applied in a deterministic setting as well using arguments that are summarized by the following points. The complexity of the approach in the stochastic setting becomes prohibitive when the amount of the substrate S becomes very large. On the other hand, this is the case in

Given $k_1, k_{-1}, k_2,$ and $\#E$	
S_1	$v_{FES}(S_1)$
S_2	$v_{FES}(S_2)$
...	...
S_n	$v_{FES}(S_n)$

Fig. 3. Flow Equivalent Server characterisation

which the stochastic (or at least the average) behaviour of the model is conveniently captured by a set of ODE, i.e., by a deterministic model. Moreover, in the case of our model, the equilibrium solution of the set of differential equations corresponding to the short-circuited model is simple enough to obtain an analytic expression for the speed of the composite transition as it is described in the following.

We assume that the initial condition is $[E]_0 = M_1$, $[S]_0 = M_2$, $[ES]_0 = 0$, and $[P]_0 = 0$. We will denote the steady state measures of the compounds by $[E], [S], [ES]$ and $[P]$. In the short-circuited version of the reactions given in (1), moles transformed in P are immediately moved back to S and consequently its steady state measure is zero (i.e., $[P] = 0$). The steady state measures of the other compounds can be determined by considering

- the fact that in steady state the rate of change of the quantities of the different compounds is zero, i.e., we have

$$\begin{aligned} \frac{d[E](t)}{dt} &= 0 = -k_1[E][S] + k_{-1}[ES] + k_2[ES] \\ \frac{d[S](t)}{dt} &= 0 = -k_1[E][S] + k_{-1}[ES] + k_2[ES] \\ \frac{d[ES](t)}{dt} &= 0 = +k_1[E][S] - k_{-1}[ES] - k_2[ES] \end{aligned} \tag{6}$$

  which are three dependent equations;
- and the following equations expressing conservation of mass

$$[E] + [ES] = M_1, \quad [S] + [ES] = M_2 \tag{7}$$

In (6) and (7) we have three independent equations for three unknowns. There are two solutions but only one of them guarantees positivity of the unknowns. The speed of producing P is given by the steady state quantity of ES multiplied by k_2. This speed is

$$v_{FES} = \frac{k_2\left([E] + [S] + k_M - \sqrt{([E] - [S])^2 + 2k_M([E] + [S]) + k_M^2}\right)}{2} \tag{8}$$

Accordingly, the set of ordinary differential equations describing the reactions given in (1) becomes

$$\begin{aligned} \frac{d[E]}{dt} &= 0 \\ \frac{d[S]}{dt} &= -\frac{k_2\left([E] + [S] + k_M - \sqrt{([E] - [S])^2 + 2k_M([E] + [S]) + k_M^2}\right)}{2} \\ \frac{d[P]}{dt} &= \frac{k_2\left([E] + [S] + k_M - \sqrt{([E] - [S])^2 + 2k_M([E] + [S]) + k_M^2}\right)}{2} \end{aligned} \tag{9}$$

which explicitly reflects the assumption of the conservation of E and the observation that substrate S is transformed into product P.

4 Numerical illustration

In this section, we first compare in Section 4.1 the MM and FES approximate kinetics from the point of view of the speed they assign to the production of P as function of the reaction rates (k_1, k_{-1}, k_2) and the concentration of the enzyme and the substrate $([E], [S])$. Subsequently, in Sections 4.2 and 4.3 we compare the quantitative behaviour of the approximations to that of the full model in the deterministic and in the stochastic setting, respectively.

It is easy to check that as the quantity of the substrate tends to infinity the two approximate kinetics lead to the the same speed of production. In both cases for the maximum speed of production we have

$$v_{\max} = \lim_{[S]\to\infty} v_{MM} = \lim_{[S]\to\infty} v_{FES} = k_2[E] \tag{10}$$

Another situation in which the two approximate kinetics show perfect correspondence is when the quantity of the enzyme is very low. This can be shown formally by observing that

$$\lim_{[E]\to 0} \frac{v_{MM}}{v_{FES}} = 1 \tag{11}$$

4.1 Production speeds

A typical way of illustrating the approximate Michaelis-Menten kinetics is to plot the production speed against the quantity of the substrate. Figure 4 gives such illustrations comparing the speeds given by the two approximate kinetics. Reaction rate k_2 is either 0.1, 1 or 10 and reaction rates k_1 and k_{-1} are varied in order to cover different situations for what concerns the ratio k_1/k_{-1}. Two different values of $[E]$ are considered. The limit behaviours expressed by (10) and (11) can be easily verified in the figures. On the left sides of the figure it can be observed that for small values of $[E]$ the two approximations are almost identical for all considered values of the reaction rates, thus in agreement with the trend conveyed by (11). It can also be seen that for larger values of $[E]$ the two approximations are rather different and the difference is somewhat increasing as k_2 increases, and becomes more significant for higher values of k_1/k_{-1}. In all cases the curves become closer to each other when the amount of $[S]$ increases.

4.2 Deterministic setting

In this section we compare the different kinetics in the deterministic setting. Once the initial quantities and the reaction rates are defined, the systems of differential equations given in (2),(5) and (9) can be numerically integrated and this provides the temporal behaviour of the involved quantities, used as references for the comparisons.

For the first experiments we choose such parameters with which the two approximate kinetics result in different speeds of production. Based on Figure 4 this is achieved whenever the quantity of the enzyme is comparable to the quantity

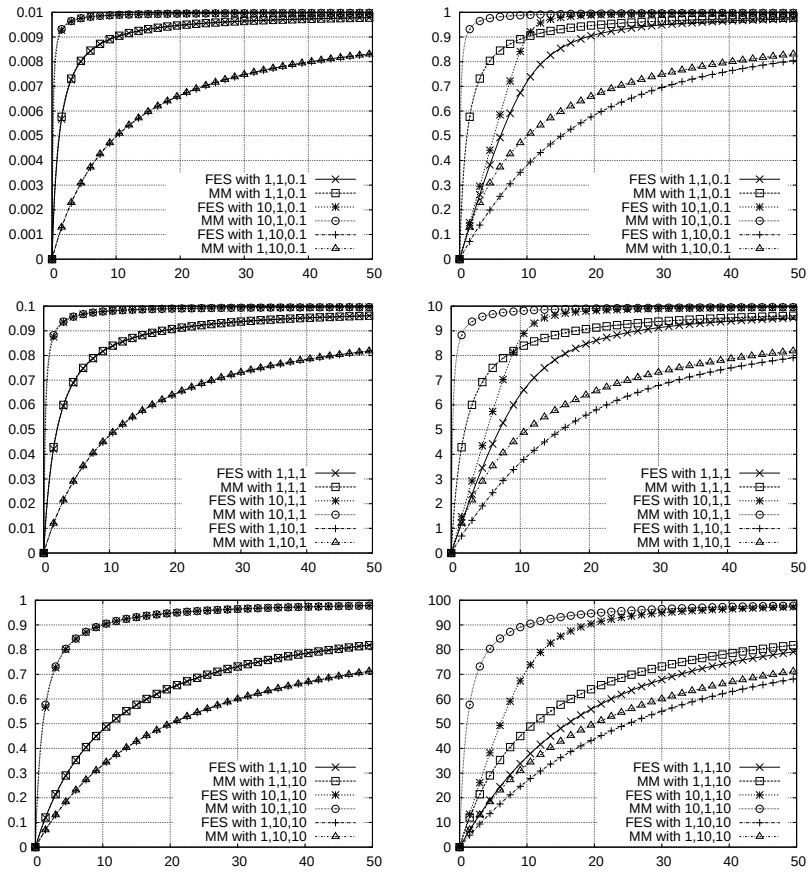

Fig. 4. Production speed as function of substrate quantity with $[E] = 0.1$ for the figures on the left side and with $[E] = 10$ on the right side; reaction rates are given in the legend in order k_1, k_{-1} and k_2

of the substrate. Accordingly, we set $[E]_0 = [S]_0 = 10$. For the full model $[ES]_0$ needs to be set too, and we choose $[ES]_0 = 0$. This choice does not help the approximations. They assume that the total enzyme concentration $[E]_0 + [ES]_0$ is immediately distributed between $[E]$ and $[ES]$, thus making possible an immediate (consistent) production of P. On the contrary, in the full model the production of $[ES]$ takes time and thus the speed of the production of P must start from 0, growing to a high value only later. Figures 5 and 6 depict the quantity of the product and the speed of its production as functions of time for two different sets of reaction rates. In both figures the kinetics based on flow equivalence provides precise approximation of the production of P. The Michaelis-Menten

kinetics instead fails to follow the full model, but this is not surprising as the derivation of this kinetics assumes small amount of enzymes. It can also be seen that high values of k_1/k_{-1} (Figure 6) lead to worst approximation in case of Michaelis-Menten kinetics. On the right hand side of the figures one can observe that for the full model the speed of producing P is 0 at the beginning and then it increases fast to the speed foreseen by the FES approximation.

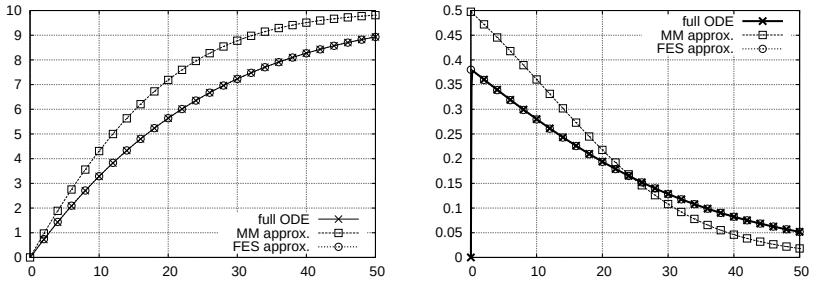

Fig. 5. Quantity of product (left) and speed of production (right) as function of time with $k_1 = 1$, $k_{-1} = 10$, $k_2 = 0.1$, $[E] = 10$ and initial quantity of substrate equals 10

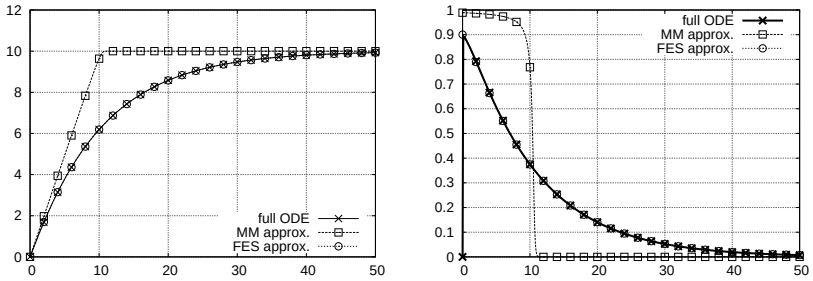

Fig. 6. Quantity of product (left) and speed of production (right) as function of time with $k_1 = 10$, $k_{-1} = 1$, $k_2 = 0.1$, $[E] = 10$ and initial quantity of substrate equals 10

A second set of experiments is illustrated in Figures 7 and 8. We choose sets of parameters with which the speed of production of the MM and FES approximations are similar. In these cases both approximations are close to the reference behaviour. Still, it can be seen that for high values of k_1/k_{-1} (Figure 8) the approximation provided by the Michaelis-Menten kinetics is slightly less precise.

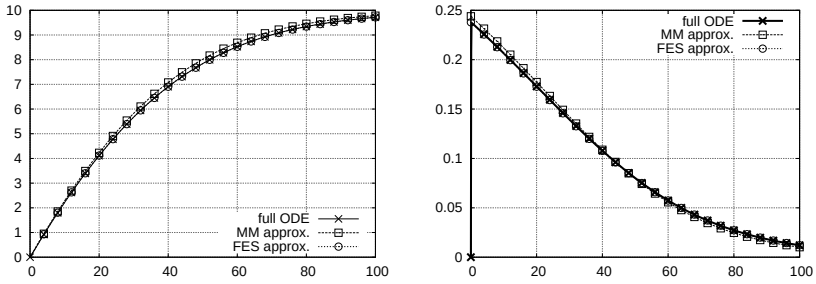

Fig. 7. Quantity of product (left) and speed of production (right) as function of time with $k_1 = 1$, $k_{-1} = 10$, $k_2 = 0.5$, $[E] = 1$ and initial quantity of substrate equals 10

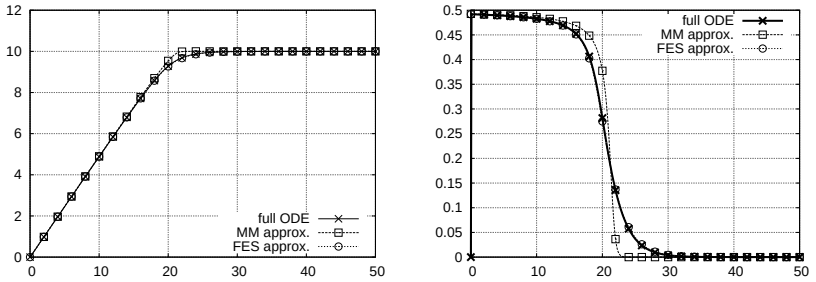

Fig. 8. Quantity of product (left) and speed of production (right) as function of time with $k_1 = 10$, $k_{-1} = 1$, $k_2 = 0.5$, $[E] = 1$ and initial quantity of substrate equals 10

In the following we turn our attention to the cases in which both the approximations are less reliable. In Figure 9 we plotted the case $k_1 = 0.1$, $k_{-1} = 0.1$, $k_2 = 0.1$, $[E] = 1$, $[S]_0 = 1$ and $[ES]_0 = 0$. As mentioned earlier, with $[ES]_0 = 0$ the initial production speed in the original model is 0 while it is immediately high in the approximate kinetics. With low values of k_1 and k_{-1}, the time taken by the system to reach the quasi-steady-state situation assumed by the approximate kinetics is quite long. For this reason there is a longer initial period in which P is produced by the approximations at a "wrong" speed. Furthermore, decreasing k_1 and k_{-1} would lead to a longer period in which the approximate kinetics are not precise (see Figure 9).

Another way of "disturbing" the approximations is to dynamically change the quantity of the substrate in the system. In the original model, because of the intermediate step yielding ES, the speed of producing P changes only after some delay. On the contrary, the approximations react immediately. The harsher the change in the quantity of the substrate the larger is the difference between the original model and the approximations. This phenomenon is reflected in the

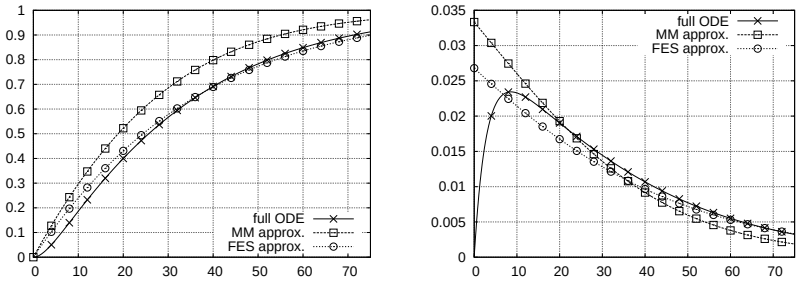

Fig. 9. Quantity of product (left) and speed of production (right) as function of time with $k_1 = 0.1$, $k_{-1} = 0.1$, $k_2 = 0.1$, $[E] = 1$ and initial quantity of substrate equals 1

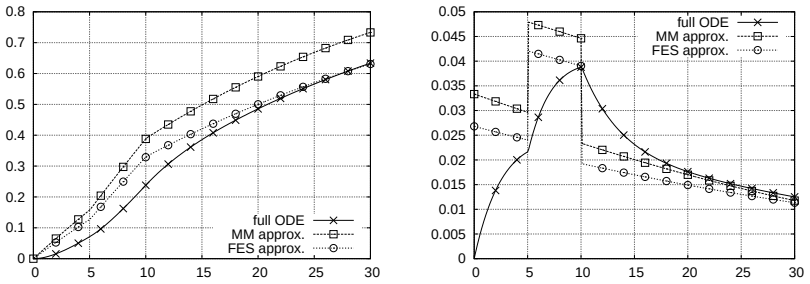

Fig. 10. Quantity of product (left) and speed of production (right) as function of time with $k_1 = 0.1$, $k_{-1} = 0.1$, $k_2 = 0.1$, $[E] = 1$, initial quantity of substrate equals 1 and adding substrate to the system according to (12)

model by adding the following term to the differential equation that describes the quantity of the substrate:

$$10(U(t-5) - U(t-5.1)) - 10(U(t-10) - U(t-10.1)) \tag{12}$$

where U denotes the unit-step function. The effect of (12) is to add 1 unit of substrate to the system in the time interval $[5, 5.1]$ and to take away 1 unit of substrate from it in the time interval $[10, 10.1]$. The resulting behaviour is depicted in Figure 10. The approximations change the speed of producing P right after the change in the quantity of the substrate while the original model reacts to the changes in a gradual manner. Naturally, if the quantity of the substrate undergoes several harsh changes then the MM and the FES kinetics can result in bad approximation of the full model.

4.3 Stochastic setting

In the following we compare the different kinetics in the stochastic setting, by analysing the corresponding CTMCs. In particular, we determine by means of

simulation the average and the variance of the quantity of the product as function of time. The simulations were carried out in Dizzy [11].

The reaction rates for the first set of experiments are $k_1 = k_{-1} = k_2 = 1$. As in the previous section, this choice allows to test a situation where the speed of the two approximations are different. For the same reason, we choose the same initial quantity for the enzyme and the substrate $[E]_0 = [S]_0 = 1$. In the stochastic setting the discretization step, denoted by δ, has to be chosen as well. This choice has a strong impact because as the granularity with which the concentrations are modeled is increased, the behaviour of the CTMC tends to the deterministic behaviour of the corresponding ODE. Figures 11 and 12 depict the average and the variance of the quantity of the product with $\delta = 0.01$ and $\delta = 0.001$, respectively. In both figures the approximate kinetics based on flow equivalence gives good approximation of the original average behaviour while the Michaelis-Menten approximation results in too fast production of P. On the right side on the figures one can observe that also the variance is approximated better by the FES approximation.

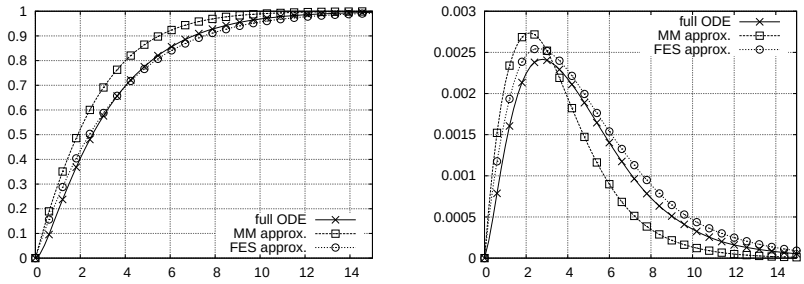

Fig. 11. The average (left) and the variance (right) of the quantity of the product as function of time with $k_1 = 1$, $k_{-1} = 1$, $k_2 = 1$, $[E]_0 = [S]_0 = 1$ and $\delta = 0.01$

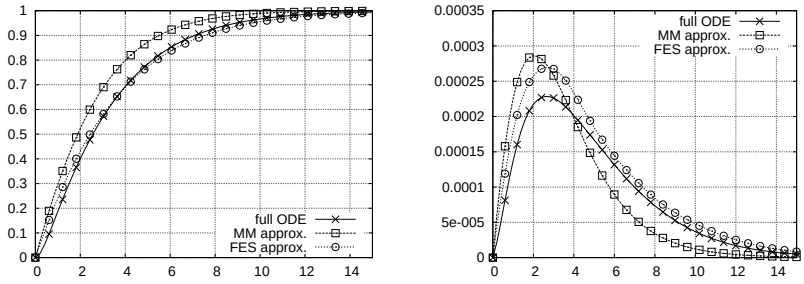

Fig. 12. The average (left) and the variance (right) of the quantity of the product as function of time with $k_1 = 1$, $k_{-1} = 1$, $k_2 = 1$, $[E]_0 = [S]_0 = 1$ and $\delta = 0.001$

For the second set of experiments we set $k_1 = 10$ and $k_{-1} = k_2 = 1$ and as initial states we choose again $[E]_0 = [S]_0 = 1$. In this case too, as it was shown in Figure 4, the speeds of production of P as predicted by the MM and FES approximations are quite different. Figures 13 and 14 depict the resulting behaviour for two different values of δ. As in case of the deterministic setting, the Michaelis-Menten approximation suffers from the increased k_1/k_{-1} ratio and becomes less precise than before. The FES based approach still results in good approximation for both the average and the variance of the production.

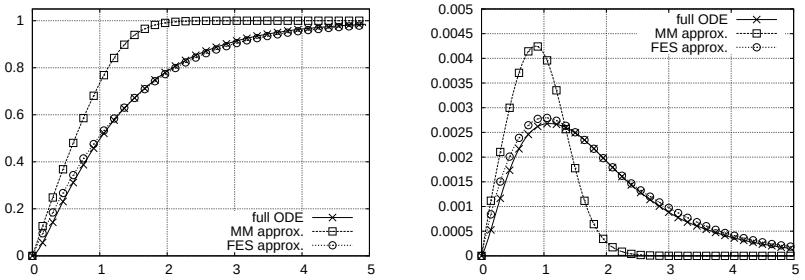

Fig. 13. The average (left) and the variance (right) of the quantity of the product as function of time with $k_1 = 10$, $k_{-1} = 1$, $k_2 = 1$, $[E]_0 = [S]_0 = 1$ and $\delta = 0.01$

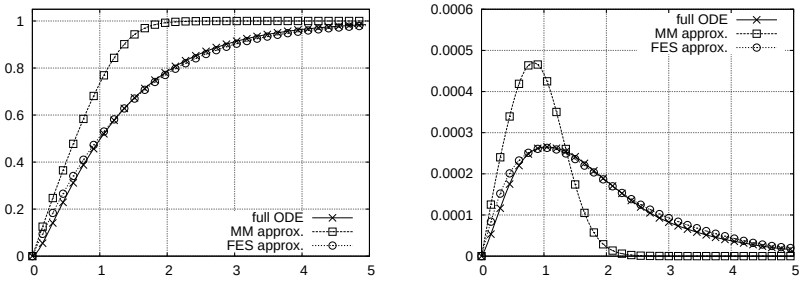

Fig. 14. The average (left) and the variance (right) of the quantity of the product as function of time with $k_1 = 10$, $k_{-1} = 1$, $k_2 = 1$, $[E]_0 = [S]_0 = 1$ and $\delta = 0.001$

5 Conclusion

In this paper we have considered the approximate treatment of the basic enzymatic reactions $E+S \rightleftharpoons ES \longrightarrow E+P$. In particular, an approximate kinetics, based on the concept of flow equivalent server, has been proposed for its analysis. This FES approximate kinetics has been compared to both the exact model and to the most common approximate treatment, namely, the Michaelis-Menten kinetics. We have shown that the FES kinetics is more robust than the one of Michaelis-Menten.

The FES approximation for the basic enzymatic reactions is computationally convenient due to the fact that it has been possible to find an analytic expression for the speed of the composite reaction in this case. While it is very unlikely for this to be true in the case of more complex kinetics, the method is very general and we will study it further within this context to see if it is possible to find other functional expressions for the speed of the composite reaction. One direction of research will be computing the flow equivalent characterization of the kinetics for a number of specific parameter sets and then of constructing the functional representations via interpolation.

References

1. Fisher, J., Henzinger, T.A.: Executable cell biology. Nature Biotechnology **25** (November 2007) 1239–1249
2. Reddy, V., Mavrovouniotis, M., Liebman, M.: Qualitative analysis of biochemical reaction systems. Comput. Biol. Med. **26** (1996) 9–24
3. Chandy, K.M., Herzog, U., Woo, L.S.: Parametric analysis of queueing networks. IBM Journal of R. & D. **19**(1) (January 1975) 36–42
4. Napione, L., Manini, D., Cordero, F., Horváth, A., Picco, A., Pierro, M.D., Pavan, S., Sereno, M., Veglio, A., Bussolino, F., Balbo, G.: On the use of stochastic Petri nets in the analysis of signal transduction pathways for angiogenesis process. In: Proc. of The 7th Conference on Computational Methods in Systems Biology (CMSB 2009). Volume 5688 of Lecture Notes in Bioinformatics., Bologna, Italy (Sept 2009) 281–295
5. Henri, V.: Recherches sur la loi de l'action de la sucrase. Compt. Rend. **133** (1901) 891–894
6. Voit, E.O.: Computational Analysis of Biochemical Systems. Cambridge University Press (2000)
7. Gillespie, D.: A rigorous derivation of the master chemical equation. Physica **188** (1992) 404–425
8. Denning, P.J., Buzen, J.P.: The operational analysis of queueing network models. ACM Comput. Surv. **10**(3) (1978) 225–261
9. Stewart, W.J.: Probability, Markov Chains, Queues, and Simulation: The Mathematical Basis of Performance Modeling. Princeton Univ. Press (2009)
10. Ajmone Marsan, M., Balbo, G., Conte, G.: A class of generalized stochastic Petri nets for the performance analysis of multiprocessor systems. ACM Transactions on Computer Systems **2**(1) (May 1984)
11. Ramsey, S., Orrell, D., Bolouri, H.: Dizzy: Stochastic simulation of large-scale genetic regulatory networks. J. Bioinformatics Comput. Biol. **3**(2) (2005) 415–436

On the Importance of the Deadlock Trap Property for Monotonic Liveness

Monika Heiner[1], Cristian Mahulea[2], Manuel Silva[2]

[1] Department of Computer Science, Brandenburg University of Technology
Postbox 10 13 44, 03013 Cottbus, Germany
monika.heiner@tu-cottbus.de
[2] Instituto de Investigación en Ingeniería de Aragón (I3A),
Universidad de Zaragoza, Maria de Luna 1, E-50018 Zaragoza, Spain
cmahulea@unizar.es, silva@unizar.es

Abstract. In Petri net systems, liveness is an important property capturing the idea of no transition (action) becoming non-fireable (unattainable). Additionally, in some situations it is particularly interesting to check if the net system is (marking) monotonically live, i.e., it remains live for any marking greater than the initial one. In this paper, we discuss structural conditions preserving liveness under arbitrary marking increase. It is proved that the deadlock trap property (DTP) is a necessary condition for liveness monotonicity of ordinary nets, and necessary and sufficient for some subclasses. We illustrate also how the result can be used to study liveness monotonicity for non-ordinary nets using a simulation preserving the firing language. Finally, we apply these conditions to several case studies of biomolecular networks.

1 Motivation

Petri nets are a natural choice to represent biomolecular networks. Various types of Petri nets may be useful – qualitative, deterministically timed, stochastic, continuous or hybrid ones, depending on the available information and the kind of properties to be analysed. Accordingly, the integrative framework demonstrated by several case studies in [GHR+08], [HGD08], [HDG10] applies a family of related Petri net models, sharing structure, but differing in their kind of kinetic information.

A key notion of the promoted strategy of biomodel engineering is the *level concept*, which has been introduced in the Petri net framework in [GHL07]. Here, a token stands for a specific amount of mass, defined by the total mass divided by the number of levels. Thus, increasing the token number to represent a certain amount of mass means to increase the resolution of accuracy.

This procedure silently assumes some kind of behaviour preservation while the marking is increased (typically multiplied by a factor) to represent a finer granularity of the mass flowing through the network. However, as it is well-known in Petri net theory, liveness is not monotonic with respect to (w.r.t.) the initial marking for general Petri nets. Thus, there is no reason to generally assume that

there is no significant change in the possible behaviour by marking increase. Contrary, under liveness monotonicity w.r.t. the initial marking we can expect continuization (fluidization) to be reasonable. However, only a particular kind of monotonicity seems to be needed for continuization: *homothetic liveness*, i.e., liveness preservation while multiplying the initial marking by k [RTS99], [SR02].

At structural level, (monotonic) liveness can be considered using transformation (reduction) rules [Ber86], [Sil85], [Mur89], [Sta90], the classical analysis for ordinary nets based on the Deadlock Trap Property (DTP) [Mur89], [Sta90], or the results of *Rank Theorems*, which are directly applicable to non-ordinary nets [TS96], [RTS98]. In this paper, we concentrate on the DTP, which will initially be used for ordinary net models, and later extended to non-ordinary ones.

This paper is organized as follows. We start off with recalling relevant notions and results of Petri net theory. Afterwards we introduce the considered subject by looking briefly at two examples, before turning to our main result yielding a necessary condition for monotonic liveness. We demonstrate the usefulness of our results for the analysis of biomolecular networks by a variety of case studies. We conclude with an outlook on open issues.

2 Preliminaries

We assume basic knowledge of the standard notions of place/transition Petri nets, see e.g. [DHP+93], [HGD08], [DA10]. To be self-contained we recall the fundamental notions relevant for our paper.

Definition 1 (Petri net, syntax).

A Petri net *is a tuple* $\mathcal{N} = \langle P, T, \boldsymbol{Pre}, \boldsymbol{Post} \rangle$*, and a* Petri net system *is a tuple* $\Sigma = \langle \mathcal{N}, \boldsymbol{m}_0 \rangle$*, where*

- P *and* T *are finite, non-empty, and disjoint sets.* P *is the set of* places. T *is the set of* transitions.
- $\boldsymbol{Pre}, \boldsymbol{Post} \in \mathbb{N}^{|P| \times |T|}$ *are the pre- and post-matrices, where* $|\cdot|$ *is the cardinality of a set, i.e., its number of elements. For a place* $p_i \in P$ *and a transition* $t_j \in T$*,* $Pre(p_i, t_j)$ *is the weight of the arc connecting* p_i *to* t_j *(*0 *if there is no arc), while* $Post(p_i, t_j)$ *is the weight of the arc connecting* t_j *to* p_i*.*
- $\boldsymbol{m}_0 \in \mathbb{N}_{\geq 0}^{|P|}$ *gives the* initial marking.
- $\boldsymbol{m}(p)$ *yields the number of tokens on place* p *in the marking* $\boldsymbol{m}$*. A place* p *with* $\boldsymbol{m}(p) = 0$ *is called* empty (unmarked) *in* $\boldsymbol{m}$*, otherwise it is called* marked *(non-empty). A set of places is called empty if all its places are empty, otherwise marked.*
- *The* preset *and* postset *of a node* $x \in P \cup T$ *are denoted by* ${}^\bullet x$ *and* $x^\bullet$*. They represent the input and output transitions of a place* x*, or the input and output places of a transition* x*. More specifically, if* $t_j \in T$*,* ${}^\bullet t_j = \{p_i \in P | Pre(p_i, t_j) > 0\}$ *and* $t_j{}^\bullet = \{p_i \in P | Post(p_i, t_j) > 0\}$*. Similarly, if* $p_i \in P$*,* ${}^\bullet p_i = \{t_j \in T | Post(p_i, t_j) > 0\}$ *and* $p_i{}^\bullet = \{t_j \in T | Pre(p_i, t_j) > 0\}$*.*
  We extend both notions to a set of nodes $X \subseteq P \cup T$ *and define the set of all prenodes* ${}^\bullet X := \bigcup_{x \in X} {}^\bullet x$*, and the set of all postnodes* $X^\bullet := \bigcup_{x \in X} x^\bullet$*.*

- *A node $x \in P \cup T$ is called* source node*, if $^\bullet x = \emptyset$, and* sink node *if $x^\bullet = \emptyset$. A* boundary node *is either a sink or a source node (but not both, because we assume a connected net).*

Definition 2 (Petri net, behaviour). *Let $\langle \mathcal{N}, \boldsymbol{m}_0 \rangle$ be a net system.*

- *A transition t is* enabled *at marking $\boldsymbol{m}$, written as $\boldsymbol{m}[t\rangle$, if $\forall p \in {}^\bullet t : \boldsymbol{m}(p) \geq Pre(p,t)$, else* disabled*.*
- *A transition t, enabled in $\boldsymbol{m}$, may* fire *(occur), leading to a new marking $\boldsymbol{m'}$, written as $\boldsymbol{m}[t\rangle\boldsymbol{m'}$, with $\forall p \in P : \boldsymbol{m'}(p) = \boldsymbol{m}(p) - Pre(p,t) + Post(p,t)$.*
- *The set of all markings* reachable *from a marking $\boldsymbol{m}_0$, written as $[\boldsymbol{m}_0\rangle$, is the smallest set such that $\boldsymbol{m}_0 \in [\boldsymbol{m}_0\rangle$, $\boldsymbol{m} \in [\boldsymbol{m}_0\rangle \wedge \boldsymbol{m}[t\rangle\boldsymbol{m'} \Rightarrow \boldsymbol{m'} \in [\boldsymbol{m}_0\rangle$.*
- *The* reachability graph (RG) *is a directed graph with $[\boldsymbol{m}_0\rangle$ as set of nodes, and the labelled arcs denote the reachability relation $\boldsymbol{m}[t\rangle\boldsymbol{m'}$.*

Definition 3 (Behavioural properties). *Let $\langle \mathcal{N}, \boldsymbol{m}_0 \rangle$ be a net system.*

- *A place p is k-*bounded *(bounded for short) if there is a positive integer number k, serving as an upper bound for the number of tokens on this place in all reachable markings of the Petri net: $\exists\, k \in \mathbb{N}_0 : \forall \boldsymbol{m} \in [\boldsymbol{m}_0\rangle : \boldsymbol{m}(p) \leq k$.*
- *A Petri net system is k-*bounded *(bounded for short) if all its places are k-*bounded*.*
- *A transition t is* dead at marking *$\boldsymbol{m}$ if it is not enabled in any marking $\boldsymbol{m'}$ reachable from $\boldsymbol{m}$: $\nexists\, \boldsymbol{m'} \in [\boldsymbol{m}\rangle : \boldsymbol{m'}[t\rangle$.*
- *A transition t is* live *if it is not dead in any marking reachable from $\boldsymbol{m}_0$.*
- *A marking $\boldsymbol{m}$ is* dead *if there is no transition which is enabled in $\boldsymbol{m}$.*
- *A Petri net system is* deadlock-free (weakly live) *if there are no reachable dead markings.*
- *A Petri net system is* live (strongly live) *if each transition is live.*

Definition 4 (Net structures). *Let $\mathcal{N} = \langle P, T, \boldsymbol{Pre}, \boldsymbol{Post} \rangle$ be a Petri net. $\mathcal{N}$ is*

- Homogeneous (HOM) *if $\forall p \in P : t, t' \in p^\bullet \Rightarrow Pre(p,t) = Pre(p,t')$;*
- Ordinary (ORD) *if $\forall p \in P$ and $\forall t \in T$, $Pre(p,t) \leq 1$ and $Post(p,t) \leq 1$;*
- Extended Simple (ES) *(sometimes also called* asymmetric choice*) if it is ORD and $\forall\, p, q \in P : p^\bullet \cap q^\bullet = \emptyset \vee p^\bullet \subseteq q^\bullet \vee q^\bullet \subseteq p^\bullet$;*
- Extended Free Choice (EFC) *if it is ORD and $\forall\, p, q \in P : p^\bullet \cap q^\bullet = \emptyset \vee p^\bullet = q^\bullet$.*

Definition 5 (DTP). *Let $\mathcal{N} = \langle P, T, \boldsymbol{Pre}, \boldsymbol{Post} \rangle$ be a Petri net.*

- *A* siphon *(structural deadlock, co-trap) is a non-empty set of places $D \subseteq P$ with $^\bullet D \subseteq D^\bullet$.*
- *A* trap *is a non-empty set of places $Q \subseteq P$ with $Q^\bullet \subseteq {}^\bullet Q$.*
- *A* minimal siphon (trap) *is a siphon (trap) not including a siphon (trap) as a proper subset.*
- *A* bad siphon *is a siphon, which does not include a trap.*

- *An* empty siphon (trap) *is a siphon (trap), not containing a token.*
- *The* Deadlock Trap Property (DTP) *asks for every siphon to include an initially marked trap, i.e., marked at* $\boldsymbol{m}_0$.

The DTP can be reformulated as: minimal siphons are not bad and the maximal traps included are initially marked.

Definition 6 (Semiflows). *Let* $\mathcal{N} = \langle P, T, \boldsymbol{Pre}, \boldsymbol{Post} \rangle$ *be a net.*

- *The* token flow matrix *(or* incidence matrix *if the net is pure, i.e., self-loop free) is a matrix* $\boldsymbol{C} = \boldsymbol{Post} - \boldsymbol{Pre}$.
- *A* place vector *is a vector* $\boldsymbol{y} \in \mathbb{Z}^{|P|}$*; a* transition vector *is a vector* $\boldsymbol{x} \in \mathbb{Z}^{|T|}$.
- *A* P-semiflow *is a place vector* $\boldsymbol{y}$ *with* $\boldsymbol{y} \cdot \boldsymbol{C} = \boldsymbol{0}$, $\boldsymbol{y} \geq \boldsymbol{0}$, $\boldsymbol{y} \neq \boldsymbol{0}$*;*
  a T-semiflow *is a transition vector* $\boldsymbol{x}$ *with* $\boldsymbol{C} \cdot \boldsymbol{x} = \boldsymbol{0}$, $\boldsymbol{x} \geq \boldsymbol{0}$, $\boldsymbol{x} \neq \boldsymbol{0}$.
- *The* support of a semiflow $\boldsymbol{x}$*, written as* $supp(\boldsymbol{x})$*, is the set of nodes corresponding to the non-zero entries of* $\boldsymbol{x}$.
- *A net is* conservative *if every place belongs to the support of a P-semiflow.*
- *A net is* consistent *if every transition belongs to the support of a T-semiflow.*
- *In a* minimal semiflow $\boldsymbol{x}$*,* $supp\,(\boldsymbol{x})$ *does not contain the support of any other semiflow* $\boldsymbol{z}$*, i.e.,* $\nexists$ *semiflow* $\boldsymbol{z} : supp\,(\boldsymbol{z}) \subset supp\,(\boldsymbol{x})$*, and the greatest common divisor of* $\boldsymbol{x}$ *is 1.*
- *A* mono-T-semiflow net *(MTS net) is a consistent and conservative net that has exactly one minimal T-semiflow.*

For convenience, we give vectors (markings, semiflows) in a short-hand notation by enumerating only the non-zero entries. Finally, we recall some well-known related propositions (see for example [Mur89], [Sta90]), which might be useful for the reasoning we pursue in this paper.

Proposition 1 (Basics).

1. *An empty siphon remains empty forever. A marked trap remains marked for ever.*
2. *If* R *and* R' *are siphons (traps), then* $R \cup R'$ *is also a siphon (trap).*
3. *A minimal siphon (trap) is a P-strongly-connected component, i.e., its places are strongly connected.*
4. *A deadlocked Petri net system has an empty siphon.*
5. *Each siphon of a live net system is initially marked.*
6. *If there is a bad siphon, the DTP does not hold.*
7. *A source place* p *establishes a bad siphon* $D = \{p\}$ *on its own, and a sink place* q *a trap* $Q = \{q\}$.
8. *If each transition has a pre-place, then* $P^\bullet = T$*, and if each transition has a post-place, then* ${}^\bullet P = T$*. Thus, in a net without boundary transitions, the whole set of places is a siphon as well as a trap (however, not necessarily minimal ones).*
9. *For a P-semiflow* $\boldsymbol{x}$ *it holds* ${}^\bullet supp(\boldsymbol{x}) = supp(\boldsymbol{x})^\bullet$*. Thus, the support of a P-semiflow is siphon and trap as well (however, generally not vice versa).*

Proposition 2 (DTP and behavioural properties).

1. *An ordinary Petri net without siphons is live.*
2. *If $\mathcal{N}$ is ordinary and the DTP holds for $\boldsymbol{m}_0$, then $\langle \mathcal{N}, \boldsymbol{m}_0 \rangle$ is deadlock-free.*
3. *If $\mathcal{N}$ is ES and the DTP holds for $\boldsymbol{m}_0$, then $\langle \mathcal{N}, \boldsymbol{m}_0 \rangle$ is live.*
4. *Let $\mathcal{N}$ be an EFC net. $\langle \mathcal{N}, \boldsymbol{m}_0 \rangle$ is live iff the DTP holds.*

We conclude this section with a proposition from [CCS91], which might be less known.

Proposition 3 (MTS net and behavioural properties). *Liveness and deadlock-freeness coincide in mono-T-semiflow net systems.*

3 Monotonic Liveness

If a property holds for a Petri net $\mathcal{N}$ with the marking $\boldsymbol{m}_0$, and it also holds in $\mathcal{N}$ for any $\boldsymbol{m} \geq \boldsymbol{m}_0$, then it is said to be *monotonic* in the system $\langle \mathcal{N}, \boldsymbol{m}_0 \rangle$. In this paper we are especially interested in monotonic liveness.

Definition 7 (Monotonic liveness).
Let $\langle \mathcal{N}, \boldsymbol{m}_0 \rangle$ be a Petri net system. It is called monotonically live, if being live for $\boldsymbol{m}_0$, it remains live for any $\boldsymbol{m} \geq \boldsymbol{m}_0$.

We are looking for conditions, at best structural conditions, preserving liveness under arbitrary marking increase. To illustrate the problem, let's consider a classical example [Sta90], [SR02].

Example 1. The net $\mathcal{N}$ in Figure 1 is ES, conservative, consistent, and covered by one T-semiflow. It is live for the given initial marking $\boldsymbol{m}_1 = (2p_1, p_4)$. Adding a token to place p_5 yields the initial marking $\boldsymbol{m}_2 = (2p_1, p_4, p_5)$ and the net system remains live for $\boldsymbol{m}_2 \geq \boldsymbol{m}_1$. However, adding a token to p_4 yields the initial marking $\boldsymbol{m}_3 = (2p_1, 2p_4)$ and the net behaviour now contains finite firing sequences, i.e., it can run into a deadlock (dead state). Thus, the net system is not live for $\boldsymbol{m}_3 \geq \boldsymbol{m}_1$. It is not monotonically live.

How to distinguish both cases? The net has two (minimal) bad siphons $D_1 = \{p_1, p_2\}$ and $D_2 = \{p_1, p_3\}$. There is no chance to prevent these siphons from getting empty for arbitrary markings. D_1 can potentially be emptied by firing $t_2 \in D_1{}^\bullet \setminus {}^\bullet D_1$, and D_2 by firing $t_1 \in D_2{}^\bullet \setminus {}^\bullet D_2$. The latter case destroyed the liveness for $\boldsymbol{m}_3$ as it will equally occur for all initial markings allowing transition sequences containing one of the troublemakers, in this example t_1 and t_2, sufficiently often. □

One lesson learnt from the previous example is, a net does not have to make use of the additional tokens. Thus, all behaviour (set of transition sequences), which is possible for $\boldsymbol{m}$ is still possible for $\boldsymbol{m}'$, with $\boldsymbol{m} \leq \boldsymbol{m}'$. However, new tokens may allow for additional system behaviour, which is actually well-known in Petri net theory, see Proposition 4.

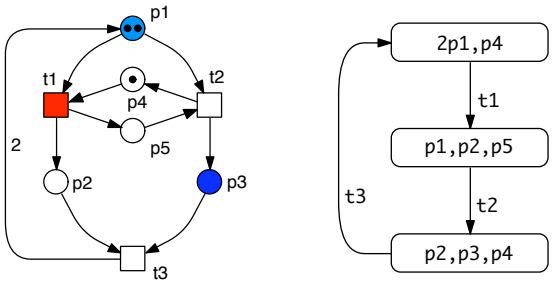

Fig. 1. A mono-T-semiflow and ES Petri net $\mathcal{N}$ and its reachability graph for the marking $\boldsymbol{m}_1 = (2p_1, p_4)$, generating the language $\mathcal{L}_{\mathcal{N}}(\boldsymbol{m}_1) = (t_1t_2t_3)^*\{\varepsilon, t_1, t_1t_2\}$. The siphon $\{p_1, p_3\}$ does not contain a trap, i.e., it is a bad siphon. If the initial marking is increased, it can potentially become empty by firing of t_1.

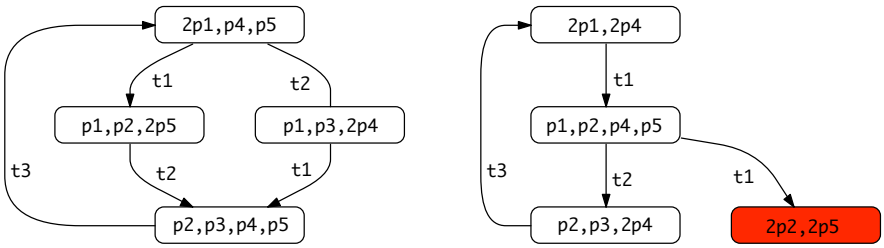

Fig. 2. Two other reachability graphs for the net $\mathcal{N}$ in Figure 1 for the initial markings $\boldsymbol{m}_2 = (2p_1, p_4, p_5)$ and $\boldsymbol{m}_3 = (2p_1, 2p_4)$; both are greater than $\boldsymbol{m}_1$. Obviously, $\mathcal{L}_{\mathcal{N}}(\boldsymbol{m}_1) \subset \mathcal{L}_{\mathcal{N}}(\boldsymbol{m}_2)$, $\mathcal{L}_{\mathcal{N}}(\boldsymbol{m}_1) \subset \mathcal{L}_{\mathcal{N}}(\boldsymbol{m}_3)$, but $\langle \mathcal{N}, \boldsymbol{m}_3 \rangle$ is not live while $\langle \mathcal{N}, \boldsymbol{m}_1 \rangle$ is live.

Proposition 4. *For any net $\mathcal{N}$ and two markings $\boldsymbol{m}$ and $\boldsymbol{m}'$, with $\boldsymbol{m} \leq \boldsymbol{m}'$, it holds $\mathcal{L}_{\mathcal{N}}(\boldsymbol{m}) \subseteq \mathcal{L}_{\mathcal{N}}(\boldsymbol{m}')$ [BRA83]; nevertheless, $\langle \mathcal{N}, \boldsymbol{m} \rangle$ may be live while $\langle \mathcal{N}, \boldsymbol{m}' \rangle$ not.*

Example 1 is a mono-T-semiflow net, i.e., a net, where liveness and deadlock-freeness coincide (see Proposition 3). We look briefly at Example 2 to understand that this does not generally hold if there are several T-semiflows breathing life into the net.

Example 2. The net $\mathcal{N}$ in Figure 3 is a slight extension of Example 1. It is ES, conservative, consistent and covered by two T-semiflows: $\boldsymbol{x}_1 = (t_1, t_2, t_3), \boldsymbol{x}_2 = (t_4, t_5)$. It is live for the initial marking $\boldsymbol{m}_1 = (2p_1, p_4)$.

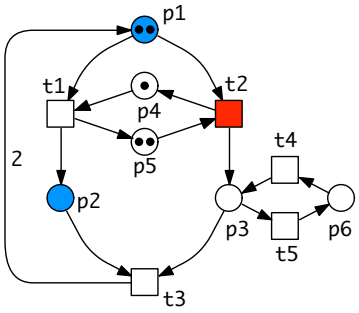

Fig. 3. An ES Petri net which is not mono-T-semiflow. It is live for the initial marking $\boldsymbol{m}_1 = (2p_1, p_4)$. The siphon $\{p_1, p_2\}$ is bad. So it can potentially become empty by firing t_2 sufficiently often. This happens for the initial marking $\boldsymbol{m}_2 = (2p_1, p_4, 2p_5)$, making the net non-live, however keeping it deadlock-free (observe that $\{p_3, p_6\}$ behaves as a trap if the firing of t_3 is blocked forever).

The net has the following minimal siphons $D_1 = \{p_1, p_2\}$, $D_2 = \{p_1, p_3, p_6\}$, and $D_3 = \{p_4, p_5\}$; the first two are bad siphons. With the initial marking $\boldsymbol{m}_2 = (2p_1, p_4, 2p_5)$, D_1 can become empty by firing twice $t_2 \in D_1{}^\bullet \setminus {}^\bullet D_1$, which destroys the liveness, without causing a dead state. The transitions t_4, t_5 are live, the others not. Thus, the net system is not live, but deadlock-free. □

The loss of liveness is not necessarily monotonic itself; i.e., a net may be live for $\boldsymbol{m}_1$, non-live for a marking $\boldsymbol{m}_2$ with $\boldsymbol{m}_2 \geq \boldsymbol{m}_1$, and live again for a marking $\boldsymbol{m}_3$ with $\boldsymbol{m}_3 \geq \boldsymbol{m}_2$ (which works for all examples in this paper). Liveness may also be lost by marking multiples (*homothetic markings*). Examples 1 and 2 are homothetically live, Example 3 in Section 5 not.

4 Monotonic Liveness of Ordinary Nets

Let us turn to liveness criteria suitable for our objective looking at *ordinary* nets first. Liveness criteria not relying on the marking obviously ensure monotonic liveness. Unfortunately, there are only a few.

First of all, there are some structural reduction rules, see, e.g., [Sil85], [Ber86], [Mur89], [SR99]. To give a sample, the following reduction rule is easy to accept: a source transition is live, and all its post-places are unbounded. The transition and its post-places can be deleted (for analysis purposes); the reduction can be iterated as many times it is applicable. Sometimes, this kind of reasoning allows to decide liveness (for examples, see Section 6).

Besides structural reduction we have the DTP, which in most cases does depend on the marking, but it is obviously monotonic w.r.t. the marking: if each siphon contains a marked trap at $\boldsymbol{m}$, then – of course – it contains a marked

trap at $\boldsymbol{m}' \geq \boldsymbol{m}$. Thus, the DTP-related conclusions on behavioural properties in Proposition 2 are monotonic as well:

Proposition 5 (Monotonic DTP).

1. *An ordinary net without siphons is monotonically live.*
2. *An ordinary net system which holds the DTP is monotonically deadlock-free.*
3. *A live ES net system which holds the DTP is monotonically live.*
4. *An EFC net system is monotonically live iff the DTP holds.*

Proposition 5.1 can be considered as a special case of the DTP. Then, there must be source transitions (see Proposition 1.8), and the net is not strongly connected and not bounded.

Lemma 1. *Let be $\mathcal{N}$ an ordinary Petri net. If $\mathcal{N}$ is monotonically live, then there are no bad siphons.*

Proof. We will prove its reverse – if there exist a bad siphon, then the net system is not monotonically live – by contradiction. Let P_S be a bad siphon. Then there exist troublemaking transitions $\Theta_i \in P_S{}^\bullet \setminus {}^\bullet P_S$. There must be such transitions, because otherwise $P_S{}^\bullet = {}^\bullet P_S$, and then the siphon P_S would be a trap as well.

Since the net system is monotonically live, the marking of the places $P \setminus P_S$ can be increased in such a way that it will never restrict the firing of the transitions $P_S{}^\bullet$, i.e., the transitions depending on the siphon. Therefore, we can consider the subnet restricted to P_S in isolation.

We will show that the subsystem restricted to P_S can be emptied eventually by increasing the marking, hence cannot be monotonically live. Obviously we can assume that P_S is a minimal siphon. We consider two cases.

(1) The siphon has no forks (t_j is a *fork* if $|t_j{}^\bullet| > 1$). Based on the P-strongly-conectedness (see Proposition 1.3), there exists at least one path from each place $p \in P_S$ to one of the troublemakers Θ_i. Moving a token from p to ${}^\bullet\Theta_i$ does not increase the marking of any other place of P_S not belonging to the considered path. Obviously, this path can contain joins (t_j is a *join* if $|{}^\bullet t| > 1$), but we can add any tokens that are missing in the input places of the join. Firing the join, the marking of the places in the siphon is not increased. Using this process we can move the tokens from any $p \in P_S$ to some ${}^\bullet\Theta_i$, and by firing Θ_i when it is enabled, P_S can be emptied. Thus, the net system can not be monotonically live.

(2) On the contrary, let us assume that there exists at least one fork t_j and let $p_1, p_2 \in t_j{}^\bullet$ be its output places. For the same reason as discussed in case (1), there exists a directed path from both places to one or several troublemakers. If all paths from p_1 to any troublemaker Θ_i contain t_j, then they form a trap. This is impossible because siphons are assumed to be bad. By symmetry, in the case in which the paths from p_2 to troublemakers contain t_j, there exists a trap as well.

Finally, let us assume that there exists a path from p_1 to a troublemaker Θ_i and one path from p_2 to a troublemakers Θ_k, none of them containing t_j.

On both paths the same kind of reasoning can be applied (in an iterative way if several forks appear). Therefore, the siphon can be emptied even if firing t_j increases the tokens in P_S. □

Lemma 1 helps to preclude monotonic liveness for Examples 1 and 2 as well as for all other non-monotonically live examples we are aware of.

Theorem 1. *Let be $\mathcal{N}$ an ordinary Petri net. If $\langle \mathcal{N}, \boldsymbol{m}_0 \rangle$ is monotonically live, then the DTP holds.*

Proof. The structural check of the DTP can have three possible outcomes.

1. If there are no siphons, then the DTP holds trivially and the net is monotonically live (see Proposition 5.1).
2. If there are bad siphons, then the DTP does not hold for any initial marking and the net is not monotonically live (see Lemma 1).
3. If each siphon includes a trap, then the *maximal* trap P_T in every minimal siphon P_S has to be initially marked to fulfill the DTP. Because we assume liveness of the net system, there has to be at least one token in each minimal siphon (see Proposition 1.5). Let us assume that a token is not in P_T, but in a place $p \in P_S \setminus P_T$. If there exists at least one path without forks from p to a troublemaking transition $\Theta_i \in P_S{}^\bullet \setminus {}^\bullet P_S$ not containing any transition belonging to the trap, ${}^\bullet P_T$, then p can be emptied using the same reasoning as used in the proof of in Lemma 1, case (1). Therefore the net can not be live. If the path from p to a troublemaking transition $\Theta_i \in P_S{}^\bullet \setminus {}^\bullet P_S$ contains a fork, then the output places of the fork will be marked when p is emptied, and the paths from the output places of the forks to the output should be considered separately.
   Finally, if *all* paths from p to the troublemaking transitions contain at least one transition ${}^\bullet P_T$, then the trap P_T is not maximal since P_T together with all places belonging to the above mentioned paths (including all non-minimal ones) from p to transitions ${}^\bullet P_T$ are also a trap. □

According to Theorem 1, the DTP establishes a necessary condition for monotonic liveness, which complements Proposition 5.3.

Corollary 1. *A live ES net system is monotonically live iff the DTP holds.*

Moreover, for those systems for which deadlock-freeness is equivalent to liveness, the DTP is a sufficient criteria for liveness monotonicity. This leads, for example, to the following theorem:

Theorem 2. *Let be $\mathcal{N}$ an ordinary mono-T-semiflow Petri net which for $\boldsymbol{m}_0$ fulfills the DTP. Then the system $\langle \mathcal{N}, \boldsymbol{m} \rangle$ is live for any $\boldsymbol{m} \geq \boldsymbol{m}_0$.*

Proof. It follows from Proposition 5.2 (DTP and deadlock-freeness monotonicity) and Proposition 3 (equivalence of liveness and deadlock freeness in

mono-T-semiflow net systems). □

Therefore, the DTP is a sufficient criterion for monotonic liveness of ordinary mono-T-semiflow net systems as well. In summary, while the DTP is in general neither necessary nor sufficient for liveness, it turns out to be the case to keep alive ordinary ES nets or ordinary mono-T-semiflow nets under any marking increase.

5 Monotonic Liveness of Non-ordinary Nets

It is well-known that non-ordinary nets can be simulated under interleaving semantics by ordinary ones [Sil85] (see Figure 4 for an example). Let us look on the net structures we get by this simulation to learn how far the results for ordinary nets of Section 4 can be uplifted to non-ordinary nets.

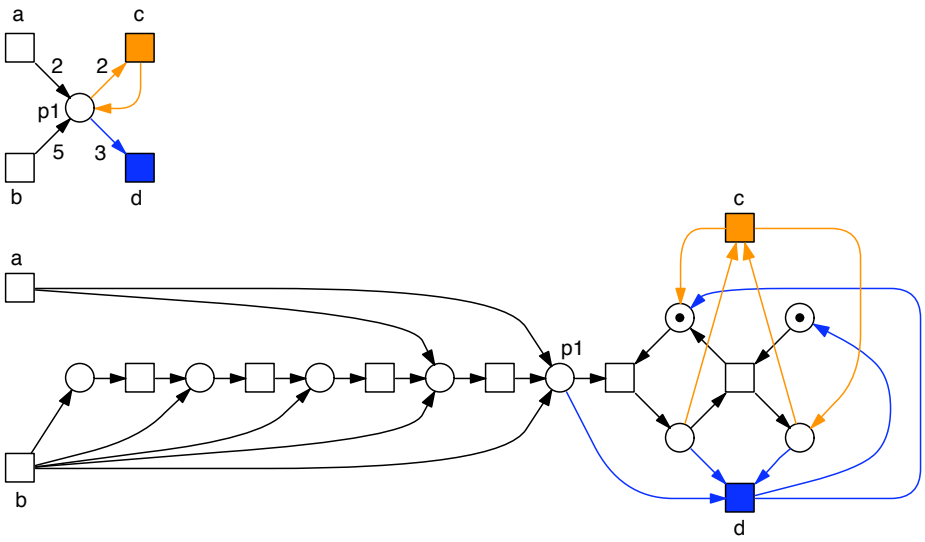

Fig. 4. A general principle to *simulate* a non-ordinary net system by an ordinary net system (here, the firing language of the second net projected on $\{a, b, c, d\}$ is always equal to that of the first) [Sil85].

Example 3. We take a non-ordinary net from [SR02] and consider its simulation by an ordinary net, which we construct according to the general principle demonstrated in Figure 4.

The two net systems in Figure 5 are conservative, consistent, and live for the given initial marking. The ordinary net on the right hand side is not ES, and it

has two minimal bad siphons $\{q_1, p_1, p_{1b}, p_{1c}\}$, $\{p_2, p_1, p_{1b}, p_{1c}\}$. Thus, according to Lemma 1, it is not monotonically live. Because our simulation preserves the projection of the firing language, in particular, preserves monotonicity of liveness. Thus, we conclude that the model on the left hand side is not monotonically live. Indeed, both nets are not live for any initial marking with an even number of tokens in p_1, but live for infinitely many other markings greater than or equal to $(1, 1)$. □

As a consequence of firing simulation by the ordinary net systems of the non-ordinary ones (preserving always the markings of the places involved in the head of the tail and complement, here q_1 and q_{1co}), liveness monotonicity can be studied on the ordinary simulation.

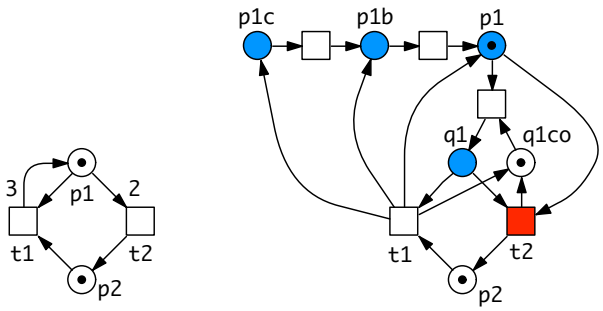

Fig. 5. A non-ordinary Petri net system and its simulation by an ordinary one. Both systems are non-live for any initial marking with an even number of tokens in p_1, and live for any other odd marking. Note that the markings of q_1 and q_{1co} should not be increased in order to keep the language simulation in the right hand model. The net system on the right has a bad siphon $\{q_1, p_1, p_{1b}, p_{1c}\}$ that can potentially become empty by firing t_2 sufficiently often.

6 Applications

We consider a variety of test cases of our benchmark repository to demonstrate the helpfulness of the DTP for biomolecular networks. The following list sketches some basic characteristics. The essential analysis results are summarized in Table 1. All models hold the DTP, they are consistent and (supposed to be) live. For non-ordinary nets, the DTP refers to its simulation by an ordinary one.

1. **Apoptosis** (size: 37 places, 45 transitions, 89 arcs) is a signal transduction network, which governs complex mechanisms to control and execute genetically programmed cell death in mammalian cells. Disturbances in the apoptotic processes may lead to various diseases. This essential part of normal physiology for most metazoan species is not really well understood; thus

there exist many model versions. The validation by Petri net invariants of the model considered here is discussed in [HKW04], [HK04].

2. **RKIP** (size: 11 places, 11 transitions, 14 arcs) models the core of the influence of the Raf-1 Kinase Inhibitor Protein (RKIP) on the Extracellular signal Regulated Kinase (ERK) signalling pathway. It is one of the standard examples used in the systems biology community. It has been introduced in [CSK+03]; the corresponding qualitative, stochastic, continuous Petri nets are scrutinized in [GH06], [HDG10].
3. **Biosensor** (size: 6 places, 10 transitions, 21 arcs) is a gene expression network extended by metabolic activity. The model is a general template of a biosensor, which can be instantiated to be adapted to specic pollutants. It is considered as qualitative, stochastic, and continuous Petri net in [GHR+08] to demonstrate a model-driven design of a self-powering electrochemical biosensor.
4. **Hypoxia** (size: 14 places, 19 transitions, 56 arcs) is one of the well-studied molecular pathways activated under hypoxia condition. It models the Hypoxia Induced Factor (HIF) pathway responsible for regulating oxygen-sensitive gene expression. The version considered here is discussed in [YWS+07]; the corresponding qualitative and continuous Petri nets are used in [HS10] to determine the core network.
5. **Lac operon** (size: 11 places, 17 transitions, 41 arcs) is a classical example of prokaryotic gene regulation. We re-use the simplified model discussed in [Wil06]. Its corresponding stochastic Petri net is considered in [HLGM09].
6. **G/PPP** (size: 26 places, 32 transitions, 76 arcs) is a simplified model of the combined glycolysis (G) and pentose phosphate pathway (PPP) in erythrocytes (red blood cells). It belongs to the classical examples of biochemistry textbooks, see e.g. [BTS02], and thus of systems biology as well. The model was first discussed using Petri net technologies in [Red94]. Its validation by Petri net invariants is shown in [HK04], and a more exhaustive qualitative analysis in [KH08].
7. **MAPK** (size: 22 places, 30 transitions, 90 arcs) models the signalling pathway of the mitogen-activated protein kinase cascade, published in [LBS00]. It is a three-stage double phosphorylation cascade; each phosphorylation/dephosphorylation step applies the mass action kinetics pattern. The corresponding qualitative, stochastic, and continuous Petri net are scrutinized in [GHL07], [HGD08].
8. **CC – Circadian clock** (size: 14 places, 16 transitions, 58 arcs) refers to the central time signals of a roughly 24-hour cycle in living entities. Circadian rhythms are used by a wide range of organisms to anticipate daily changes in the environment. The model published in [BL00] demonstrates that circadian network can oscillate reliably in the presence of stochastic biomolecular noise and when cellular conditions are altered. It is also available as PRISM model on the PRISM website (http://www.prismmodelchecker.org). Its corresponding stochastic Petri net belongs to the benchmark suite used in [SH09]. We consider here a version with inhibitor arcs modelled by co-places.

9. **Halo** (size: 37 places, 38 transitions, 138 arcs) is a cellular signaling and regulation network, describing the phototaxis in the halobacterium salinarum [NMOG03]. It models the sophisticated survival strategy, which the halobacterium developed for harsh conditions (high temperature, high salt). A light sensing system and flagellar motor switching allows the cells to swim to those places of their habitat where the best light conditions are available. The model is the result of prolonged investigations by experimentally working scientists [Mar10].
10. **Pheromone** (size: 42 places, 48 transitions, 119 arcs) is a signal transduction network of the well understood mating pheromone response pathway in *Saccharomyces cerevisiae*. The qualitative Petri net in [SHK06] extends a former ODE model [KK04]. The Petri net was validated by Petri net invariants and a partitioning of the transition set.
11. **Potato** (size: 17 places, 25 transitions, 78 arcs) describes the main carbon metabolism, the sucrose-to-starch breakdown in Solanum tuberosum (potato) tubers. The qualitative Petri net model was developed in cooperation with experimentally working scientists, experienced in ODE modelling. Its validation by Petri net invariants is discussed in [HK04], and a more detailed pathway exploration in [KJH05].

Table 1. Some biomolecular case studies; all of them hold the DTP, are consistent and live.

#	case study	multiplicities	net class	bounded	liveness shown by
1	apoptosis	ORD	ES	no	Proposition 2.1
2	RKIP	ORD	ES	yes	Proposition 2.3
3	biosensor	ORD	ES	no	Proposition 2.3
4	hypoxia	ORD	not ES	no	structural reduction
5	lac operon	HOM	not ES	no	structural reduction
6	G/PPP	HOM	not ES	no	structural reduction
7	MAPK	ORD	not ES	yes	dynamic analysis (RG)
8	CC	HOM	not ES	yes	dynamic analysis (RG)
9	halo	not HOM	not ES	yes	dynamic analysis (RG)
10	pheromone	HOM	not ES	no	by reasoning
11	potato	not HOM	not ES	no	by reasoning

Contrary, the model of signal transduction events involved in the angiogenesis processes, which is discussed in [NMC$^+$09] as a stochastic and continuous Petri net model (size: 39 places, 64 transitions, 185 arcs) is to a large extent covered by a (non-minimal) bad siphon. Thus, even if the net is live for a certain marking $\boldsymbol{m}$, there is always a larger marking $\boldsymbol{m'}$, which will allow to remove all tokens from the bad siphon. Consequently, an arbitrary marking increase will not preserve liveness.

7 Tools

The Petri nets for the case studies have been constructed using Snoopy [RMH10], a tool to design and animate or simulate hierarchical graphs, among them qualitative, stochastic and continuous Petri nets as used in the case studies in Section 6. Snoopy provides export to various analysis tools as well as import and export of the Systems Biology Markup Language (SBML).

The qualitative analyses have been made with the Petri net analysis tool Charlie [Fra09], complemented by the structural reduction rules supported by the Integrated Net Analyser INA [SR99].

8 Conclusions

We have discussed the problem of monotonic liveness, with one of the motivations originating from bio-model engineering. We have presented a new result showing the necessity of the DTP for monotonic liveness.

Moreover, we immediately know – thanks to the well-known propositions of the DTP – that ordinary ES nets are monotonically iff the DTP holds. Furthermore, we know – because the DTP monotonically ensures deadlock freeness – that for any net class, in which liveness and deadlock freeness coincide, monotonic liveness is characterized by the DTP. We have shown one instance for this case: the mono-T-semiflow nets (MTS).

We have demonstrated the usefulness of our results by applying them to a variety of biomolecular networks.

One of the remaining open issues is: what are sufficient conditions for monotonic liveness for more general net structures? While none of our test cases is an MTS net, this line might be worth being explored more carefully, e.g. by looking at FRT nets (Freely Related T-Semiflows) [CS92] and extensions.

Acknowledgements. This work has been partially supported by CICYT - FEDER grant DPI2006-15390 and by the European Community's Seventh Framework Programme under project DISC (Grant Agreement n. INFSO-ICT-224498). The work of M. Heiner was supported in part by the grant DPI2006-15390 for a stay with the Group of Discrete Event Systems Engineering (GISED); the main ideas of this paper have been conceived during this period.

References

Ber86. G. Berthelot. Checking properties of nets using transformations. In G. Rozenberg, editor, *Advances in Petri Nets 1985*, volume 222 of *Lecture Notes in Computer Science*, pages 19–40. Springer, 1986.

BL00. N. Barkai and S. Leibler. Biological rhythms: Circadian clocks limited by noise. *Nature*, 403(6767):267–268, 2000.

BRA83. G. W. BRAMS. Reseaux de Petri. Theorie et pratique (2 tomes). *Masson*, 1983.

BTS02. J.M. Berg, J.L. Tymoczko, and L. Stryer. *Biochemistry, 5th ed.* WH Freeman and Company, New York, 2002.

CCS91. J. Campos, G. Chiola, and M. Silva. Ergodicity and Throughput Bounds of Petri Nets with Unique Consistent Firing Count Vector. *IEEE Transactions on Software Engineering*, 17:117–125, 1991.

CS92. J. Campos and M. Silva. Structural techniques and performance bounds of stochastic Petri net models. In *Advances in Petri Nets 1992, volume 609 of Lecture Notes in Computer Science*, pages 352–391. Springer-Verlag, 1992.

CSK+03. K.-H. Cho, S.-Y. Shin, H.-W. Kim, O. Wolkenhauer, B. McFerran, and W. Kolch. Mathematical modeling of the influence of RKIP on the ERK signaling pathway. In *Proc. CMSB*, pages 127–141. Springer, LNCS 2602, 2003.

DA10. R. David and H. Alla. *Discrete, Continuous, and Hybrid Petri Nets.* Springer, 2010.

DHP+93. F. DiCesare, G. Harhalakis, J.M. Proth, M. Silva, and F.B. Vernadat. *Practice of Petri nets in manufacturing.* Chapman & Hall, 1993.

Fra09. A. Franzke. *Charlie 2.0 - a multi-threaded Petri net analyzer.* Diploma Thesis, Brandenburg University of Technology at Cottbus, CS Dep., 2009.

GH06. D. Gilbert and M. Heiner. From Petri nets to differential equations - an integrative approach for biochemical network analysis. In *Proc. ICATPN 2006*, pages 181–200. LNCS 4024, Springer, 2006.

GHL07. D. Gilbert, M. Heiner, and S. Lehrack. A unifying framework for modelling and analysing biochemical pathways using Petri nets. In *Proc. CMSB*, pages 200–216. LNCS/LNBI 4695, Springer, 2007.

GHR+08. D. Gilbert, M. Heiner, S. Rosser, R. Fulton, Xu Gu, and M. Trybiło. A Case Study in Model-driven Synthetic Biology. In *Proc. 2nd IFIP Conference on Biologically Inspired Collaborative Computing (BICC), IFIP WCC 2008, Milano*, pages 163–175, 2008.

HDG10. M. Heiner, R. Donaldson, and D. Gilbert. *Petri Nets for Systems Biology, in Iyengar, M.S. (ed.), Symbolic Systems Biology: Theory and Methods.* Jones and Bartlett Publishers, Inc., in Press, 2010.

HGD08. M. Heiner, D. Gilbert, and R. Donaldson. Petri nets in systems and synthetic biology. In *Schools on Formal Methods (SFM)*, pages 215–264. LNCS 5016, Springer, 2008.

HK04. M. Heiner and I. Koch. Petri Net Based Model Validation in Systems Biology. In *Proc. ICATPN, LNCS 3099*, pages 216–237. Springer, 2004.

HKW04. M. Heiner, I. Koch, and J. Will. Model Validation of Biological Pathways Using Petri Nets - Demonstrated for Apoptosis. *BioSystems*, 75:15–28, 2004.

HLGM09. M. Heiner, S. Lehrack, D. Gilbert, and W. Marwan. Extended Stochastic Petri Nets for Model-Based Design of Wetlab Experiments. *Transactions on Computational Systems Biology XI*, pages 138–163, 2009.

HS10. M. Heiner and K. Sriram. Structural analysis to determine the core of hypoxia response network. *PLoS ONE*, 5(1):e8600, 01 2010.

KH08. I. Koch and M. Heiner. *Petri Nets, in B.H. Junker and F. Schreiber (eds.), Biological Network Analysis*, chapter 7, pages 139–179. Wiley Book Series on Bioinformatics, 2008.

KJH05. I. Koch, B.H. Junker, and M. Heiner. Application of Petri Net Theory for Modeling and Validation of the Sucrose Breakdown Pathway in the Potato Tuber. *Bioinformatics*, 21(7):1219–1226, 2005.

KK04. B. Kofahl and E. Klipp. Modelling the dynamics of the yeast pheromone pathway. *Yeast*, 21(10):831–850, 2004.

LBS00. A. Levchenko, J. Bruck, and P.W. Sternberg. Scaffold proteins may biphasically affect the levels of mitogen-activated protein kinase signaling and reduce its threshold properties. *Proc Natl Acad Sci USA*, 97(11):5818–5823, 2000.

Mar10. W. Marwan. Phototaxis in halo bacterium as a case study for extended stochastic Petri nets. *Private Communication*, 2010.

Mur89. T. Murata. Petri Nets: Properties, Analysis and Applications. *Proc.of the IEEE 77*, 4:541–580, 1989.

NMC+09. L Napione, D Manini, F Cordero, A Horvath, A Picco, M De Pierro, S Pavan, M Sereno, A Veglio, F Bussolino, and G Balbo. On the Use of Stochastic Petri Nets in the Analysis of Signal Transduction Pathways for Angiogenesis Process. In *Proc. CMSB*, pages 281–295. Springer, LNCS/LNBI 5688, 2009.

NMOG03. T. Nutsch, W. Marwan, D. Oesterhelt, and E.D. Gilles. Signal processing and flagellar motor switching during phototaxis of Halobacterium salinarum. *Genome research*, 13(11):2406–2412, 2003.

Red94. V. N. Reddy. Modeling Biological Pathways: A Discrete Event Systems Approch. Master thesis, University of Maryland, 1994.

RMH10. C. Rohr, W. Marwan, and M. Heiner. Snoopy - a unifying Petri net framework to investigate biomolecular networks. *Bioinformatics*, 26(7):974–975, 2010.

RTS98. L. Recalde, E. Teruel, and M. Silva. On linear algebraic techniques for liveness analysis of P/T systems. *Journal of Circuits, Systems, and Computers*, 8(1):223–265, 1998.

RTS99. L. Recalde, E. Teruel, and M. Silva. Autonomous continuous P/T systems. In *Proc. ICATPN*, pages 107–126. Springer, LNCS 1689, 1999.

SH09. M. Schwarick and M. Heiner. CSL model checking of biochemical networks with Interval Decision Diagrams. In *Proc. CMSB*, pages 296–312. Springer, LNCS/LNBI 5688, 2009.

SHK06. A. Sackmann, M. Heiner, and I. Koch. Application of Petri Net Based Analysis Techniques to Signal Transduction Pathways. *BMC Bioinformatics*, 7:482, 2006.

Sil85. M. Silva. *Las Redes de Petri: en la Automática y la Informática*. Editorial AC, 1985.

SR99. P.H. Starke and S. Roch. *INA - The Intergrated Net Analyzer*. Humboldt University Berlin, www.informatik.hu-berlin.de/∼starke/ina.html, 1999.

SR02. M. Silva and L. Recalde. Petri nets and integrality relaxations: A view of continuous Petri net models. *IEEE Transactions on Systems, Man, and Cybernetics, Part C: Applications and Reviews*, 32(4):314–327, 2002.

Sta90. P.H. Starke. *Analysis of Petri Net Models (in German)*. B. G. Teubner, Stuttgart, Stuttgart, 1990.

TS96. E. Teruel and M. Silva. Structure theory of equal conflict systems. *Theoretical Computer Science*, 153:271–300, 1996.

Wil06. D.J. Wilkinson. *Stochastic Modelling for System Biology*. CRC Press, New York, 1st Edition, 2006.

YWS+07. Y. Yu, G. Wang, R. Simha, W. Peng, F. Turano, and C. Zeng. Pathway switching explains the sharp response characteristic of hypoxia response network. *PLoS Comput Biol*, 3(8):e171, 2007.

Modelling Gradients Using Petri Nets

Laura M.F. Bertens[1], Jetty Kleijn[2], Maciej Koutny[3], and Fons J. Verbeek[1]

[1] Imaging and Bioinformatics group, LIACS, Leiden University
Leiden, 2300 RA The Netherlands
lbertens@liacs.nl, fverbeek@liacs.nl
[2] LIACS, Leiden University
Leiden, 2300 RA The Netherlands
kleijn@liacs.nl
[3] School of Computing Science, Newcastle University
Newcastle upon Tyne, United Kingdom
maciej.koutny@ncl.ac.uk

Abstract. Motivated by the graded posteriorization during the AP axis development in the frog *Xenopus laevis*, we propose an abstract Petri net model for the formation of a gradient of proteins in a chain of cells.

Keywords: gradient formation, planar signalling, Petri net model

1 Introduction

Petri nets have been shown to be very promising for molecular and cellular biology, in particular for metabolic, signalling and gene-regulatory networks (see e.g. [1, 2, 6, 9, 10, 14, 20, 30, 31]). In this paper we propose Petri nets as an abstract modelling tool for higher level developmental processes in the organism, e.g., on tissue and organ level, taking cells as central elements.

Currently, we are working on a case study: the embryonic development of the anterior-posterior i.e., head-to-tail axis (AP axis) in the model organism *Xenopus laevis*, the African clawed frog. The development of this model embryo has been studied thoroughly and a huge amount of literature is available to draw from when building and validating the model, see references in [3, 15]. Moreover, this case study comprises several different subprocesses, found in many biological processes, that require modelling solutions. The aim of our project is to eventually model the entire process of AP axis development. Hence we envisage a final model consisting of several building blocks, most of which describing generic biological processes. Each of the subprocesses poses modelling challenges which, when solved, may lead to templates for similar developmental processes, incorporating multiple levels of both spatial and temporal information, also in other organisms. Petri nets are particularly useful in modelling such biological processes, due to their intuitive graphical component, which resembles biological diagrams, and their ability to model concurrency. Our case study appears to be very well suited to explore new ways in which Petri nets can be applied to developmental biology.

In this paper we present a fundamental approach to modelling a particular subprocess: the *formation of a morphogen gradient*, which helps instigate the differentiation of the cells along the developing axis. This subprocess is a good starting point, since it is relatively simple conceptually, in comparison to the other subprocesses in the case study. In early development, gradients are crucial ([36]) and finding a modelling solution for the generic process of gradient formation will not only serve the modelling of this case study, but will also be useful for the modelling of other developmental processes. By staying very close to the biological sequence of events in gradient formation, rather than focusing on a concrete outcome, the model should be generally applicable and robust.

Throughout this paper the emphasis will be on abstraction and modelling decisions, as opposed to implementation of specific biological data; we present a basic Petri net modelling gradient formation, which serves as a proof of concept for our approach. In the remainder of this paper we outline the biological background of gradient formation in general and in this particular case study. Subsequently we describe our modelling decisions and we present the model. In the last section the possibilities of the model and future work are discussed.

2 PT-nets with activator arcs

For a general introduction to Petri nets we refer to [27]. In this paper, we use PT-nets with activator arcs ([17]), and a maximally concurrent execution rule [5].

Petri nets are defined by an underlying structure consisting of *places* and *transitions*. These basic elements are connected by directed, *weighted arcs*. In the Petri net model considered in this paper, there are moreover *activator arcs* connecting places to transitions. In modelling, places are usually the passive elements, representing local states, and transitions the active elements. Here, global states, referred to as *markings*, are defined as mappings assigning to each place a natural number (of *tokens* corresponding to available resources).

A *PTA-net*, is a tuple $N = (P, T, W, Act, m_0)$ such that:

- P and T are finite disjoint sets, of the *places* and *transitions* of N, resp.
- $W : (T \times P) \cup (P \times T) \to \mathbb{N}$ is the *weight function* of N.
- $Act \subseteq P \times T$ is the set of *activator* arcs of N.
- $m_0 : P \to \mathbb{N}$ is the *initial marking* of N.

In diagrams, places are drawn as circles, and transitions as boxes. Activator arcs are indicated by black-dot arrowheads. If $W(x, y) \geq 1$, then (x, y) is an *arc* leading from x to y; it is annotated with its weight if this is greater than one. A marking m is represented by drawing in each place p exactly $m(p)$ tokens as small black dots. We assume that each transition t has at least one input place (there is at least one place p such that $W(p, t) \geq 1$).

When a single transition t occurs ('fires') at a marking, it takes tokens from its input places and adds tokens to its output places (with the number of tokens consumed/produced given by the weights of the relevant arcs). Moreover, if there

is an activator arc $(p,t) \in Act$, then transition t can only be executed at the given marking if p contains at least one token, without the implication of tokens in p being consumed or produced when t occurs. Thus, the difference with a *self-loop*, i.e., an arc from p to t and vice versa, is that the activator arc only tests for the presence of tokens in p.

We define the executions of N in the more general terms of simultaneously occurring transitions. A *step* is a multiset of transitions $U : T \to \mathbb{N}$. Thus $U(t)$ specifies how many times transition t occurs in U. (Note that if we exclude the empty multiset, single transitions can be considered as minimal steps.) Step U is *enabled* (to occur) at a marking m if m assigns enough tokens to each place for all occurrences of transitions in U and, moreover, all places tested through an activator arc by a transition in U, contain at least one token.

Formally, step U is enabled at marking m of N if, for all $p \in P$:

- $m(p) \geq \sum_{t \in T} U(t) \cdot W(p,t)$
- $m(p) \geq 1$ whenever there is a transition t such that $U(t) \geq 1$ and $(p,t) \in Act$.

If U is enabled at m, it can be *executed* leading to the marking m' obtained from m throught the accumulated effect of all transition occurrences in U:

- $m'(p) = \sum_{t \in T} U(t) \cdot (W(t,p) - W(p,t))$ for all $p \in P$.

Finally, a step U is said to be *max-enabled* at m if it is enabled at m and there is no step U' that strictly contains U (meaning that $U' \neq U$ and $U(t) \leq U'(t)$ for all transitions t) and which is also enabled at m. We denote this by $m[U\rangle m'$. A (max-enabled) *step sequence* is then a sequence $\sigma = U_1 \dots U_n$ of non-empty steps U_i such that $m_0\,[U_1\rangle\, m_1 \cdots m_{n-1}\,[U_n\rangle\, m_n$, for some markings $m_1, \dots, m_n$ of N. Then m_n is said to be a *reachable* marking of N (under the maximally concurrent step semantics).

To conclude this preliminary section, we elaborate a bit on the choice of this particular net model. First, it should be observed that it follows from the above definitions that the semantics allows *auto-concurrency*, the phenomenon that a transition may be executed concurrently with itself. This approach makes it possible to use transitions for a faithful modeling of natural events like the independent (non-sequential) occurrence in vast numbers of a biochemical reaction in a living cell. Note that the degree of auto-concurrency of a transition can easily be controlled by a dedicated place with a fixed, say k, number of tokens connected by a self-loop with that transition implying that never more than k copies of that transition can fire simultaneously.

Activator arcs were introduced in [16] as a means of *testing* for the presence of at least one token in a place, and so they are similar to other kinds of net features designed for the same reason. We mentioned already self-loops by which the presence of a token in a place can be tested only by a single transition (which 'takes and returns' the token) and not simultaneously by an arbitrary number of transition occurrences in a step. Two other mechanisms which do allow such multiple testing are *context* arcs [25] and *read (or test)* arcs [34]. Both, however, display important differences when compared with activator arcs. A context arc

testing for the presence of a token in place p by transition t indicates that after a step in which t participates has been executed, p must still contain a token which precludes the occurrence in the same step of transitions that have p as an output place. A read arc is also different, but less demanding in that there must exist a way to execute sequentially (i.e., one-by-one) all transition occurrences in the step, without violating the read arc specification. In both cases, one can easily see that activator arcs are most permissive since they only check for the presence of a token *before* the step is executed (this is often referred to as *a priori* testing). We feel that *a priori* testing is more appropriate for biological applications as the 'lookahead' implied by the other two kinds of test arcs is hard to imagine in reality.

Finally, we rely in this paper on *maximal* concurrency in the steps that are executed which reflects the idea that execution of transitions is never delayed. This may also be viewed as a version of time-dependent Petri nets where all transitions have a firing duration of 1. However, the maximal concurrency we apply in this paper does not derive from Petri nets with time, but rather from Petri nets with *localities* [19] leading to a *locally maximal* semantics. This semantics is what we plan to use to model other aspects of the development as well. Here one may think of e.g., the locally synchronous occurrence (in pulses) of reactions in individual compartments of a cell.

3 Biological background and modelling decisions

In biology, the term gradient is used to describe a gradual and directed change in concentration of a morphogen through a group of cells, e.g., a tissue. Morphogens are signalling molecules that cause cells in different places in the body to adopt different fates and thereby help establish embryonic axes. Morphogens are produced in a localized source of a tissue, the source cell(s), and emanate from this region, forming a concentration gradient ([13, 32]). A morphogen gradient has an immediate effect on the differentiation of the cells along it; cells are able to 'read' their position along the gradient and determine their developmental fate accordingly. They have a range of possible responses and the morphogen concentration dictates which response will be exhibited ([13, 32]). In establishing their developmental fate, cells take into account the morphogen concentration. When the morphogen concentration over the entire gradient is increased (or decreased), the cells should accordingly change their response to that corresponding to a higher (or lower) level of morphogen.

The mechanisms by which the morphogen travels through a cell layer have been the topic of some debate and are not yet fully understood. Three mechanisms have been described, shown schematically in Figure 1: (A) diffusion through the extracellular matrix ([8, 11, 23]), either passively, like a drop of ink in water ([11]), or facilitated by receptors on the cell surface which guide the morphogens along ([8]), as shown in the figure; (B) sequential internalization of the morphogen molecules in vesicles in the cells, a process called endocytosis, and subsequent re-emission ([7, 8, 32]); (C) direct contact between the cells by

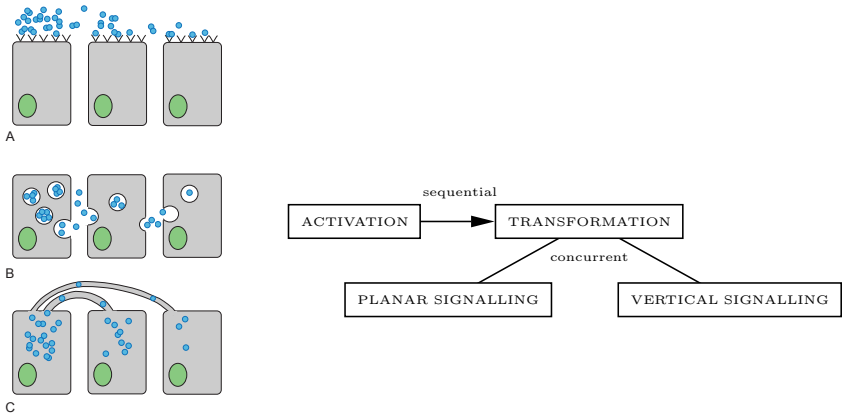

Fig. 1. Left: three possible mechanisms for gradient formation: diffusion (A), endocytosis and subsequent re-emission (B) and transport through cytonemes (C). Right: an overview of the process of AP axis formation in *Xenopus laevis*

means of tentacle-like threads of cytoplasm, called cytonemes, connecting the cells ([13]). These mechanisms are not necessarily mutually exclusive and some studies conclude that a combination of mechanisms underlies the formation of a gradient. It is important to note that both diffusion and endocytosis take place between neighbouring cells, while cytonemes connect all cells directly to the source. This makes it very different from a modelling perspective, as will be discussed below.

Unfortunately, knowledge of the exact concentrations and shapes of most gradients is limited. This is mainly due to the transient nature of morphogen gradients and the low concentrations at which they are effective, both of which make it difficult to visualize the morphogens ([11]). Many morphogens are rapidly degraded or prevented from binding to receptors by antagonistic proteins ([11]). Much of the information on gradients is therefore obtained indirectly, by observing their effect, i.e., the responses of the cells along it ([11]).

AP axis formation in *Xenopus laevis*: a case study. The AP axis formation in *Xenopus laevis* takes place during the early embryonic stage of gastrulation and ensures the development of anterior structures near the head and posterior structures towards the tail. The process can be seen as divided into two steps, which take place sequentially ([26]), cf. Figure 1. The first step is activation; a group of cells in the outer cell layer of the embryo, the ectoderm, change their developmental identity and form a rectangular strip of tissue, called the neurectoderm ([3, 15]). It is this strip of cells in which the AP axis will ultimately be established, leading to gradual posteriorization of cells nearer to the tail-end of the embryo.

During the second step, transformation, the axis is formed in the neurectoderm by means of two mechanisms: vertical and planar signalling between neighbouring cells ([3, 15]). Here we focus on the second. Planar signalling occurs within the neurectoderm in a direction parallel to the future axis (and is therefore called 'planar'). Concentration gradients of several morphogens are formed in the neurectoderm along the future AP axis. Source cells on the posterior end of the neurectoderm produce the morphogens, which then get distributed throughout the tissue. Individual cells sense their position along these gradients and take on a more or less posterior fate according to the concentration of these posteriorizing molecules ([12, 15]), thereby establishing the formation of an AP axis. In the planar signalling of our case study three types of signalling molecules play a role: retinoic acid (RA), fibroblast growth factors (Fgf) and Wnts ([22, 29, 35]). All of these are produced at the posterior end of the embryo and together these promote posterior cell fates, while inhibiting anterior fates. Although it is clear that all three types are important in axis formation, it is not yet fully understood how these proteins interact in establishing cell fate. A general and abstract modelling approach, focusing on the underlying common process of gradient formation, makes it possible to later add specific data on any of the morphogens in particular or on combinations of these.

Modelling decisions. We have chosen cells as the elementary units in our model to be represented as places in a Petri net. Earlier studies ([4, 21, 24]) have successfully modelled cell-to-cell signalling, starting from a lower biological level, using places to represent genes and proteins. Although this allows a high level of detail, it also complicates the net and makes it difficult to identify single cells. In our approach the cellular level represents the intermediate level between the subcellular levels, on which the morphogen signalling between cells takes place, and the tissue/organ level, where whole cell layers may move.

Tokens are used to represent a certain level of concentration (see [10]) within the overall gradient of the morphogen system, without differentiation between morphogens or their quantities. As mentioned before, in most cases no quantitative data are available, since morphogen gradients are often transient and difficult to visualize ([13]). As in [21], our approach is therefore partially qualitative and partially quantitative. The significance of tokens in a place is not purely qualitative; not only the presence or absence but also the exact number of tokens determine the course of events. However, the numbers of tokens do not represent actual numbers of molecules, making the model semi-qualitative. Our Petri net model can, however, also be used to model specific morphogens, incorporating quantitative data, by assigning exact concentrations to the tokens and thereby making the model completely quantitative. For certain morphogens quantitative data exist, for instance for the gradient of Fgf8 in zebrafish, which can be seen to spread extracellularly through the processes of diffusion, endocytosis and degradation ([28]). Also, for some gradients found in biological processes, experimental data have enabled to deduce mathematical expressions, describing the

quantitative morphogen concentrations ([33]). When modelling these gradients, these formulas can be incorporated in the parameters of our Petri net model.

Neighbourhood communication. It is our aim to develop a faithful model for gradient formation. Rather than having the net simply distribute the proper pre-computed amount of tokens over the places representing the cells, the actual transport of morphogen between cells can be read off from the Petri net model during execution. Consequently, when building the model we have to specify explicitly which process of gradient formation is to be modelled. Here we choose to model morphogens moving between neighbouring cells, i.e., the Petri net will implement a mechanism similar to diffusion or endocytosis and subsequent re-emission, but not transport through cytonemes (since this does not take place between neighbouring cells). However, we foresee no problems in the abstract implementation of the latter process. The difference between diffusion and endocytosis is apparent on a lower biological level and could be modeled by subnets. Furthermore, often the ratio of the concentrations between neighbouring cells is not known due to lack of quantitative data, and it may vary depending on the gradient considered. Therefore we have a parameter ρ in our model to represent this ratio and to determine the amount of tokens to be transported between places during the simulation of gradient formation. Since we do not distinguish the molecular mechanisms of diffusion, endocytosis and degradation of morphogens in this model, ρ represents the final ratio of morphogens between neighbouring cells and morphogen degradation is implicit. To model explicitly both the production of morphogens in the local source cells and the degradation in the target cells, subnets could be added. This should make the source and sink mechanisms of gradient formation transparent and allow the user to experiment with different configurations.

Implementation. In the organism, gradient ratios arise passively as a consequence of physical laws. However, to accurately reflect the biological process of gradient formation underlying the spread of morphogens from cell to cell, our formal model has to compute the number of tokens passed on based on the ratio ρ. Hence the model includes explicit separate computational units for the necessary calculations. In particular, these parts of the net control the transport of tokens between places. In this way a close relation to the biological process can be maintained in one part of the net, with the underlying computations performed by a subnet in the background. At all times, the marking of the net will be consistent with biological observations of (the effect of) the gradient, i.e., the ratio is maintained and places corresponding to cells further away from the source will never have more tokens than places (cells) closer to it. Another important feature of the model is the use of concurrent steps rather than individually occurring transitions. Cells only react to their environment and have no knowledge of other cells than their immediate neighbours. Non-adjacent cells can be simultaneously involved in the transport of morphogens. This leads to an execution mode consisting of concurrent *steps*. Moreover, these steps are *maxi-*

mal to reflect that also in the net model morphogens are moved to a next cell as soon as possible.

4 Gradients and Petri Nets

Following the ideas outlined in the previous section, we will propose a formal model for the formation of a gradient.

Our assumptions regarding the biological process of gradient formation are as follows. Given is a segment of k adjacent cells with the i-th cell immediate neighbour of the $(i+1)$-th cell. Morphogens can be transported only between immediate neighbours. Morphogens move from cells with higher concentration to neighbours with lower concentration, as long as their concentration ratio does not exceed a given gradient ratio $0 < \rho < 1$. We assume that ρ is a rational number, i.e., $\rho = \frac{N}{M}$, where $M > N \geq 1$. Initially, the first cell x_1 contains a quantity (has concentration level) K of a morphogen. These assumptions lead to the following modelling problem.

> Given are $k \geq 1$ places $x_1, \ldots, x_k$, representing a segment of k cells with place x_i corresponding to the i-th cell. In the initial marking m_0, the first place x_1 contains K tokens and there are no tokens in the other places.
> In the net modelling the mechanism of gradient formation, we need to shift tokens from x_1 in the direction of the last place x_k. Places and/or transitions may be added, but in such a way that for any reachable marking m the following hold.
>
> 1. The number of tokens in the x_i's remains constant, i.e.,
>
> $$m(x_1) + \cdots + m(x_k) = K \qquad \textbf{token preservation}$$
>
> 2. The tokens are distributed monotonically along the sequence of k places, i.e.,
>
> $$m(x_1) \geq \ldots \geq m(x_k) \qquad \textbf{monotonicity}$$
>
> 3. The ratio of the numbers of tokens in two neighbouring places does not exceed ρ, i.e., for every $1 \leq i < k$ with $m(x_i) \geq 1$:
>
> $$\frac{m(x_{i+1})}{m(x_i)} \leq \rho \qquad \textbf{ratio}$$
>
> 4. Shifting continues until moving even one token would violate the above, i.e., if no tokens are shifted after marking m was reached, then for every $1 \leq i < k$ with $m(x_i) > 1$:
>
> $$\frac{m(x_{i+1})+1}{m(x_i)-1} > \rho \qquad \textbf{termination}$$
>
> Moreover, the relative position of a place within the sequence plays no role. In particular, the mechanism should be easily scalable and **insensitive** to the specific values of k and K. □

If we look at the above formulation of properties (2) and (3) — monotonicity and preservation of the gradient ratio — and recall that $\rho = \frac{N}{M}$ and $M > N$, it is easy to observe that these two properties are together equivalent to stating that, for every $1 \leq i < k$, $N{\cdot}m(x_i) - M{\cdot}m(x_{i+1}) \geq 0$. We will call a marking m satisfying this inequality *consistent* and denote $\alpha_i \stackrel{\text{df}}{=} N{\cdot}m(x_i) - M{\cdot}m(x_{i+1})$, for every $1 \leq i < k$. Note that the initial marking is consistent.

Similarly, if we look at the above formulation of properties (2) and (4) — monotonicity and termination — it is easy to observe that together they are equivalent to the statement that, for every $1 \leq i < k$, $N{\cdot}m(x_i) - M{\cdot}m(x_{i+1}) < M + N$. We will call a consistent marking m satisfying this inequality *stable*. Note that for a given ρ, k and K, there may be more than one stable marking. For example, if $\rho = \frac{1}{2}$, $k = 5$ and $K = 111$, then the following are two different stable markings:

x_1	x_2	x_3	x_4	x_5
59	29	14	6	3

x_1	x_2	x_3	x_4	x_5
58	29	14	7	3

We are now ready to propose a generic solution for the above problem.
For a given consistent marking m and each $1 \leq i < k$, move β_i tokens from x_i to x_{i+1} where $\beta_i \leq \left\lfloor \frac{\alpha_i}{M+N} \right\rfloor$, and at least one β_i must be non-zero if at least one of the values $\left\lfloor \frac{\alpha_i}{M+N} \right\rfloor$ is non-zero. We denote the resulting marking by $m_{\beta_1 \ldots \beta_{k-1}}$.

An intuitive reason for proposing such a mechanism for shifting tokens is that the number of tokens in x_i that are 'balanced' by tokens in x_{i+1} is $\frac{M}{N}{\cdot}m(x_{i+1})$, because each token in x_{i+1} is equivalent to $\frac{M}{N}$ tokens in x_i. Hence there are $m(x_i) - \frac{M}{N}{\cdot}m(x_{i+1})$ unbalanced tokens in x_i. The 'portion' of each unbalanced token that could be safely transferred to x_{i+1} is $\frac{N}{M+N}$. Hence in total we may safely transfer $\left\lfloor \frac{N}{M+N}{\cdot}(m(x_i) - \frac{M}{N}{\cdot}m(x_{i+1})) \right\rfloor$ tokens, which is precisely $\left\lfloor \frac{\alpha_i}{M+N} \right\rfloor$ tokens. Clearly, some of the numbers $\beta_1, \ldots, \beta_{k-1}$ can be zero, and by the condition above, all β_i's are zeros if and only if the marking is stable:

Proposition 1. *$\beta_1 = \cdots = \beta_{k-1} = 0$ if and only if m is stable.*

Crucially, by the mechanism proposed consistent markings are always transformed into consistent markings.

Proposition 2. *If m is a consistent marking then $m_{\beta_1 \ldots \beta_{k-1}}$ is also consistent.*

According to the above, any number of tokens not exceeding $\left\lfloor \frac{\alpha_i}{M+N} \right\rfloor$ can be moved *simultaneously* from x_i to x_{i+1} (for every $i < k$), and consistency will be preserved. Clearly, the new consistent marking is different from the previous one if and only if, for at least one i, we have $\beta_i \geq 1$. The idea now is to keep changing the marking on $x_1, \ldots, x_k$ until a marking m has been reached such that $\left\lfloor \frac{\alpha_i}{M+N} \right\rfloor = 0$, for all $1 \leq i < k$, which is equivalent to $\alpha_i < M + N$, for all $1 \leq i < k$. In other words, this m is a stable marking. Since tokens cannot

be shifted forever, this procedure will always terminate in a stable marking (formally, we can show this by considering a weighted distance to the end of the chain of the K tokens; it never increases and always decreases in a non-stable state).

Looking now from the point of view of a Petri net implementation of the proposed mechanism, what we are after is a net N_{shift} comprising the places $x_1, \ldots, x_k$ and such that if m is a marking of N_{shift} whose projection on these k places is consistent, then a step U can occur at m if

- it moves at most $\left\lfloor \frac{\alpha_i}{M+N} \right\rfloor$ tokens from x_i to x_{i+1}, for all $1 \leq i < k$;
- at least one token is moved from x_i to x_{i+1} for at least one $1 \leq i < k$, unless the projection of m onto $x_1, \ldots, x_k$ is stable.

In fact, in the proposed implementation, we will be preceding the 'token-shifting' with a 'pre-processing' stage which seems to be unavoidable unless one uses some kind of arcs with complex weights depending on the current net marking.

Implementation. In the implementation of the proposed shifting mechanism, as many tokens as possible should be shifted from one neighbour to the next. That means that, at each stage we have, for every $1 \leq i < k$, $\beta_i = \left\lfloor \frac{\alpha_i}{M+N} \right\rfloor$. Moreover, tokens are shifted from a place without any assumptions whether new tokens will come to that place from its other neighbour. Thus we need to provide a Petri net structure capable of 'calculating' the value of expressions like

$$\left\lfloor \frac{N{\cdot}m(x_i) - M{\cdot}m(x_{i+1})}{M+N} \right\rfloor .$$

Our proposed gradient forming mechanism distinguishes three phases: I, II and III. An auxiliary net N_{3phase}, shown in Figure 2(b), is used to schedule the transitions implementing the calculations. It controls these transitions via the places w^I and w^{II} and activator arcs. For the full picture of the system one should combine the figures for all pairs (x_i, x_{i+1}) with a single copy of the net in Figure 2(b). Note that all places with identical label (in particular w^I, w^{II}, and w^{III}) should be identified. That other parts of the encompassing net model do not interfere with the calculations carried out during phases I and II can be ensured by connecting the relevant transitions with the place w^{III} using activator arcs.

For every $1 \leq i < k$, transition t_i is intended to shift tokens from x_i to x_{i+1} (phase III). To achieve this, we use two disjoint sets of new, auxiliary places, $x'_1, \ldots, x'_k$ and $x''_1, \ldots, x''_k$. These places are initially empty. The idea is to fill x'_i with $N{\cdot}m(x_i)$ tokens and x''_{i+1} with $M{\cdot}m(x_{i+1})$ tokens (phase I). The latter are used for the removal of $M{\cdot}m(x_{i+1})$ tokens from x'_i (phase II). After this, there are α_i tokens remaining in x'_i. Finally, for each group of $N+M$ tokens in x'_i, one token is shifted from x_i to x_{i+1}. The construction (for x_i and x_{i+1}) is shown in Figure 2(a).

The overall mechanism operates in cycles of three consecutive, maximally concurrent steps such that for every $1 \leq i < k$:

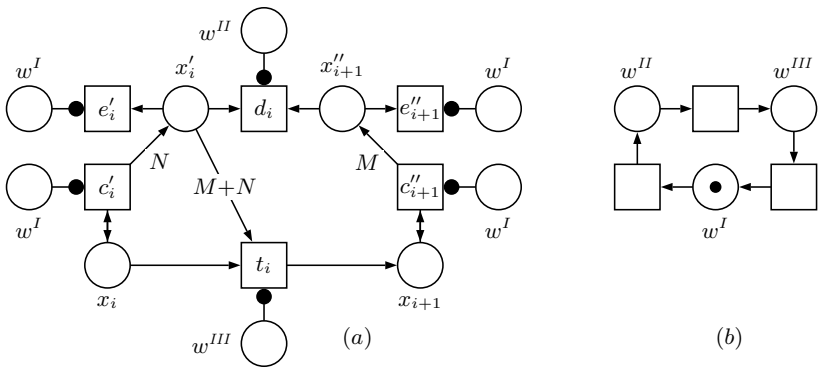

Fig. 2. (a) The main part of the construction for the solution (note that e''_{i+1} is introduced for later use when one might want to remove or add tokens to the x_i's from 'outside'; in the standard (consistent) situation it is never activated as after phase 2, place x''_{i+1} is empty.); and (b) the subnet N_{3phase} enforcing the three phases.

I. Transition c'_i, inserts (in $m(x_i)$ auto-concurrent occurences) $N{\cdot}m(x_i)$ tokens into x'_i. In the same step, transition c''_{i+1}, inserts (in $m(x_i)$ auto-concurrent occurences) $M{\cdot}m(x_{i+1})$ tokens into x''_{i+1}. Simultaneously, transitions e'_i and e''_{i+1} empty x'_i and x''_{i+1} of any residual tokens left from the previous cycle.
II. Next, transition d_i (in $M{\cdot}m(x_{i+1})$ auto-concurrent occurences) empties x''_{i+1} and leaves in x'_i the difference $\alpha_i = N{\cdot}m(x_i) - M{\cdot}m(x_{i+1})$.
III. In the third step, the occurrences of transition t_i transfer $\beta_i = \left\lfloor \frac{\alpha_i}{M+N} \right\rfloor$ tokens from x_i to x_{i+1}.

Proposition 3. *Each cycle results in transferring β_i tokens from x_i to x_{i+1}.*

Note that in this implementation with the control net N_{3phase}, neighbouring pairs are either all involved in calculations (step 1 and 2 of the cycle) or tokens are transferred between neighbours (step 3). During the whole operation of the adjustment process (except for the transfer phase), the token counts in the places x_i representing the cells are unchanged and they can be accessed for reading by other transitions (and thus influence neighbouring cells). In other words, calculations are *orthogonal* to the basic operation of the net (the gradient formation).

As an example, let us consider the case when $\rho = \frac{1}{2}$, $k = 4$ and $K = 100$. Then executing the constructed net in a maximally concurrent manner leads to the following sequence of markings on the x_i after each cycle and eventually to a stable marking:

x_1	100	67	67	60	60	57	57	56	56	55	54
x_2	0	33	22	29	25	28	26	27	26	25	26
x_3	0	0	11	8	12	10	12	12	13	12	12
x_4	0	0	0	3	3	5	5	5	5	6	6

The next example shows what happens if we start from a (non-initial) consistent marking (again $\rho = \frac{1}{2}$):

x_1	200	167	156	...
x_2	50	67	67	...
x_3	0	16	22	...
x_4	0	0	5	...

The construction works without any problems, if we start with a consistent marking. In case $0 > \alpha_i$ for some i, then transition t_i is not executed, but the transitions t_{i-1} and t_{i+1} may still be executed and lead to an adjustment of the marking causing t_i to become active in the next cycle. A further observation is that adding (or removing) tokens at some point, will trigger a re-adjustment process which tries to re-establish the correct ratios between the markings of adjacent places x_i. This process is unpredictable, but to deal with that case we have included transition e''_{i+1} which in the standard (consistent) situation is never activated since then, after phase 2, place x''_{i+1} is empty.

An important characteristics of the proposed solution is that it is purely *local* and does not assume anything about the number of tokens which may appear in the x_i's nor the length of the chain. In other words, it is truly generic. What's more it also works if M and N are different for different pairs of neighbouring places, i.e., if rather than a uniform gradient ratio ρ there is a ratio ρ_i for each pair of neighbours x_i and x_{i+1}.

Another feature of our solution is the maximal concurrency semantics intended to reflect the idea of morphogens (simultaneously) moving from cell to neighbouring cell whenever that is possible. The preliminary sequential semantics model we developed (but not reproduced here) is more complicated as it also needs *inhibitor arcs* which test for *absence* of tokens (to decide whether or not tokens should still be shifted). Moreover, one needs to decide that x_i either receives or sends tokens at each stage. In a step model it can both receive and send. Also, with the maximal concurrency semantics, the number of states of the model is dramatically reduced.

The auxiliary net N_{3phase} is used to partly sequentialize the behaviour in order to separate the pre-processing phases from the actual shifting phase. This net could also have been made local to the subnet in Figure 2(a), with different copies of it assigned to different localities. This would have given the additional possibility of controlling the degree of synchronisation between different parts of the gradient model by using a locally maximal step semantics.

Finally, we would like to point out that the activator arcs in our implementation are used only to control the calculation and can actually be avoided in case there would be a limit on the number of tokens in each place x_i at any time. (Then the activator arcs can be eliminated basically by having separate copies of N_{3phase} for each $1 \leq i < k$, transfer around sufficiently many tokens in a bundle, and replace activator arcs by self-loops). This assumption corresponds to having (or knowing) some capacity bound on the concentration levels of morphogens in a cell and so may be biologically sound!

5 Conclusion

Starting from gradient formation in the AP axis development in the model organism *Xenopus laevis*, we have presented a novel approach to using Petri nets in developmental biology by focusing on the cellular rather than subcellular levels and abstracting from concrete proteins and genes. This has led to a parameterized Petri net model for the general process of gradient formation through diffusion and endocytosis.

Assumptions regarding gradient formation have been formulated based on essential features of this process as reported in the literature. These assumptions underlie the precise requirements given that should be satisfied by an abstract Petri net model of gradient formation. A crucial point here is the consistency that is maintained during the execution of the model. Hence the realization of the gradient is faithfully reflected. Moreover the close relationship between biological process and evolution of the formal model makes it possible to apply existing Petri net techniques to analyse what happens during gradient formation. In particular cause-effect relations should be properly reflected in the process semantics of the modelling Petri net ([17, 18]).

Another main contribution of this approach is its generic nature, leading to a model that is scalable and applicable to a plethora of specific gradients. Also scalability is a consequence of the faithful reflection of the biological process. Since the final token (morphogen) distribution is not directly computed from the initial amount of morphogen and the length of the chain of cells, but rather simulates the communication between neighbouring cells, the length plays no role in the occurrence of the steps. The model as presented here represents a one-morphogen system without relying on quantitative data, but exact values could be assigned to ratio and individual tokens. Moreover, it provides a basis for simulation of simultaneous gradient formation (different morphogens with different experimental initial markings) and for inhibiting/activating interactions between them. Simulation with actual biological data to validate the model should be a next step. In addition, we will focus our attention on the extension of this still rather basic model to more dimensions, e.g., rather than having just a single line of cells, we consider the spread of morphogens from a source throughout a tissue plane or volume.

In [4, 21], Petri nets are used to model developmental processes in a way similar to our approach when it comes to the semi-qualitative use of tokens and the use of maximal concurrency. In these papers however, the focus is on subcellular levels. Petri net places are used to represent genes and gene products, where in our approach cells, as basic units in a tissue, are modelled by places. Having cells as basic units should prove to be a useful intermediate position convenient for 'zooming in and out' between subcellular and tissue level. It is our aim to model more subprocesses of the AP axis formation. For instance the different molecular processes underlying diffusion and endocytosis could be modeled in subnets, allowing the user to compare the different effects of these mechanisms. Also the degradation of morphogens could be modeled by a subnet, making the entire process more explicit. The choice of cells as main elements is

expected to be particularly suitable not only in this 'vertical' linking processes, but also for the 'horizontal' connections between processes taking place on the same cellular level. Having molecules or genes as places would result in specific net models for certain processes, as would taking tissue structures, such as the neurectoderm. Cells however can play a role in different processes simultaneously.

The next step in the modelling of the AP axis development in *Xenopus laevis* will focus on the vertical signalling (see Figure 1). This process occurs concurrently with the planar signalling of gradient formation and involves the same cells. This will challenge us to explore further the possibilities of Petri nets as a model for concurrent and independent processes in high level developmental biology.

Acknowledgments We are grateful to all referees for their remarks and suggestions which helped us to improve the paper. We would like to express also our appreciation to A.Durston and H.Jansen for discussing *Xenopus* biology.

References

1. R.Banks: Qualitatively Modelling Genetic Regulatory Networks: Petri Net Techniques and Tools. Ph.D. Thesis, Newcastle University, 2009
2. R.Banks, V.Khomenko, L.J.Steggles: A Case for Using Signal Transition Graphs for Analysing and Refining Genetic Networks. ENTCS 227, 2009, 3–19
3. N.Bardine: Hox in Frogs. PhD Thesis, University of Leiden, 2008
4. N.Bonzanni et. al: Executing Multicellular Differentiation: Quantitative Predictive Modelling of *C.elegans* Vulval Development. Bioinformatics 25, 2009
5. H.-D.Burkhard: On Priorities of Parallelism: Petri Nets under the Maximum Firing Strategy. LNCS 146, 1983, 86–97
6. C.Chaouiya: Petri Net Modelling of Biological Networks. Briefings in Bioinformatics 8, 2007, 210–219.
7. E.Entchev, M.Gonzalez-Gaitan: Morphogen Gradient Formation and Vesicular Trafficking. Traffic 3, 2002, 98–109
8. J.A.Fischer, S.H.Eun, B.T.Doolan: Endoytosis, Endosome Trafficking, and the Regulation of *Drosophila* Development. The Annual Review of Cell and Developmental Biology 22, 2006, 181–206
9. D.Gilbert, M.Heiner: From Petri Nets to Differential Equations - an Integrative Approach for Biochemical Network Analysis. LNCS 4024, 2006, 181–200
10. D.Gilbert, M.Heiner, S.Lehrack: A Unifying Framework for Modelling and Analysing Biochemical Pathways Using Petri Nets. LNBI 4695, 2007, 200–216
11. J.B.Gurdon et. al: Activin Signalling and Response to a Morphogen Gradient. Nature 371, 1994, 487–492
12. J.B.Gurdon et. al: Single Cells Can Sense their Position in a Morphogen Gradient. Development 126, 1999, 5309–5317
13. J.B.Gurdon, P.Bourillot: Morphogen Gradient Interpretation. Nature 413, 2001, 797–803
14. M.Heiner, D.Gilbert, R.Donaldson: Petri Nets for Systems and Synthetic Biology. LNCS 5016, 2008, 215–264
15. H.J.Jansen: Anterior-posterior Axis Formation in *Xenopus laevis*. PhD Thesis, University of Leiden, 2009

16. R.Janicki, M.Koutny: Semantics of Inhibitor Nets. Information and Computation 12, 1995, 1–16
17. J.Kleijn and M.Koutny: Processes of Petri Nets with Range Testing. Fundamenta Informaticae 80, 2007, 199–219
18. J.Kleijn and M.Koutny: Processes of Membrane Systems with Promoters and Inhibitors. Theoretical Computer Science 404, 2008, 112–126
19. J.Kleijn, M.Koutny, G.Rozenberg: Towards a Petri Net Semantics for Membrane Systems. LNCS 3850, 2006, 292–309
20. I.Koch, B.H.Junker, M.Heiner: Application of Petri Net Theory for Modelling and Validation of the Sucrose Breakdown Pathway in the Potato Tuber. Bioinformatics 21, 2004, 1219–1226
21. E.Krepska et. al: Design Issues for Qualitative Modelling of Biological Cells with Petri Nets. LNBI 5054, 2008, 48–62
22. T.Kudoh, S.W.Wilson, I.B.Dawid: Distinct roles for Fgf, Wnt and Retinoic Acid in Posteriorizing the Neural Ectoderm. Development 129, 2002, 4335–4346
23. A.D.Lander, Q.Nie, F.Y.M.Wan: Do Morphogen Gradients Arise by Diffusion? Developmental cell 2, 2002, 785–796
24. H.Matsuno et. al: Boundary Formation by Notch Signaling in Drosophila Multicellular Systems: Experimental Observations and Gene Network Modeling by Genomic Object Net. Pacific Symposium on Biocomputing 8, 2003, 152–163
25. U.Montanari, F.Rossi: Contextual Nets. Acta Informatica 32, 1995, 545–596
26. P.D.Nieuwkoop: Activation and Organisation of the Central Nervous System in Amphibians. III. Synthesis of a New Working Hypothesis. Journal of Experimental Zoology 120, 1952, 83–108
27. W.Reisig, G.Rozenberg (Eds.): Lectures on Petri Nets I and II. LNCS 1491 and 1492, 1998
28. S.Scholpp, M.Brand: Endocytosis Controls Spreading and Effective Signaling Range of Fgf8 Protein. Current Biology 14, 2004, 1834–1841
29. J.Shiotsuguet et. al: Multiple Points of Interaction between Retinoic Acid and Fgf Signaling During Embryonic Axis Formation. Development 131, 2004, 2653–2667
30. L.J.Steggles, R.Banks, O.Shaw et al.: Qualitatively Modelling and Analysing Genetic Regulatory Networks: a Petri Net Approach. Bioinformatics 23, 2006, 363–343
31. C.Talcott, D.L.Dill: Multiple Representations of Biological Processes. Transactions on Computational Systems Biology, 2006
32. A.A.Teleman, M.Strigini, S.M.Cohen: Shaping Morphogen Gradients. Cell 105, 2001, 559–562
33. C.J.Tomlin, J.D.Axelrod: Biology by Numbers: Mathematical Modelling in Developmental Biology. Nature Reviews Genetics 8, 2007, 331–340
34. W.Vogler: Partial Order Semantics and Read Arcs. Theoretical Computer Science 286, 2002, 33–63
35. R.J.White et. al: Complex Regulation of *cyp26a1* Creates a Robust Retinoic Acid Gradient in the Zebrafish Embryo. Plos biology 5, 2007, 2522–2533
36. L.Wolpert: Principles of Development. Oxford University Press, 2002

Colored Petri nets to model and simulate biological systems

Fei Liu and Monika Heiner

Department of Computer Science, Brandenburg University of Technology
Postbox 10 13 44, 03013 Cottbus, Germany
{liu, monika.heiner}@informatik.tu-cottbus.de

Abstract. Petri nets have become an effective formalism to model biological systems. However, attempts to simulate biological systems by low-level Petri nets are restricted to relatively small models, and they tend to grow quickly for modeling complex systems, which makes it more difficult to manage and understand the nets. Motivated by this, we propose a colored Petri net-based framework for modeling, simulating, and analyzing complex biological systems. We give the definitions of biochemically interpreted colored qualitative Petri nets (QPN^C) and colored stochastic Petri nets (SPN^C) and describe their functionalities and features implemented in the Petri net tool Snoopy. We use two examples, the cooperative ligand binding and the repressilator, to demonstrate how to construct and simulate QPN^C and SPN^C models, respectively.

1 Motivation

With the rapid growth of data being generated in the biological field, it has become necessary to organize the data into coherent models that describe system behavior, which are subsequently used for simulation, analysis or prediction. A large variety of modeling approaches has already been applied to modeling a wide array of biological systems (see [HK09] for a review). Among them, Petri nets are especially suitable for representing and modeling the concurrent, asynchronous, and dynamic behavior of biological systems, which were first introduced to the qualitative analysis of the biochemical reaction systems by Reddy et al. [RML93]. Motivated by the qualitative analysis of Petri nets, many applications of Petri nets (e.g. stochastic Petri nets, timed Petri nets, continuous Petri nets, and hybrid Petri nets, etc.) have been developed for modeling and simulating biological systems [GH06]. Since biological processes are inherently stochastic, stochastic Petri nets have recently become a modeling paradigm for capturing their complex dynamics, which can help to understand the behavior of complex biological systems by integrating detailed biochemical data and providing quantitative analysis results, see e.g. [JP98], [NOG+05], [PRA05].

Petri nets provide a formal and clear representation of biological systems based on their firm mathematical foundation for the analysis of biochemical properties. However, low-level Petri nets do not scale. So attempts to simulate biological systems by low-level Petri nets have been mainly restricted so far

to relatively small models. They tend to grow quickly for modeling complex systems, which makes it more difficult to manage and understand the nets, thus increasing the risk of modeling errors [Mur07]. Two known modeling concepts improving the situation are hierarchy and color. Hierarchical structuring has been discussed a lot, see e.g. [MWW09], while the color has gained little attention so far. Thus, we investigate how to apply colored Petri nets to modeling and analyzing biological systems. To do so, we not only provide compact and readable representations of complex biological systems, but also do not lose the analysis capabilities of low-level Petri nets, which can still be supported by automatic unfolding. Moreover, another attractive advantage of colored Petri nets for a biological modeler is that they provide the possibility to easily increase the size of a model consisting of many similar subnets just by adding colors.

In this paper, we propose a colored Petri net-based framework for modeling, simulating, and analyzing biological systems. We are developing tools to support this new framework. Two prototypes for colored qualitative Petri nets (QPN^C) and colored stochastic Petri nets (SPN^C) have been implemented in Snoopy, a tool for modeling and animating/simulating hierarchical graph-based formalisms [Sno10]. We will describe these two prototypes and some applications.

This paper is organized as follows. Section 2 outlines the colored Petri net-based framework for modeling, simulating and analyzing biological systems and gives the definitions of QPN^C and SPN^C. Section 3 discusses the functionalities and features for QPN^C and SPN^C, which have been implemented in Snoopy. Section 4 shows how to construct basic colored Petri net components, and gives two examples to demonstrate QPN^C and SPN^C, respectively. Section 5 summarizes related work. Finally, conclusions and outlook are given.

2 Colored Petri net-based framework

In this section, we propose a colored Petri net-based framework for modeling, and simulating/analyzing biological systems, illustrated in Fig. 1, which extends the Petri net-based framework for modeling, and simulating/analyzing biological systems introduced in [GHL07], i.e., the new proposed framework is in fact the colored version of the existing framework. Both of these frameworks unify the qualitative, stochastic and continuous Petri net paradigms, but the colored version provides more compact and readable representations of complex biological systems.

The new framework relates three modeling paradigms: QPN^C, SPN^C, and colored continuous Petri nets (CPN^C), just like the Petri net-based framework that relates qualitative Petri nets (QPN), stochastic Petri nets (SPN) and continuous Petri nets (CPN). QPN^C is an abstraction of SPN^C and CPN^C, while SPN^C and CPN^C are mutually related by approximation. The user can refer to [GHL07] to take a closer look at the detailed relationship between these three paradigms. In the following, we will describe QPN^C and SPN^C in detail, but not CPN^C as we have not investigated CPN^C yet.

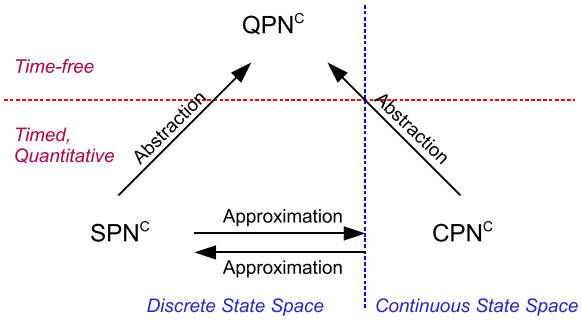

Fig. 1. Colored Petri net-based framework for modeling, and simulating/analyzing biological systems.

2.1 Colored qualitative Petri Nets (QPN^C)

We assume basic knowledge of the standard notions of qualitative place/transition Petri nets, see e.g. [Mur89], [HGD08]. In the following, we will briefly describe QPN, and then give the definition of QPN^C.

QPN is the basic Petri net class, which consists of places, transitions, and arcs. QPN does not associate a time with transitions or the sojourn of tokens at places, and thus is time-free [GHL07]. QPN^C is a colored extension of QPN.

Colored Petri nets were first proposed by Jensen [Jen81], which combine Petri nets with capabilities of programming languages to describe data types and operations, thus providing a flexible way to create compact and parameterizable models. In colored Petri nets, tokens are distinguished by the "color", rather than having only the "black" one. Besides, arc expressions, an extended version of arc weights, specify which tokens can flow over the arcs, and guards that are in fact Boolean expressions define additional constraints on the enabling of the transitions [JKW07]. In the following, we give the definition of the QPN^C based on the definition of colored Petri nets by Jensen [JKW07]. Here we denote by EXP the set of expressions that comply with a predefined syntax, which are used as arc expressions, guards, etc.

Definition 1. *A QPN^C is a tuple $< P, T, F, \sum, C, g, f, m_0 >$, where:*

- *P is a finite, non-empty set of places.*
- *T is a finite, non-empty set of transitions.*
- *F is a finite set of directed arcs, such that $F \subseteq (P \times T) \cup (T \times P)$.*
- *$\sum$ is a finite, non-empty set of types, also called color sets.*
- *$C : P \to \sum$ is a color function that assigns to each place $p \in P$ a color set $C(p) \in \sum$.*
- *$g : T \to EXP$ is a guard function that assigns to each transition $t \in T$ a guard expression that has the Boolean type.*

- $f : F \rightarrow EXP$ *is an arc function that assigns to each arc* $a \in F$ *an arc expression that has a multiset type* $C(p)_{MS}$*, where* p *is the place connected to the arc* a*, and* $C(p)_{MS}$ *is the multiset on the color set* $C(p)$*.*
- $m_0 : P \rightarrow EXP$ *is an initialization function that assigns to each place* $p \in P$ *an initialization expression that has a multiset type* $C(p)_{MS}$*.*

QPN^C is a colored extension of the qualitative place/transition net extended by different kinds of arcs, e.g., inhibitor arc and read arc [HRR+08]. These kinds of arcs are not explicitly denoted in the definition above.

2.2 Colored Stochastic Petri Nets (SPN^C)

In this section, we will briefly recall stochastic Petri nets (SPN) and their extensions, and then introduce colored stochastic Petri nets (SPN^C).

SPN are an extension of qualitative place/transition Petri nets. As with a qualitative Petri net, a stochastic Petri net maintains a discrete number of tokens on its places. But contrary to the time-free case, a firing rate (waiting time) is associated with each transition, which is a random variable, defined by an exponential probability distribution. The semantics of a stochastic Petri net is described by a continuous time Markov chain (CTMC). The CTMC of a stochastic Petri net without parallel transitions is isomorphic to the reachability graph of the underlying qualitative Petri net, while the arcs between the system states are now labelled by the transition rates [HLG+09].

There are quite a number of various extensions based on the fundamental stochastic Petri net class SPN, see e.g. [MBC+95], [Ger01]. For example, generalized stochastic Petri nets ($GSPN$) are stochastic Petri nets (SPN) extended by inhibitor arcs and immediate transitions. Deterministic and stochastic Petri nets ($DSPN$) are generalized stochastic Petri nets ($GSPN$) extended by deterministic transitions [HLG+09].

While SPN and its extensions offer enormous modeling power, managing large-scale Petri net models is difficult due to the fact that tokens are indistinguishable. To alleviate this limitation, the SPN^C is presented to uplift biochemically interpreted extended stochastic Petri nets introduced in [HLG+09] to a colored version. As in the QPN^C, in the SPN^C, tokens are distinguished by the "color", and arc expressions and guards have the same meaning. Before expressions are evaluated to values, the variables in the expressions must get assigned values, which is called binding. A binding of a transtion $t \in T$ exactly corresponds to a transition instance, denoted by $t(b)$, i.e., each binding will become an uncolored transition after unfolding. The set of all bindings for a transition t constitutes the set of all the instances of transition t, denoted by $TI(t)$. The set of all instances for all transitions T of a net is denoted by $TI(T)$. In contrast, each color $c \in C(p)$ for a place $p \in P$ exactly corresponds to a place instance, denoted by $p(c)$, i.e., each color will become an uncolored place after unfolding. We let $PI(p)$ denote all the instances of a place p and $PI(P)$ all the instances of all places P of a net. In the following, we give the definition of SPN^C based on QPN^C.

Definition 2. *A biochemically interpreted colored stochastic Petri net* SPN^C *is a tuple* $< P, T, F, \sum, C, g, f, v, l, m_0 >$*, where:*

- $< P, T, F, \sum, C, g, f, m_0 >$ *is a* QPN^C*.*
- T *is refined as the union of three disjoint transition sets, i.e.* $T := T_{stoch} \cup T_{im} \cup T_{timed}$ *with:*
  - T_{stoch}*, the set of stochastic transitions with exponentially distributed waiting time,*
  - T_{im}*, the set of immediate transitions with waiting time zero, and*
  - T_{timed}*, the set of transitions with deterministic waiting time.*
- F *is refined as the union of two disjoint arc sets, i.e.,* $F := F_N \cup F_I$ *with:*
  - $F_N \subseteq (P \times T) \cup (T \times P)$ *is the set of directed standard arcs,*
  - $F_I \subseteq P \times T$ *is the set of directed inhibitor arcs.*
- $v : TI(T_{stoch}) \rightarrow H$ *is a function that assigns a stochastic hazard function* $h(t(b))$ *to each transition instance* $t(b) \in TI(t)$ *of each transition* $t \in T_{stoch}$*, whereby* $H := \bigcup_{t(b) \in TI(T)} \{h_{t(b)} | h_{t(b)} : \mathbb{N}_0^{|{}^\bullet t(b)|} \rightarrow \mathbb{R}^+\}$ *is the set of all stochastic hazard functions, and* $v(t(b)) = h(t(b))$ *for all transitions* $t \in T_{stoch}$*.*
- $l : TI(T_{timed}) \rightarrow \mathbb{R}^+$ *assigns a non-negative deterministic waiting time to each transition instance* $t(b) \in TI(t)$ *of each deterministic transition* $t \in T_{timed}$*.*

Please note, the stochastic hazard function in SPN^C is defined for each transition instance of each colored transition. The domain of $h(t(b))$ is restricted to the set of preplace instances of $t(b)$, denoted by ${}^\bullet t(b)$ with ${}^\bullet t(b) := \{p(c) \in PI(P) | f(p(c), t(b)) \neq 0\}$. For sake of simplicity, such features as read arcs and scheduled transitions are not explicitly mentioned in the definition above. For the semantics of SPN^C refer to [HLG+09].

Colored Petri nets, such as QPN^C and SPN^C, allow to build more compact and parametric representations of biological systems by, e.g., folding similar subnets which are then distinguished by colors. Therefore, it is possible to concisely represent complex systems that would have required a huge low-level Petri net. This provides an effective way to model and simulate very complex biological systems which would have been difficult with other modeling approaches.

3 Colored Petri net implementation in Snoopy

Snoopy is a generic and adaptive tool for modeling and animating/simulating hierarchical graph-based formalisms. Snoopy runs on Windows, Linux, and Mac operating systems. It is available free of charge for non-commercial use, and can be obtained from our website [Sno10]. However QPN^C and SPN^C are still prototypes and thus not included in the official release so far.

Snoopy provides the following functionalities for QPN^C and SPN^C:

- Rich data types for color set definition, consisting of dot, integer, string, Boolean, enumeration, index, product and union. The user can use these data types to define distinguishable tokens.

- Colored Petri net models as drawn as usual, and automatic syntax checking of declarations and expressions.
- Automatic animation, and single-step animation by manually choosing a binding. Thus, the user can run animation automatically or control the animation manually.
- Simulation is done on an automatically unfolded Petri net, and simulation results for colored or uncolored places/transitions are given together or separately. This functionality only applies to SPN^C.
- Several simulation algorithms to simulate SPN^C, including the Gillespie stochastic simulation algorithm (SSA) [Gil77].
- QPN^C and SPN^C are exported to different net formalisms, and thus can be analyzed by different tools such as CHARLIE [Fra09] and IDD-CSL [SH09].

In addition, there are some functionalities and features that are especially helpful for modeling biological systems, which are described as follows.

- Concise specification of initial markings. In a biological model, there are often large quantities of species to be modeled. So the initial markings may be set in many different ways.
  - Specifying the color and its corresponding tokens as usual.
  - Specifying a set of colors with the same number of tokens.
  - Using a predicate to choose a set of colors and then specifying the number of tokens.
  - Using the $all()$ function to specify a specific number of tokens for all colors.
- Specifying a rate function for each instance of a colored transition. For a transition, we may define different rate functions for different transition binding instances, and we use predicates to reach this goal.
- Supporting several extended arc types, such as inhibitor arc, read arc (often also called test arcs), equal arc, reset arc, and modifier arc, which are popular add-ons enhancing modeling comfort [HRR+08].
- Supporting extended transitions. Snoopy supports stochastic transitions with freestyle rate functions and rate functions of some predefined patterns as well as several deterministically timed transition types: immediate firing, deterministic firing delay, and scheduled firing (see [HLG+09] for details).

All these functionalities and features for QPN^C and SPN^C facilitate the modeling and simulation of biological systems. As a result, we not only can obtain a more compact and readable model for a complex biological system, but also do not lose simulation or analysis capabilities compared with low-level Petri nets.

4 Constructing colored Petri net models

In this section, we will demonstrate how to construct a colored Petri net model using Snoopy. We first show how to construct basic colored Petri net components, and then present two examples to illustrate QPN^C and SPN^C, respectively.

4.1 Constructing basic colored Petri net components

The key step in the design of a colored Petri net is to construct basic colored Petri net units, through which we can obtain the whole colored Petri net model step by step. This process is also called folding. In the following we will introduce some folding ways to construct basic colored Petri net components, which are illustrated in Fig. 2.

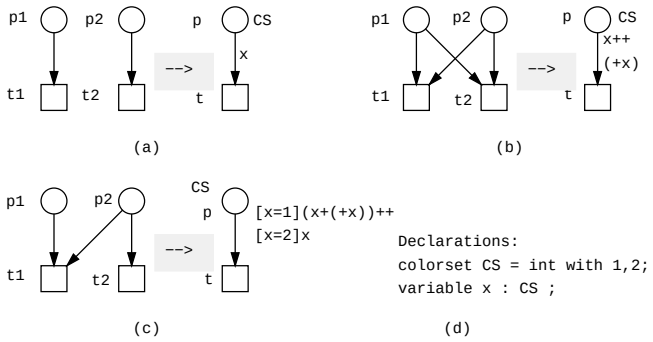

Fig. 2. Basic colored Petri net components.

Fig. 2(a) shows the folding of two isolated subnets with the same structure. For this simple case, we can define a color set containing two colors. For example, we define the color set as "CS" with two integer colors: 1 and 2 (see Fig. 2(d)). We then assign the color set "CS" to the place. We define the arc expression as x, where x is a variable of the type "CS". Thus, we get a basic colored Petri net component, illustrated on the right hand of Fig. 2(a).

In Fig. 2(b), the net to be folded is extended by two extra arcs from p2 (p1) to t1 (t2), respectively. To fold it, we use the same color set, and just modify the arc expression to $x++(+x)$, where the "+" in the $(+x)$ is the successor operator, which returns the successor of x in an ordered finite color set. If x is the last color, then it returns the first color. The "++" is the multiset addition operator.

In Fig. 2(c), the net to be folded gets one extra arc from p2 to t1. To fold it, we use the same color set, and just modify the arc expression to $[x = 1](x++(+x))++[x = 2]x$, meaning: if $x = 1$, then there are two arcs connecting p with t, while if $x = 2$, then there is only one arc connecting p with t.

In summary, the following rules apply when folding two similar nets to a colored Petri net. If the two subnets share the same structure, we just have to define a color set and set arc expressions without predicates. If the subnets are similar, but not the same in structure, we may need to define arc expressions with predicates or guards. However, in either case, if we want to continue to

add other similar nets, what we should do is usually to add new colors, and slightly change arc expressions or guards. Using these basic colored Petri net components, we can construct the whole colored Petri net model step by step.

In the next two sections, we will give two simple examples to demonstrate the application of colored Petri nets. The first example is to demonstrate QPN^C, and the second one is to demonstrate SPN^C.

4.2 Cooperative ligand binding

We consider an example of the binding of oxygen to the four subunits of a hemoglobin heterotetramer. The hemoglobin heterotetramer in the high and low affinity state binds to none, one, two, three or four oxygen molecules. Each of the ten states is represented by a place and oxygen feeds into the transitions that sequentially connect the respective places. The qualitative Petri net model is illustrated in Fig. 3 (taken from [MWW09]).

Using the folding ways demonstrated above we obtain for Fig. 3 a QPN^C model (Fig. 4), and further a more compact QPN^C model (Fig. 5). From Fig. 4, we can see that the colored Petri net model reduces the size of the corresponding low-level Petri net model. Moreover, comparing Fig. 4 with Fig. 5, we can also see that we can build colored Petri net model with different level of structural details, which is especially helpful for modeling complex biological systems. After automatic unfolding, these two colored models yield exactly the same Petri net model as given in Fig. 3, i.e., the colored models and the uncolored model are equivalent. The declarations for these two QPN^C models of the cooperative ligand binding are given in Table 1.

From these two colored nets, we can also see that the folding operation does reduce the size of the net description for the prize of more complicated inscriptions. The graphic complexity is reduced, but the annotations of nodes and edges creates a new challenge. This is not unexpected since a more concise write-up must rely on more complex components. Therefore, it is necessary to build a colored Petri net model at a suitable level of structural details.

Table 1. Declarations for the QPN^C models of the cooperative ligand binding.

Declarations
colorset Dot = dot;
colorset HbO2 = int with 0-4;
colorset Level = enum with H,L;
colorset P = product with HbO2 ×Level;
variable x: HbO2;
variable y: Level;

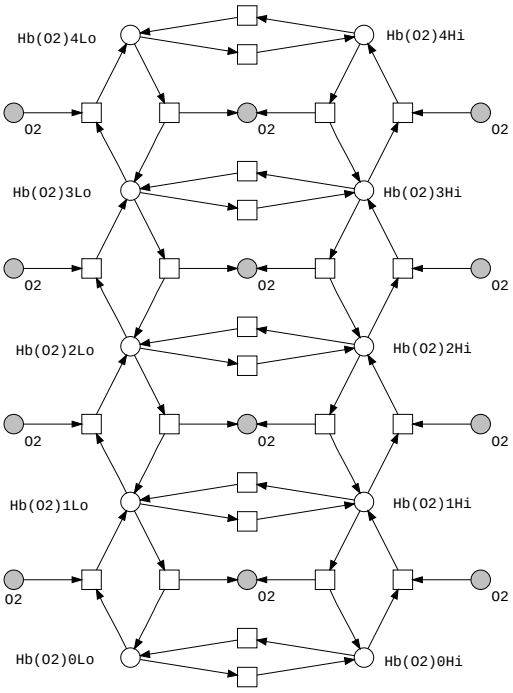

Fig. 3. Cooperative binding of oxygen to hemoglobin represented as a Petri net model. For clarity, oxygen is represented in the form of multiple copies (logical places) of one place.

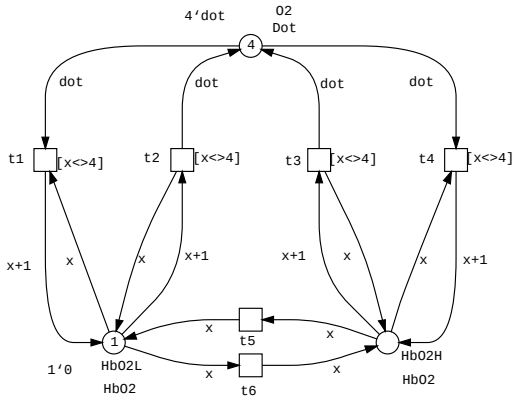

Fig. 4. QPN^C model for the cooperative binding of oxygen to hemoglobin, given as a low-level Petri net in Fig. 3. For declarations of color sets and variables, see Table 1.

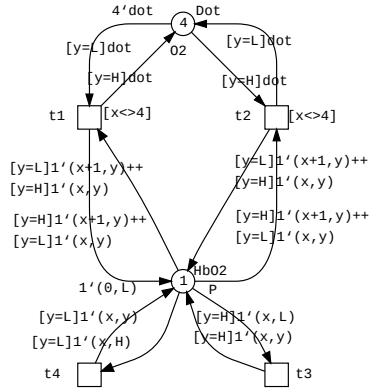

Fig. 5. QPN^C model for the cooperative binding of oxygen to hemoglobin, given as a low-level Petri net in Fig. 3. For declarations of color sets and variables, see Table 1.

4.3 Repressilator

In this section, we will demonstrate the SPN^C using an example of a synthetic circuit - the repressilator, which is an engineered synthetic system encoded on a plasmid, and designed to exhibit oscillations [EL00]. The repressilator system is a regulatory cycle of three genes, for example, denoted by g_a, g_b and g_c, where each gene represses its successor, namely, g_a inhibits g_b, g_b inhibites g_c, and g_c inhibites g_a. This negative regulation is realized by the repressors, p_a, p_b and p_c, generated by the genes g_a, g_b and g_c respectively [LB07].

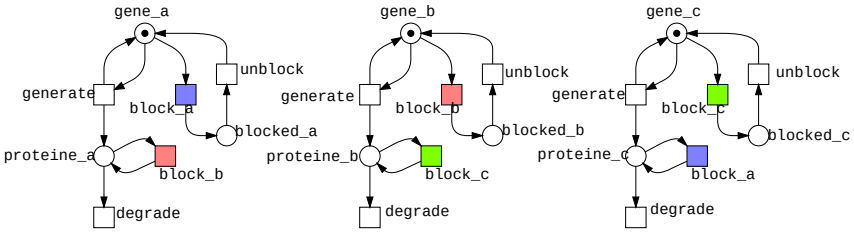

Fig. 6. Stochastic Petri net model for the repressilator. The highlighted transitions are logical transitions.

As our purpose is to demonstrate the SPN^C, we only consider a relatively simple model of the repressilator, which was built as a stochastic π-machine in [BCP08]. Based on that model, we build a stochastic Petri net model (Fig. 6), and further a SPN^C model for the repressilator (shown on the left hand of Fig.

7). This colored model when unfolded yields the same uncolored Petri net model in Fig. 6.

Table 2 gives the declarations for this SPN^C model. There are three colors, a, b, and c to distinguish three similar components in Fig. 6. The predecessor operator "-" in the arc expression $-x$ returns the predecessor of x in an ordered finite color set. If x is the first color, then it returns the last color.

As described above, the SPN^C will be automatically unfolded to a stochastic Petri net, and can be simulated with different simulation algorithms. On the right hand of Fig. 7 a snapshot of a simulation run result is given. The rate functions are given in Table 3 (coming from [PC07]). The SPN^C model exhibits the same behavior compared with that in [PC07].

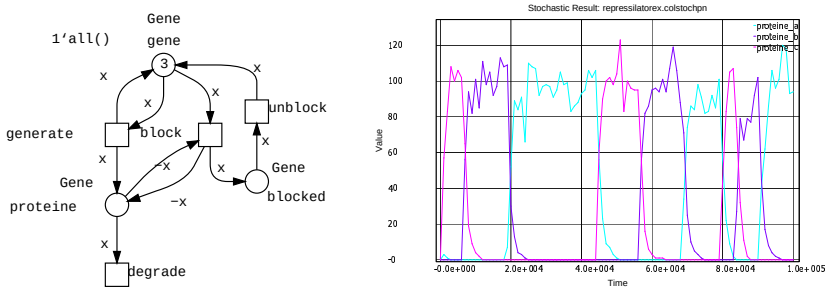

Fig. 7. SPN^C model of the low-level Petri net given in Fig. 6, and one simulation run plot for the repressilator. For rate functions, see Table 3.

Table 2. Declarations for the SPN^C model of the repressilator.

Declarations
colorset Gene = enum with a,b,c;
variable x: Gene;

From Fig. 7, we can see that the SPN^C model reduces the size of the original stochastic Petri net model to one third. More importantly, when other similar subnets have to be added, the model structure does not need to be modified and what has to be done is only to add extra colors.

For example, we consider the generalized repressilator with an arbitrary number n of genes in the loop that is presented in [MHE+06]. To build its SPN^C model, we just need to modify the color set as n colors, and do not need to

Table 3. Rate functions for the SPN^C model of the repressilator.

Transition	Rate function
generate	$0.1 * gene$
block	$1.0 * proteine$
unblock	$0.0001 * blocked$
degrade	$0.001 * proteine$

modify anything else. For example, Fig. 8 gives the conceptual graph of the generalized repressilator with $n = 9$ (on the left hand), and one simulation plot (on the right hand), whose rate functions are the same as in Table 3. Please note, the SPN^C model for the generalized repressilator is the same as the one for the three-gene repressilator, and the only difference is that we define the color set as n colors rather than 3 colors. This demonstrates a big advantage of color Petri nets, that is, to increase the colors means to increase the size of the net.

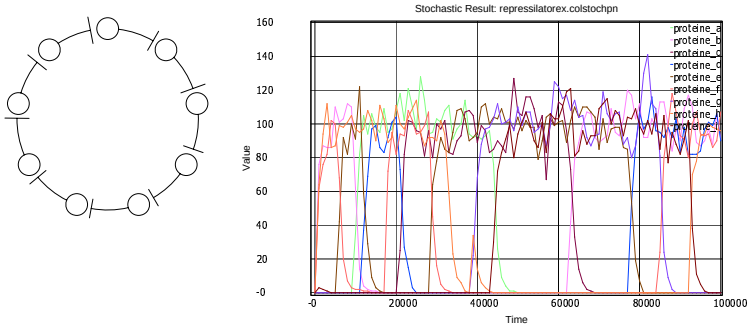

Fig. 8. Conceptual graph and one simulation run plot for the repressilator with 9 genes.

5 Related work

Heiner et al. modeled metabolic pathways with high-level Petri nets using the software packages Design/CPN [Des01]. Colors discriminate metabolites, and thus they got a number of valuable insights by combining symbolic analysis and simulation for colored metabolic steady state system models [HKV01]. Genrich et al. discussed the steps to establish and tune high-level net models, and

modeled metabolic pathways of the glycolysis and citric acid cycle with colored Petri nets using also Design/CPN. By assigning enzymatic reaction rates to the transitions, they implemented the simulation and quantitative study of networks of metabolic processes [GKV01]. Bahi-Jaber et al. investigated the application of colored stochastic Petri nets to epidemic models using a very simple model [BP03]. Although this study had no tool support, it really demonstrated the advantages of colored stochastic Petri nets. Runge described a systematic semi-automatic procedure, exploiting the place/transition net's T-invariants to construct an equivalent bounded and live coloured net. As case study, an extended glycolysis was used [Run04]. However, he only considered modeling and qualitative analysis of biological model based on CPN tools [JKW07]. Lee et al. built a colored Petri net model for the signal transduction system stimulated by epidermal growth factor (EGF) based on CPN tools, in which they use the conservation and kinetic equations to quantitatively examine the dynamic behavior of the EGF signaling pathway [LYL+06]. Tubner et al. used the UML class diagram to understand the static structure of molecules involved in the TLR4 pathway, and then modeled and simulated the TLR4 pathway to get the behavior of the system with colored Petri nets based on CPN tools [TMK+06]. In their model, they did not consider any time information.

In summary, the existing studies usually resort to Design/CPN or its successor CPN tools to realize the modeling and analysis of biological systems. But CPN tools are not designed for modeling and analyzing biological systems. So it is not suitable in many aspects, like rate function definition and simulative analysis by stochastic simulation algorithms.

In contrast, in Snoopy we provide specific functionalities and features to support editing, simulating, and analyzing of biological models based on colored Petri nets, as shown in Section 3.

6 Conclusion and outlook

In this paper we have described our on-going work of a colored Petri net-based framework to model, simulate, and analyze complex biological systems. This framework consists of three parts: QPN^C, SPN^C, and CPN^C, and only the first two parts have been described in this paper. Their definitions are given, and functionalities and features implemented in Snoopy are described, followed by two examples to demonstrate their application. The colored Petri nets allow a more concise representation of biological systems, making it possible and convenient to construct and analyze large-scale biological models.

We are working on improvements of these two paradigms: QPN^C and SPN^C. In the next step, we will focus on the development of analysis tools for SPN^C, and we will include the CPN^C in our work. We are also developing a method to automatically create colored Petri nets from non-coloured Petri nets (automatic folding). This development will provide much stronger support to construct and analyze large-scale biological models. Besides, we are working on a case study

with a size of the underlying uncolored model of about 110,000 places and 135,000 transitions.

Acknowledgments

This work has been supported by the Modeling of Pain Switch (MOPS) program of Federal Ministry of Education and Research (Funding Number: 0315449H). We would like to thank Wolfgang Marwan, Christian Rohr, and Martin Schwarick for their assistance in model construction and software development. We also would like to thank the anonymous referees for many constructive comments.

References

[BCP08] R. Blossey, L. Cardelli, A. Phillips: Compositionality, Stochasticity and Cooperativity in Dynamic Models of Gene Regulation. HFSP Journal. 2(1), 17-28 (2008)

[BP03] N. Bahi-Jaber, D. Pontier: Modeling Transmission of Directly Transmitted Infectious Diseases Using Colored Stochastic Petri Nets. Mathematical Biosciences. 185, 1-13 (2003)

[Des01] Design/CPN: http://www.daimi.au.dk/designCPN. (2001)

[EL00] M. B. Elowitz, S. Leibler: A Synthetic Oscillatory Network of Transcriptional Regulators. Nature. 403, 335-338 (2000)

[Fra09] A. Franzke: Charlie 2.0 - a Multi-Threaded Petri Net Analyzer. Diploma Thesis, Brandenburg University of Technology Cottbus. (2009)

[Ger01] R. German: Performance Analysis of Communication Systems With Non-Markovian Stochastic Petri Nets. John Wiley and Sons Ltd. (2001)

[GH06] D. Gilbert, M. Heiner: From Petri Nets to Differential Equations - an Integrative Approach for Biochemical Network Analysis. Proc. ICATPN. LNCS, 4024, 181-200 (2006)

[GHL07] D. Gilbert, M. Heiner, S. Lehrack : A Unifying Framework for Modelling and Analysing Biochemical Pathways Using Petri Nets. Proc. International Conference on Computational Methods in Systems Biology. LNCS/LNBI, 4695, 200-216 (2007)

[GKV01] H. Genrich, R. Kffner, K. Voss: Executable Petri Net Models for the Analysis of Metabolic Pathways. International Journal on Software Tools for Technology Transfer. 3(4), 394-404 (2001)

[Gil77] D. T. Gillespie: Exact Stochastic Simulation of Coupled Chemical Reactions. Journal of Physical Chemistry. 81(25), 2340-2361 (1977)

[HGD08] M. Heiner, D. Gilbert, R. Donaldson: Petri Nets for Systems and Synthetic Biology. In Schools on Formal Methods (SFM), LNCS, 5016, 215-264 (2008)

[HK09] A. P. Heath, L. E. Kavraki: Computational Challenges in Systems Biology. Computer Science Review. 3(1), 1-17 (2009)

[HKV01] M. Heiner, I. Koch, K. Voss: Analysis and Simulation of Steady States in Metabolic Pathways with Petri Nets. Proc. Third Workshop CPN. Univ. of Aarhus, 15-34 (2001)

[HLG+09] M. Heiner, S. Lehrack, D. Gilbert, W. Marwan: Extended Stochastic Petri Nets for Model-based Design of Wetlab Experiments. Transaction on Computational Systems Biology XI. LNCS/LNBI, 5750, 138-163 (2009)

[HRR+08] M. Heiner, R. Richter, C. Rohr, M. Schwarick: Snoopy - A Tool to Design and Execute Graph-Based Formalisms. [Extended Version]. Petri Net Newsletter. 74, 8-22 (2008)

[Jen81] K. Jensen: Coloured Petri Nets and the Invariant-Method. Theor. Comput. Sci. 14, 317-336 (1981)

[JKW07] K. Jensen, L. M. Kristensen, L. M. Wells: Coloured Petri Nets and CPN Tools for Modelling and Validation of Concurrent Systems. International Journal on Software Tools for Technology Transfer. 9(3/4) 213-254 (2007)

[JP98] P. J. E. Goss, J. Peccoud: Quantitative Modeling of Stochastic Systems in Molecular Biology by Using Stochastic Petri Nets. Proc. Natl. Acad. Sci. 95, 6750-6755 (1998)

[LB07] A. Loinger, O. Biham: Stochastic Simulations of the Repressilator Circuit. Phisical Review. 76(5), 051917(9) (2007)

[LYL+06] D. Lee, R. Zimmer, S. Lee, S. Park: Colored Petri Net Modeling and Simulation of Signal Transduction Pathways. Metabolic Engineering. 8, 112-122 (2006)

[MBC+95] M. Ajmone Marsan, G. Balbo, G. Conte, S. Donatelli, and G. Franceschinis: Modelling with Generalized Stochastic Petri Nets. Wiley Series in Parallel Computing. John Wiley and Sons, 2nd Edition. (1995)

[MHE+06] S. Muller, J. Hofbauer, L. Endler, C. Flamm, S. Widder, P. Schuster: A Generalized Model of the Repressilator. Journal of Mathematical Biology. 53, 905-937 (2006)

[Mur89] T. Murata: Petri Nets: Properties, Analysis and Applications. Proc.of the IEEE. 4, 541-580 (1989)

[Mur07] I. Mura: Simplifying the Stochastic Petri Nets Formalism for Representing Biological Phenomena. Technical Report TR-19-2007, CoSBi (Center for Computational and Systems Biology), University of Trento (2007)

[MWW09] W. Marwan, A. Wagler, R. Weismantel: Petri Nets as a Framework for the Reconstruction and Analysis of Signal Transduction Pathways and Regulatory Networks. Natural Computing. 9 (2009)

[NOG+05] T. Nutsch, D. Oesterhelt, E. D. Gilles, W. Marwan: A Quantitative Model of the Switch Cycle of an Archaeal Flagellar Motor and Its Sensory Control. Biophysical Journal. 89(4), 2307-2323 (2005)

[PC07] A. Phillips, L. Cardelli: Efficient, Correct Simulation of Biological Processes in the Stochastic Pi-calculus. Proc. Computational Methods in Systems Biology. LNCS, 4695, 184-199 (2007)

[PRA05] M. Peleg, D. Rubin, R. B. Altman: Using Petri Net Tools to Study Properties and Dynamics of Biological Systems. Journal of the American Medical Informatics Association. 12(2), 181-199 (2005)

[RML93] V. N. Reddy, M. L. Mavrovouniotis, M. N. Liebman: Petri Net Representation in Metabolic Pathways. Proc. First International Conference on Intelligent System for Molecular Biology. 328-336 (1993)

[Run04] T. Runge: Application of Coloured Petri Nets in Systems Biology. Proc. 5th Workshop CPN. 77-95 (2004)

[SH09] M. Schwarick, M. Heiner: CSL Model Checking of Biochemical Networks with Interval Decision Diagrams. Proc. 7th International Conference on Computational Methods in Systems Biology (CMSB 2009), Springer LNBI 5688, 296-312 (2009)

[Sno10] Snoopy Website: Snoopy - Tool to Design and Animate/Simulate Graphs. http://www-dssz.informatik.tu-cottbus.de/software/snoopy.html (2010)

[TMK+06] C. Tubner, B. Mathiak, A. Kupfer, N. Fleischer, S. Eckstein: Modelling and Simulation of the TLR4 Pathway with Coloured Petri Nets. Proc. IEEE EMBS Annual International Conference. 2009-2012 (2006)

Control of Metabolic Systems Modeled with Timed Continuous Petri Nets

Roberto Ross-León[1], Antonio Ramirez-Treviño[1], José Alejandro Morales[2], and Javier Ruiz-León[1]

[1] Centro de Investigaciones y Estudios Avanzados del I.P.N. Unidad Guadalajara
{rross,art,jruiz}@gdl.cinvestav.mx
[2] Centro Universitario de Ciencias Exactas e Ingenierías, Universidad de Guadalajara
alejandro.morales@cucei.udg.mx

Abstract. This paper is concerned with the control problem of biological systems modeled with Timed Continuous Petri Nets under infinite server semantics. This work introduces two main contributions. The first one is a bottom-up modeling methodology that uses $TCPN$ to represent cell metabolism.
The second contribution is the control wich solves the Regulation Control Problem (RCP) (to reach a required state and maintain it). The control is based on a Lyapunov criterion that ensures reaching the required state.

Key words: Cell metabolome, Petri nets, Controllability, Stability.

This work was supported by project No. 23-2008-335, COETCYJAL-CEMUE, Mexico. R. Ross-León was supported by CONACYT, grant No. 13527.

1 Introduction

Petri nets PN [1], [2], [3] are a formal paradigm for modelling and analysis of systems that can be seen as discrete dynamical systems. Unfortunately, due to state explosion problem, most of the analysis techniques cannot be applied in heavy marked Petri nets. In order to overcome this problem, the Petri net community developed the Timed Continuous Petri Nets ($TCPN$) [4], [5], a relaxation of the Petri Nets where the marking becomes continuous and the state equation is represented by a positive, bounded set of linear differential equations.

The main $TCPN$ characteristics such as the nice pictorially representation, the mathematical background, the synchronization of several products to start an activity and the representation of causal relationship make $TCPN$ amenable to represent biochemical reactions and cell metabolism. In fact $TCPN$ marking captures the concentration of molecular species while differential equations together with the firing vectors represent the reaction velocity and the graph captures the metabolic pathways. The entire $TCPN$ captures the cell metabolome.

Several works model [6], [7], analyse [8], [9] and control [10], [11] metabolic pathways. Most of them deal with pseudo-steady states of the biochemical reaction dynamic. Nowadays, the scientific community is exploring the use of PN and

their extensions [12], [13] to model biological systems since the former are able to capture the compounds flow, the reaction velocity, the enabling/inhibiting reactions and both the transitory and steady states of reaction dynamic into a single formalism.

This work is concerned on how to model the entire metabolome with $TCPN$. It proposes a bottom-up modeling methodology where biochemical reactions are modeled through elementary modules, and shows how these modules are merged to form metabolic pathways, and at the end the cell metabolism. The resulting model captures both, the transitory and steady state metabolome dynamics. It is worth noticing that the derived $TCPN$ model condenses several particular behaviors represented by the set of differential equations generated by the $TCPN$ itself. For instance, a single transition with four input places (a reaction needing four substrates) generates a set of four possible differential equations while two transitions with four input places each will generate a set of sixteen possible differential equations. Therefore highly complex behaviors emerging from few compounds interacting can be captured by $TCPN$.

This work also presents the control problem of reaching a required state (marking) representing a certain metabolite concentration. In order to solve this problem, an error equation is stated and stabilized using a Lyapunov approach. The solution is the reaction rate vector which is greater or equal to zero and lower or equal to the maximum settled by the kinetics of Michaelis-Menten for the current enzyme concentration. Thus, if a solution exists, it could be implemented *in vivo* by directed genetic mutation, knock-in (or knock-out) strategies or pharmacological effects.

Present paper is organized as follows. Section 2 gives $TCPN$ basic definitions, controllability and cell metabolic concepts. Next section introduces the proposed metabolome modeling methodology. Section 4 presents the problem of reaching a required state and synthesizes Lyapunov like transition flow for solving this problem. Following section presents an illustrative example to show the performance of the computed control law. In the last section the conclusions and future work are presented.

2 Basic Definitions

This section presents briefly the basic concepts related with PN, *Continuous* PN and $TCPN$. An interested reader can review [3], [14], [15] and [16] for further information. At the end of this section a useful form of the state equation for $TCPN$ under infinite server semantics is presented.

2.1 Petri Net concepts

Definition 1. *A Continuous Petri Net (ContPN) system is a pair* (N, m_0)*, where* $N = (P, T, Pre, Post)$ *is a Petri net structure (PN) and* $m_0 \in \{\mathbb{R}^+ \cup 0\}^{|P|}$ *is the initial marking.* $P = \{p_1, ..., p_n\}$ *and* $T = \{t_1, ..., t_k\}$ *are finite sets of elements named places and transitions, respectively.* $Pre, Post \in \{\mathbb{N} \cup 0\}^{|P| \times |T|}$

are the Pre and Post incidence matrices, respectively, where $Pre[i,j]$, $Post[i,j]$ represent the weights of the arcs from p_i to t_j and from t_j to p_i, respectively. The Incidence matrix denoted by C is defined by $C = Post - Pre$.

Each place p_i has a marking denoted by $m_i \in \{\mathbb{R}^+ \cup 0\}$. The set ${}^\bullet t_i = \{p_j \mid Pre[j,i] > 0\}$, $(t_i^\bullet = \{p_j \mid Post[j,i] > 0\})$ is the preset (postset) of t_i. Similarly the set ${}^\bullet p_i = \{t_j \mid Post[i,j] > 0\}$, $(p_i^\bullet = \{t_j \mid Post[i,j] > 0\})$ is the preset (postset) of p_i.

A transition $t_j \in T$ is enabled at marking m iff $\forall p_i \in {}^\bullet t_j$, $m_i > 0$. Its enabling degree is:

$$enab(t_j, m) = \min_{p_i \in {}^\bullet t_j} \frac{m_i}{Pre\,[i,j]} \tag{1}$$

and it is said that m_i constraints the firing of t_j. Equation (1) denotes the maximum amount that t_j can be fired at marking m; indeed t_j can fire in any real amount α, where $0 < \alpha < enab(t_j, m)$ leading to a new marking $m\prime = m + \alpha C[\bullet, j]$. If m is reachable from m_0 through a finite sequence σ of enabled transitions, then m can be computed with the equation:

$$m = m_0 + C\sigma \tag{2}$$

named the *ContPN* state equation, where $\sigma \in \{\mathbb{R}^+ \cup 0\}^{|T|}$ is the firing count vector, i.e., σ_j is the cumulative amount of firing of t_j in the sequence σ. The set of all reachable markings from m_0 is called the reachability space and it is denoted by $RS\,(N, m_0)$. In the case of a *ContPN* system, $RS\,(N, m_0)$ is a convex set [17].

Definition 2. *A contPN is bounded when every place is bounded ($\forall p \in P, \exists b_p \in \mathbb{R}$ with $m\,[p] \leq b_p$ at every reachable marking m). It is live when every transition is live (it can ultimately occur from every reachable marking). Liveness is extended to lim-live when infinitely long sequence can be fired. A transition t is non lim-live iff a sequence of successively reachable markings exists which converge to a marking such that none of its successors enables a transition t.*

2.2 Timed continuous Petri nets

Definition 3. *A timed ContPN is the 3-tuple $TCPN = (N, \lambda, m_0)$, where N is a ContPN, $\lambda : T \to \{\mathbb{R}^+\}^{|T|}$ is a function that associates a maximum firing rate to each transition, and m_0 is the initial marking of the net N.*

The state equation of a $TCPN$ is

$$\overset{\bullet}{m}(\tau) = Cf(\tau) \tag{3}$$
$$\text{where } f(\tau) = \overset{\bullet}{\sigma}(\tau)$$

And under the infinite server semantics, the flow of transition t_j is given by

$$f_j(\tau) = \lambda_j enab(t_j, m(\tau)) \tag{4}$$

where λ_j represents the maximum firing rate of transition t_j. Notice that $TCPN$ under infinite server semantics is a piecewise linear system (a class of hybrid systems) due to the *minimum* operator that appears in the enabling function of the flow definition.

Definition 4. *A configuration of a $TCPN$ at m is a set of (p,t) arcs describing the effective flow of all transitions.*

$$\Pi(m)[i,j] = \begin{cases} \frac{1}{Pre[i,j]} & \text{if } p_i \text{ is constraining } t_j \\ 0 & \text{otherwise} \end{cases} \tag{5}$$

Definition 5. *The maximum firing rate matrix is denoted by*

$$\Lambda = diag\left(\lambda_1, \ldots, \lambda_{|T|}\right). \tag{6}$$

According to previous notation, the state equation and the flow vector are described by:

$$\begin{aligned} \dot{m} &= C\Lambda\Pi(m) \cdot m \\ f &= \Lambda\Pi(m) \cdot m \end{aligned} \tag{7}$$

The only action that can be applied to a $TCPN$ system is to slow down the firing flow. The forced flow of a controlled transition t_i becomes $f_i - u_i$ where f_i is the flow of the unforced system (i.e. without control) and u is the control action, with $0 \leq u_i \leq f_i$. The controlled state equation is:

$$\dot{m} = C\left[\Lambda\Pi(m) \cdot m - u\right] \tag{8}$$

$$0 \leq u_i \leq \left[\Lambda\Pi(m) \cdot m\right]_i \tag{9}$$

In order to obtain a simplified version of the state equation, the input vector u is rewritten as $u = I_u\Lambda\Pi(m) \cdot m$, where $I_u = diag\left(I_{u_1}, \ldots, I_{u_{|T|}}\right)$ and $0 \leq I_{u_i} \leq 1$. Then the matrix $I_c = I - I_u$ is constructed and the controlled state equation can be rewritten as:

$$\dot{m} = CI_c\Lambda\Pi(m) \cdot m \tag{10}$$

Notice that $0 \leq I_{c_i} \leq 1$.

2.3 Controllability

The classical linear systems definition of controllability cannot be applied to $TCPN$ systems because the required hypothesis are not fulfilled, that is, the input should be unbounded and the state space should be $\mathbb{R}^{|P|}$. The next definitions are taken from [18].

Definition 6. *Let N be net of a $TCPN$. The structural admissible states set is defined as $SASS(N) = \{\mathbb{R}^+ \cup \{0\}\}^{|P|}$ (all inital markings that can be imposed to a net). Let B be the base of the left annuller of the incidence matrix C. The equivalence relation $\beta : SASS(N) \rightarrow SASS(N)$ is defined as $m_1 \beta m_2$ iff $B^T m_1 = B^T m_2$, $\forall m_1, m_2 \in SASS(N)$. The system admissible states set is the equivalent class of the initial marking $Class(m_0)$ under β.*

In the sequel, let us denote by $int\left(Class\left(m_0\right)\right)$ the set of relative interior of $Class\left(m_0\right)$.

Definition 7. *Let (N, λ, m_0) be a TCPN system. It is fully controllable with bounded input $(BIFC)$ if there is an input such that for any two markings $m_1, m_2 \in Class\left(m_0\right)$, it is possible to transfer the marking from m_1 to m_2 in finite or infinite time, and the input fulfills (9) along the trajectory, and is controllable with bounded input (BIC) over $S \subseteq Class\left(m_0\right)$ if there is an input such that for any two markings $m_1, m_2 \in S$, it is possible to transfer the marking from m_1 to m_2 in finite or infinite time, and the input fulfills (9) along the trajectory.*

Definition 8. *Let (N, λ, m_0) be a TCPN system. Let $m_r \in RS\left(N, m_0\right)$ and $0 \leq I_{c_r}[i, i] \leq 1$. Then $\left(m_r, I_{c_r}\right)$ is an equilibrium point if $\dot{m}_r = CI_{c_r}\Lambda\Pi\left(m_r\right) \cdot m = 0$. Then, the steady state flow for $\left(m_r, I_{c_r}\right)$ is $f_{ss}\left(m_r, I_{c_r}\right) = I_{c_r}\Lambda\Pi\left(m_r\right) \cdot m_r$.*

An equilibrium point represents a state in which the system can be maintained using the defined control action. Given an initial marking m_0 and a required marking m_r, one control problem is to reach m_r and then keep it. For a further information about equilibrium points an interested reader can review [19].

2.4 Cell Metabolism

For the wellbeing of an given organism, each cell of that organism must transform the substances available in its surroundings to useful molecules. Such transformations take place as chemical reactions catalyzed by enzymes. In these reactions, a substrate tightly binds non-covalently to its enzyme active site to build an enzyme-substrate complex. At that moment, the enzyme chemically changes the substrate into one or more products and then releases it. The enzyme did not suffer any irreversible alterations in the process, and now is free to accept a new substrate [20].

There is no limit to the number of possible reactions occurring in nature. Nonetheless, after exhaustive analysis certain general patterns had emerged that became useful to describe several characteristics of biochemical reactions. In the case where a sole substrate becomes a single product, the reaction process is represented by the scheme:

$$E + S \rightleftharpoons ES \rightarrow EQ \rightleftharpoons E + Q \tag{11}$$

where E is the enzyme, S is the substrate, ES and EQ are the bound complexes and Q is the product.

Typically, the rate of these reactions is settled by the kinetics of Michaelis-Menten [21]. Under this kinetic model, the enzyme and substrate react rapidly to form an enzyme-substrate complex while $[S]$ and $[ES]$ are considered to be at concentration equilibrium (the same applies to $[EQ]$ and $[Q]$), that is, the rate

at which ES dissociates into $E + S$ is much faster than the rate at which ES brakes down to EQ.

Throughout the present work, we will consider a physiological cellular state where $[S] >> [E]$, which means that $[S] \rightleftharpoons [ES]$ equilibrium will always tend to complex formation. Therefore, ES dissociation rate is irrelevant and Scheme 11 can be abbreviated as follows:

$$E + S \rightarrow E + Q \tag{12}$$

where the association-dissociation is implicit.

In reactions with more than one substrate, binding can occur in different sequences; for instance, the following scheme represents an enzyme system with two substrates and all the possible sequences:

$$E + S_1 + S_2 \rightleftharpoons \begin{cases} ES_1 + S_2 \\ \quad \uparrow\downarrow \\ ES_1S_2 \rightarrow E + Q_1 + ... + Q_n \\ \quad \uparrow\downarrow \\ ES_2 + S_1 \end{cases} \tag{13}$$

Frequently the product of an enzyme is the substrate of another reaction and so on, to build a chain of reactions called metabolic pathways represented by $MP^j = \Gamma_1^j \Gamma_2^j \cdots \Gamma_n^j$ where Γ_i^j is a reaction (12) or (13) of a pathway j and Γ_k^j uses one or more products of Γ_i^m. Notice that j and m may represent different pathways.

Then a (Cell) Metabolome is $CM = \left\{ MP^i \,\middle|\, MP^i \text{ is a metabolic pathway} \right\}$, and the purpose of CM is to produce a particular set of metabolites in certain concentrations, essential to that cell.

3 Modelling the Metabolome

In order to model the metabolome using $TCPN$ it is necessary to identify how the elements involved in it will be represented. The next table relates the meaning of each element of the $TCPN$ with respect to metabolic reactions.

TCPN term	**Molecular interpretation**
Place	Molecular Species
Marking	Concentration
Transition	Reaction
Firing Rate	Rate of Reaction
Arc Weights	Stoichiometric Coefficients

The bottom-up approach herein proposed to model the metabolome consists of: a) representing reactions, the results of this stage are the elementary modules; b) merging elementary modules, where places of elementary modules representing the same molecular species on the same physical space in the cell will merge

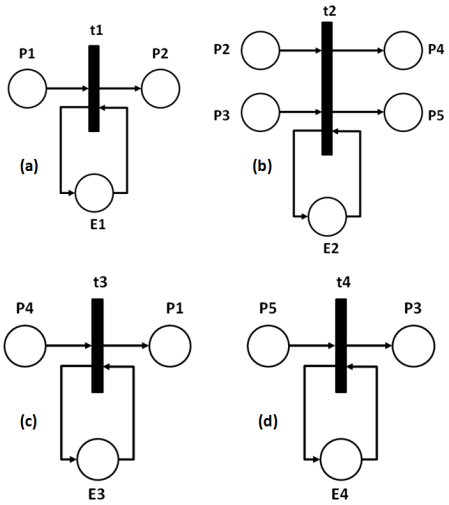

Fig. 1. Four elementary modules representing four diferent reactions.

into a single place. The results of this stage are pathway modules; and c) merging pathways modules, where places of pathways modules representing the same molecular species on the same cellular space will merge into a single place; the result of this stage is the metabolome model. For stages b and c, any specie being protein-mediated transported into a different organelle shall be modeled through the same elementary module, representing instead of substrate and product the same molecule in different spaces.

Next section describes these stages.

3.1 Representing Reactions

In order to represent each reaction Γ_i with $TCPN$ elementary modules representing the Scheme (12) or (13) are constructed. There exists one place p_j for each molecular species at the same physical space ms_j and one transition t_i to represent the reaction Γ_i. There exists one arc (p_s, t_i) if p_s represents a substrate. There exists one arc (t_i, p_q) if p_q represents a product. Finally, there exists a self-loop around p_e and t_i if p_e represents an enzyme. The initial marking $m_0\,[p_j]$ is the concentration of the molecular species ms_j at time $\tau = 0$.

Associated to transition t_i is λ_i representing the rate of reaction.

Example 1. Let $P1 + E1 \rightarrow P2 + E1$ be the Γ_1 reaction. There is one place for each molecular species ($P1$, $P2$ and $E1$), and one transition t_1 representing Γ_1. Finally, arcs are fixed in the way depicted in Figure 1a.

Assuming that the substrate concentration will remain higher than the enzyme concentration (this is an expected behavior of the system), the conflict

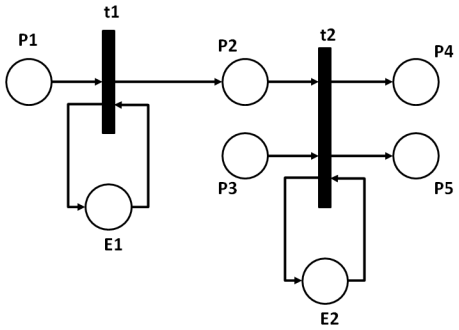

Fig. 2. Example of a Pathway Module.

between substrate and enzyme can be ignored. Hence, if a system has 2^n configurations originated by the n number of enzymes in conflict with substrates, all those configurations are eliminated because $\min([E],[S]) = [E]$ for all $\tau \geq 0$.

3.2 Merging Elementary Modules

Let N^1 and N^2 be two elementary modules, then the merging N is such that $N = (P, T, Pre, Post)$ where $P = P^1 \cup P^2$, $T = T^1 \cup T^2$, $Pre = Pre^1 \cup Pre^2$ and $Post = Post^1 \cup Post^2$. Notice that places representing the same molecular species in the same physical space are merged into a single place.

After a merging of elementary modules is made, pathway modules are obtained.

Example 2. Let $N^1 = \left(P^1, T^1, Pre^1, Post^1\right)$ and $N^2 = \left(P^2, T^2, Pre^2, Post^2\right)$ be two elementary modules showed in Figure 1a and Figure 1b respectively. Then, the merging is $N = (P, T, Pre, Post)$ where $P = P^1 \cup P^2 = \{P1, ..., P5, E1, E2\}$, $T = T^1 \cup T^2 = \{t_1, t_2\}$ and arcs are fixed in the way depicted in Figure 2, where the merging is showed.

3.3 Merging Pathway Modules

Let N^1 be a pathway module and N^2 be a pathway or an elementary module, then the merging N is such that $N = (P, T, Pre, Post)$ where $P = P^1 \cup P^2$, $T = T^1 \cup T^2$, $Pre = Pre^1 \cup Pre^2$ and $Post = Post^1 \cup Post^2$. Notice that places representing the same molecular species are merged into a single place.

After a merging of pathway modules is made, a metabolic model is obtained.

Example 3. Let $N^1 = \left(P^1, T^1, Pre^1, Post^1\right)$ be the pathway module showed in Figure 2. Let $N^2 = \left(P^2, T^2, Pre^2, Post^2\right)$ and $N^3 = \left(P^3, T^3, Pre^3, Post^3\right)$ be two elementary modules showed in Figure 1c and Figure 1d respectively. Then

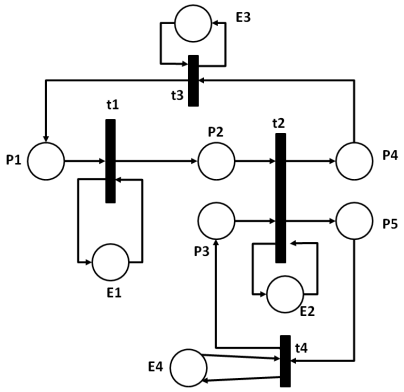

Fig. 3. Metabolic Model.

the merging is $N = (P, T, Pre, Post)$, where $P = \cup P^i = \{P1, ..., P5, E_1, ..., E_4\}$, $T = \cup T^i = \{t_1, t_2, t_3, t_4\}$ for $i = 1, ..., 4$. Arcs are fixed in Figure 3, where the merging is showed.

Although obtained metabolic models could be not live, the addition of a virtual transition and arcs going from the last place representing final products to the virtual transition and from virtual transition to the places representing initial products with an appropriate virtual reaction velocity will make the metabolic model live. For instance, consider the net of Figure 1a, it is a non-live net, but if we add a virtual input transition t_v to the place S and a virtual output transition t_v to the place Q the system will gain liveness, see Figure 4. Notice that t_v must to be the same transition added to the inital and final metabolites, this is because it is necessary to maintain the conservativeness of the matter of the system. This notion is based assuming that each module belongs to a bigger system, therefore, although the real input and output transitions could be not the same, they must have the same firing ratio.

4 Control Law

An important control problem in the metabolic engineering area is to reach a certain metabolome state such that the production of selected metabolites is regulated or particular processes are limited or favored. This problem is captured in $TCPN$ as the reachability problem, i.e. to reach a required state m_r from an initial state m_0 by means of an appropriate control action. This is formalized as follows.

Definition 9. *Let $TCPN$ be a metabolic model. Then the* `Regulation Control Problem` *in (m_r, I_{c_r}) $(RCP(m_r, I_{c_r}))$ deals with the computation of a control law*

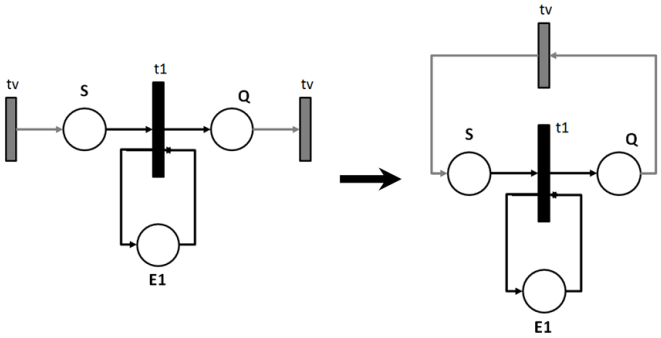

Fig. 4. Module forced to be live with the addition of a virtual transition t_v (in gray).

$I_c(\tau)$, $0 \leq \tau < \tau_f$ *feasible in the TCPN such that* $m(\tau_{ss}) = m_r$ *and* $I_c(\tau_{ss}) = I_{c_r}$, $\forall \tau_{ss} \geq \tau_f$.

In order to solve this problem, some extra places are added to the $TCPN$ metabolic model to detect the material passing through transitions. The following definition shows how these places are added to the $TCPN$.

Definition 10. *Let* (N, m_0, λ) *be a metabolic model* $TCPN$, *where* $N = (P, T, F)$. *Its extension is defined by* $xTCPN = (N_x, m_{0_x}, \lambda)$, *where* $N_x = (P \cup P_a, T, F \cup F_a)$, $|P_a| = |T|$, $m_{0_x} = \left[m_0 \; 0_{|T|} \right]^T$, $F_a = \{(t_i, p_{a_i}) \,|\forall t_i \in T \text{ and } \forall p_{a_i} \in P_a\}$. *Then the incidence matrix of* $xTCPN$ *is* $C_x = \left[C \; I_{|T|} \right]^T$.

Since $\Pi_x(m_x) = \left[\Pi(m) \; 0_{|T| \times |T|} \right]$, then the state equation of $xTCPN$ is:

$$\dot{m}_x = \begin{bmatrix} \dot{m} \\ \dot{m}_a \end{bmatrix} = \begin{bmatrix} CI_c \Lambda \Pi(m) \cdot m \\ I_c \Lambda \Pi(m) \cdot m \end{bmatrix} \tag{14}$$

$$m(0) = m_0, \; m_a(0) = 0 \tag{15}$$

Remark 1. Notice that the extension has the same dynamic over the metabolic model places and the extra places can only increase its marking. In fact, due to the $TCPN$ is live, then by construction the $xTCPN$ is also live. Then there exists at least one enabled transition. Hence $\Pi(m) \cdot m > \mathbf{0}$ (or equivalently $\dot{m}_a \geq \mathbf{0}$, the zero could be forced by an appropriate control law I_c).

Example 4. An example of an extended net is presented in Figure 5.

4.1 Solution to the RCP (m_r, I_{c_r})

Theorem 1. *Let* (N, m_0, λ) *be a metabolic model* $TCPN$ *and let* $xTCPN = (N_x, m_{0_x}, \lambda)$ *be its extension. If* (N, m_0, λ) *is BIC over int* $(Class(m_0))$ *(notice*

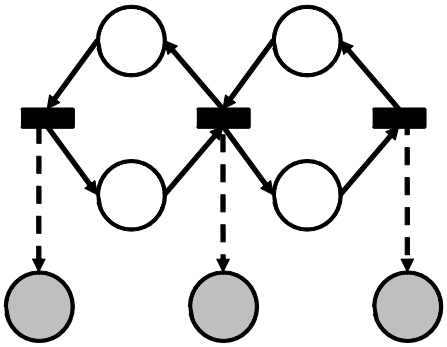

Fig. 5. Example of an extended net. The gray places are the set of added places P_a and the intermittent arrows are the set of added arcs F_a.

that neither the initial marking nor the required marking could be zero components) and (I_{c_r}, m_r) *is an arbitrary equilibrium point, then there exists* $I_c(\tau)$, $0 \leq \tau \leq \tau_f$ *feasible in the TCPN such that* $m(\tau_{ss}) = m_r$, $I_c(\tau_{ss}) = I_{c_r}$, $\forall \tau_{ss} \geq \tau_f$.

Proof. If the system is *BIC* over $int\left(Class\left(m_0\right)\right)$, then there exists a positive solution $\sigma_r(\tau)$ feasible such that

$$m_r = m_0 + C\sigma_r \tag{16}$$

This result was taken from [18]. Thus there exists $f(\tau)$ such that:

$$\int_0^{\tau_f} f(\tau)d\tau = \int_0^{\tau_f} I_c \Lambda \Pi\left(m\right) \cdot m d\tau = \sigma_r \tag{17}$$

From (14):

$$m_a(\tau_f) = \sigma_r \tag{18}$$

Now, let

$$\begin{gathered} e_x(\tau) = \left[e(\tau)\ e_a(\tau)\right]^T,\ 0 \leq \tau \leq \tau_f \\ \left[e(\tau)\ e_a(\tau)\right]^T = \left[m_r - m(\tau)\ \sigma_r - m_a(\tau)\right]^T \end{gathered} \tag{19}$$

and

$$V\left(e_x\right) = e_x^T P_L e_x \tag{20}$$

where

$$P_L = \begin{bmatrix} 0 & 0 \\ 0 & I_{|T|} \end{bmatrix} \tag{21}$$

and $I_{|T|}$ is an identity matrix of order $|T| \times |T|$. We claim that $V\left(e_x\right)$ is a Lyapunov function, i.e it is positive definite and its derivative is negative definite.

Since Equation (20) is clearly non-negative definite, then we assume that (22) is positive semidefinite, then there exists $e_x(\tau') \neq 0$ such that:

$$V\left(e_x(\tau')\right) = \left[\, e^T \; e_a^T \,\right] \begin{bmatrix} 0 & 0 \\ 0 & I_{|T|} \end{bmatrix} \begin{bmatrix} e \\ e_a \end{bmatrix} = 0 \tag{22}$$

From (22), it is clear that $e_a(\tau') = 0$, then from (19) $m_a(\tau') = \sigma_r$. Thus, from (14) and (17) and letting $\tau_f = \tau'$:

$$\begin{aligned} \int_0^{\tau_f} \overset{\bullet}{m}(\tau) d\tau &= C\sigma_r \\ m(\tau_f) - m(0) &= C\sigma_r \end{aligned} \tag{23}$$

Thus, from Equation 16 $m(\tau_f) = m_r$, then $e_x = 0$, a contradiction. Hence $V\left(e_x\right)$ is positive definite.

Now , we prove that $\overset{\bullet}{V}\left(e_x\right)$ is negative definite. The differentiate of $V\left(e_x\right)$ is:

$$\overset{\bullet}{V}\left(e_x\right) = 2e_a^T \overset{\bullet}{e}_a = -2\left[\sigma_r - m_a\right]^T \overset{\bullet}{m}_a \tag{24}$$

Then, choosing I_c such that:

$$I_{c_i} = \begin{cases} 1 \text{ if } m_a\left[i\right] < \sigma_r\left[i\right] \\ 0 \quad otherwhise \end{cases} \tag{25}$$

we obtain:

$$\left[\sigma_r - m_a\right]^T I_c > \mathbf{0} \tag{26}$$

and

$$\left[\sigma_r - m_a\right]^T I_c = 0 \text{ iff } \left[\sigma_r - m_a\right]^T = \mathbf{0}$$

thus $\overset{\bullet}{V}\left(e_x\right) < 0$ and $\overset{\bullet}{V}\left(0\right) = 0$.

Since $m_a(0) = 0$ and it only increase its value, then I_{c_i} is feasible leading from $m_a(0) = 0$ to $m_a(\tau_f) = \sigma_r$, i.e. from m_0 to m_r. Moreover, assuming $m_r \in int\left(Class\left(m_0\right)\right)$ it is reached in finite time because $\overset{\bullet}{m}_a\left[i\right] = m\left(\min\left({}^{\bullet}t_i\right)\right) e^{\lambda\tau}$ and $m\left(\min\left({}^{\bullet}t\right)\right) \neq 0 \; \forall\tau$. At τ_f the control law must be switched from $I_c(\tau_f)$ to $I_c(\tau_{ss}) = I_{c_r}$ and the regulation control problem is solved.

■

The solution to the $RCP\ (m_r, I_{c_r})$ include both, the transitory and steady state control of metabolic systems. It is an improvement to current control solutions, where the biologist and metabolic engineers use stoichiometric non-dynamical approaches such as FBA (Flux Balance Analysis) [22], [23], [24] for the control of metabolic systems. Those are based on a pseudo-stationary state model, represented by the equation:

$$Sv = 0 \tag{27}$$

where S is the matrix of stoichiometry coefficients and the solution v gives the balance of mass for a single equilibrium point at that state (v is the reaction rates vector in a steady state).

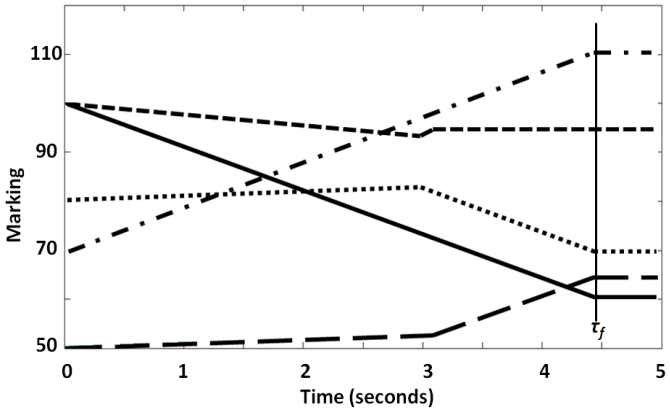

Fig. 6. Marking evolution of the net of Figure 3 applying $RCP\ (m_r, I_{c_r})$.

5 Illustrative Controlling Metabolic System Example

In order to illustrate the $RCP\ (m_r, I_{c_r})$ applied to a metabolic system, suppose the pathway module of Figure 2 together with modules c and d of Figure 1 comprise a cell metabolome. The initial marking used for this example is an arbitrary but physiologically possible initial state for the alleged metabolic model.

Example 5. Let the metabolome model of the Figure 3 be the system $TCPN = (N, \lambda, m_0)$ with $\Lambda = diag\,(2, 3, 4, 1)$ and $m_0 = \left[\begin{array}{cccccccc} 100 & 80 & 100 & 50 & 70 & 5 & 3 & 2 & 4 \end{array}\right]^T$. Let $m_r = \left[\begin{array}{ccccccccc} 95 & 70 & 60 & 65 & 110 & 5 & 3 & 2 & 4 \end{array}\right]^T$ be a required marking. We make the extended system like the procedure showed in the Figure 5. We need the solution of σ_r from $m_r = m_0 + C\sigma_r$. Notice that there are a lot of solutions for σ_r but we only focus on the smallest solution of σ_r. For this example the solution is:

$$\sigma_r = \left[\begin{array}{cccc} 30 & 40 & 25 & 0 \end{array}\right]^T$$

Solving the $RCP\ (m_r, I_{c_r})$ and applying the control (25) to the $TCPN = (N, \lambda, m_0)$, the metabolite concentrations are depicted in Figure 6. The reaction velocities (transition flux) is depicted in Figure 7. Notice that from $\tau = 0$ to $\tau = \tau_f \approx 4.5$ occurs the transitory dynamics, and for $\tau > \tau_f$ the steady state is reached.

Example 6. In Figure 8 the evolution of marking m_a is depicted. When occurs $m_a[i] = \sigma_r[i]$ the control $I_{c_i} = 0$ makes $f_i = 0$ and $m_a[i]$ is maintained until $\tau = \tau_f\ (m_a = \sigma_r)$. Then I_c switches to I_{c_r} for the steady state control.

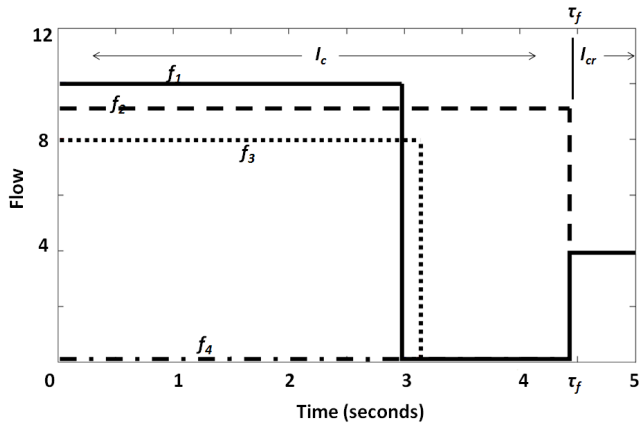

Fig. 7. Reaction velocities (transition flows) of the controlled metabolic model of the Example 5. Notice that $I_c(\tau)$ is applied for $0 \leq \tau < \tau_f$ and $I_{cr}(\tau)$ for $\tau > \tau_f$.

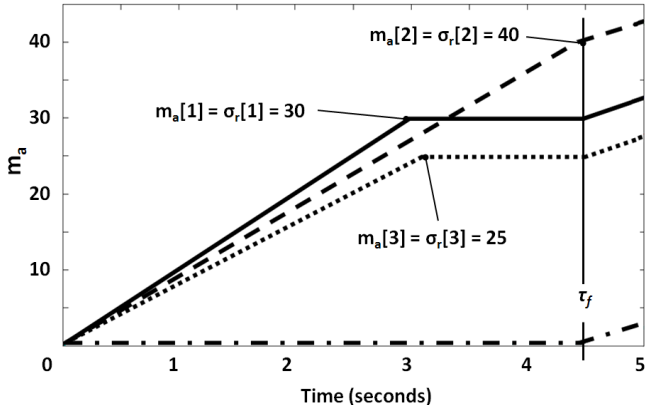

Fig. 8. Marking m_a of the Example 5.

6 Conclusions

This work presented a model methodology to capture the metabolome behavior. It uses a bottom-up approach where each individual biochemical reaction is modeled by elementary $TCPN$ modules and, afterwards, all the modules are merged into a single one to capture the whole metabolome behavior. Such characteristic of the methodology makes it simple and easy to use while the complex cell metabolic behavior is captured. This work also presented the problem of reaching a required metabolome state. The solution to this problem are the instantaneous reaction velocities that are realizable in biological system.

Present results are being applied to optimize metabolome fermentation in the production of tequila and to biofuels generation.

Future perspective involves introduction of stochastic modelling and merging the metabolome with the signaling and genetic networks.

References

1. Murata, T.: Petri nets: Properties, analysis and applications. In: Proceedings of IEEE. Volume 77. (1989) 541–580
2. Javier, Esparza; Manuel, S.: Compositional synthesis of live and bounded free choice petri nets. LNCS **571** (1991) 172–187
3. Jorg Dessel, J.E.: Free Choice Petri Nets. Cambridge University Press (1995)
4. Manuel Silva, L.R.: Continuization of timed petri nets: From performance evaluation to observation and control. 26th International Conference On Application and Theory of Petri Nets and Other Models of Concurrency (2006)
5. R. David, H.A.: Continuous petri nets. In: In Proc. Of the 8th European Workshop on Application and Theory of Petri Nets. (1987) 275–294
6. Peter J. E. Goss, J.P.: Quantitative modeling of stochastic systems in molecular biology by using stochastic petr nets. In: Natl. Acad. Sci. USA. Volume 95. (1998) 6750–6755
7. Masao Nagasaki, Atsushi Doi, H.M.S.M.: Petri net based description and modeling of biological pathways. Algebraic Biology (2005) 19–31
8. Monika Heiner, David Gilbert, R.D.: Petri nets for systems and syntethic biology. (2008) 215–264
9. David Angeli, Patrick De Leenheer, E.S.: A petri net approach to persistance analysis in chemical reaction networks. Biology and Control Theory: Current Challenges (2007) 181–216
10. Riel, N.A.W.V.: Dynamic modelling and analysis of biochemical networks: Mechanism-based models and model-based experiments. Briefings In Bioinformatics **7** (2006) 364–374
11. Nevoigt, E.: Progress in metabolic engineering of saccharomyces cerevisiae. Microbiology And Molecular Biology Reviews **72** (2008) 379–412
12. Mor Peleg, Daniel Rubin, R.B.A.: Using petri net tools to study properties and dynamics of biological systems. Journal of the American Medical Informatics Association **12** (2005) 181–199
13. Hiroshi Matsuno, Atsushi Doi, M.N.S.M.: Hybrid petri net representation of gene regulatory network. Pacific Symposium on Biocomputing **5** (2000) 338–349

14. Cassandras, C.G.: Discrete Event Systems. Modelling and Performance Analysis. Asken Associates (1993)
15. René David, H.A.: Continuous and hybrid petri nets. Journal of Circuites, Systems and Computers **8** (1998) 159–188
16. R. David, H.A.: Continuous petri nets. Proceedings of the 8th European Workshop on Application and Theory of Petri Nets (1987) 275–294
17. Manuel Silva, L.R.: On fluidification of petri net models: From discrete to hybrid and continuous model. Annual Reviews in Control 28 (2004) 253–266
18. C. R. Vázquez, A. Ramírez-Treviño, L.R.M.S.: On controllability of timed continuous petri nets. 11th Int. Workshop Hybrid Systems: Computational and Control **4981** (2008) 528–541
19. Cristian Mahulea, Antonio Ramirez, L.R.M.S.: Steady state control, zero valued poles and token conservation law in continuous net systems. Proceedings of the International Workshop on Control of Hybrid and Discrete Event Systems (2005)
20. Laszlo Kurti, B.C.: Strategic Applications of Named Reactions in Organic Synthesis. Elsevier Academic Press. USA (2005)
21. Segel, I.H.: Enzyme Kinetics. New York: Wiley-Interscience (1975)
22. J. M. Lee, E. P. Gianchandani, J.A.P.: Flux balance analysis in the era of metabolomics. Briefs in Bioinformatics **7** (2006) 140–150
23. J. S. Edwards, M. Covert, B.P.: Metabolic modelling of microbes: The flux-balance approach. Environmental Microbiology **4** (2002) 133–140
24. Francisco Llaneras, J.P.: Stoichiometric modelling of cell metabolism. Journal of Bioscience and Bioengineering **105** (2008) 1–11

Model transformation of metabolic networks using a Petri net based framework

Daniel Machado[1], Rafael S. Costa[1], Miguel Rocha[2], Isabel Rocha[1], Bruce Tidor[3], and Eugénio C. Ferreira[1]

[1] IBB-Institute for Biotechnology and Bioengineering/Centre of Biological Engineering, University of Minho, Campus de Gualtar, 4710-057 Braga, Portugal
{dmachado,rafacosta,irocha,ecferreira}@deb.uminho.pt
[2] Department of Informatics/CCTC, University of Minho, Campus de Gualtar, 4710-057 Braga, Portugal
mrocha@di.uminho.pt
[3] Department of Biological Engineering/Computer Science and Artificial Intelligence Laboratory, Massachusetts Institute of Technology, Cambridge, MA 02139, USA
tidor@mit.edu

Abstract. The different modeling approaches in Systems Biology create models with different levels of detail. The transformation techniques in Petri net theory can provide a solid framework for zooming between these different levels of abstraction and refinement. This work presents a Petri net based approach to Metabolic Engineering that implements model reduction methods to reduce the complexity of large-scale metabolic networks. These methods can be complemented with kinetics inference to build dynamic models with a smaller number of parameters. The central carbon metabolism model of *E. coli* is used as a test-case to illustrate the application of these concepts. Model transformation is a promising mechanism to facilitate pathway analysis and dynamic modeling at the genome-scale level.

1 Introduction

Systems Biology provides a new perspective in the study of living systems and embraces the complexity emerging of interactions among all biological components. Combining theory and experiments, scientists build models to explain and predict the behavior of the systems under study. Metabolic Engineering is one of the fields where this perspective has proven useful through the optimization of metabolic processes for industrial applications [28, 2].

Modeling in Systems Biology is an iterative process as the life-cycle of a model is comprised of successive refinements using experimental data. Different approaches, such as top-down, bottom-up or middle-out [18] are used depending on the purpose of the model and the type of data available for its construction. In Metabolic Engineering there are macroscopic kinetic models that consider the cell as a black-box converting substrates into biomass and products, which are typically used for bioprocess control. On the other hand, there are reaction-network-level models, either medium-scale dynamic models with detailed kinetic

information derived from literature and experimental data [3], or genome-scale stoichiometric reconstructions derived from genome annotation complemented with literature review [5].

Although the ultimate goal of Systems Biology is a complete understanding of the cell as a whole, not only it is extremely difficult to collect all the kinetic information necessary to build a fully detailed whole-cell model due to the lack of experimental data and model identifiability concerns, but also the computational cost of simulating the dynamics of a system with such detail would be tremendous. Therefore, there is a need to fit the level of detail of a model to the specific problem at hand. For instance, Metabolic Pathway Analysis (MPA) has been useful in the analysis of metabolism as a way to determine, classify and optimize the possible pathways throughout a metabolic network. However, due to the combinatorial explosion of pathways with increasing number of reactions, it is still infeasible to apply these methods in genome-scale metabolic reconstructions without decomposing the network into connected modules [23, 24]. This zooming in and out between different levels of abstraction and connecting parts with different levels of detail is a feature where formal methods and particularly Petri nets may play an important role. Concepts such as subnetwork abstraction, transition refinement or node fusion, among others, have been explored in Petri net theory [8] and may provide the theoretical background for method development.

In previous work, we reviewed different modeling formalisms used in Systems Biology from a Metabolic Engineering perspective and concluded that Petri nets are a promising formalism for the creation of a common framework of methods for modeling, analysis and simulation of biological networks [15]. They are a mathematical and graphical formalism, therefore intuitive and amenable to analysis. The different extensions available (*e.g.:* stochastic, continuous, hybrid) provide the flexibility required to model and integrate the diversity of phenomena occurring in the main types of biological networks (metabolic, regulatory and signaling). Moreover, one may find biological meaning in several concepts in Petri net theory; for instance, the incidence matrix of a Petri net is the equivalent of the stoichiometric matrix, and the minimal *t-invariants* correspond to the elementary flux modes (EFMs).

In this work, we explore strategies of model reduction for Petri net representations of metabolic networks, and the integration of this methodology with recent approaches such as genome-scale dynamic modeling. This paper is organized as follows. Section 2 explores the motivation for the work. Section 3 presents the model reduction and kinetics inference methods, Section 4 discusses their application to *E. coli* and Section 5 elaborates on conclusions and future work.

2 Background

There are different examples of model reduction in the literature. One such method was developed in [17], based on timescale analysis for classification of metabolite turnover time using experimental data. The fast metabolites are

removed from the differential equations and their surrounding reactions are lumped. In [20] the EFMs of a reaction network are calculated in order to create a macroscopic pathway network, where each EFM is a macro-reaction connecting extracellular substrates and products. A simple Michaelis–Menten rate law is assumed for each macro-reaction and the parameters are inferred from experimental data. The method is applied in a network with 18 reactions and a total of 7 EFMs. However it does not scale well to larger networks because, in the worst case, the number of EFMs grows exponentially with the network size.

The combinatorial pathway explosion problem is well known; there are methods for network decomposition in the literature that address this issue. In [23] the authors perform a genome-scale pathway analysis on a network with 461 reactions. After estimating the number of extreme pathways (EPs) to be over a million, the network is decomposed into 6 subsystems according to biological criteria and the set of EPs is computed separately for each subsystem. A similar idea in [24] consists on automatic decomposition based on topological analysis. The metabolites with higher connectivity are considered as external and connect the formed subnetworks. An automatic decomposition approach based on Petri nets is the so-called *maximal common transition sets* (MCT-sets) [22], and consists on decomposing a network into modules by grouping reactions by participation in the minimal *t-invariants* (equivalent to EFMs). A related approach relies on clustering of *t-invariants* for network modularization [9]. A very recent network coarsening method based on so-called *abstract dependent transition sets* (ADT-sets) is formulated without the requirement of pre-computation of the *t-invariants* and thus may be a promising tool for larger networks [12].

Another problem in genome-scale metabolic modeling is the study of dynamic behavior. Genome-scale metabolic reconstructions are stoichiometric and usually analyzed under steady-state assumption using constraint-based methods [1]. Dynamic flux balance analysis (dFBA) allows variation of external metabolite concentrations, and simulates the network dynamics assuming an internal pseudo steady-state at each time step [16]. It is used in [19] to build a genome-scale dynamic model of *L. lactis* that simulates fermentation profiles. However, this approach gives no insight into intracellular dynamics, neither it integrates reaction kinetics. In [26] the authors build a kinetic genome-scale model of *S. cerevisiae* using linlog kinetics, where the reference steady-state is calculated using FBA. Some of the elasticity parameters and metabolite concentrations are derived from available kinetic models, while the majority use default values. Using the stoichiometric coefficients as elasticity values is a rough estimation of the influence of the metabolites on the reaction rates. Moreover, no time-course simulation is performed. Mass action stoichiometric simulation (MASS) models are introduced in [14] as a way to incorporate kinetics into stoichiometric reconstructions. Parameters are estimated from metabolomic data. Regulation can be included by incorporating the mechanistic metabolite/enzyme interactions. A limitation of these models is that mass-action kinetics do not reflect the usual non-linearity of enzymatic reactions and the incorporation of regulation leads to a significant increase in network size.

3 Methods

The idea of this work is closer to the reduction concepts of [17, 20] than the modularization concepts in [23, 24]. In the latter cases a large model is decomposed into subunits to ease its processing by analyzing the parts individually. Instead, our objective is to facilitate the visualization, analysis and simulation of a large-scale model as a whole by abstracting its components. This reduction is to be attained by reaction lumping in a way that maintains biological meaning and valid application of current analysis and simulation tools. The Michaelis–Menten kinetics is a typical example of abstraction, where the small network of mass-action reactions are lumped into one single reaction.

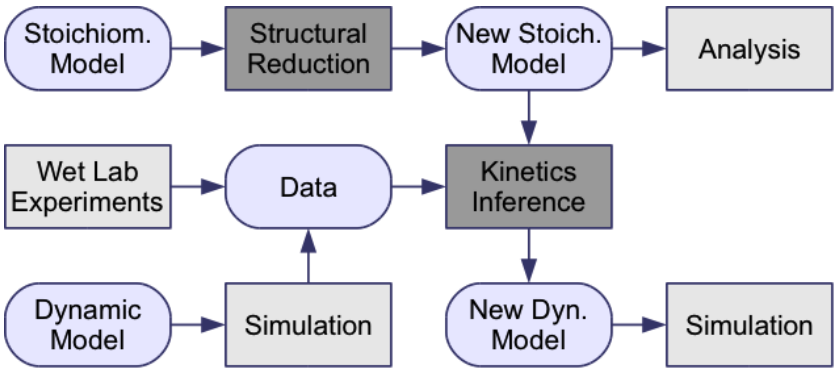

Fig. 1. Overall concept of model reduction and kinetics inference.

The overall idea of the model reduction method is depicted in Fig. 1. A large-scale stoichiometric model can be structurally reduced into a simplified version that can be more easily analyzed by methods such as MPA. Also, one may infer a kinetic structure to build a dynamic version of the reduced model. Due to the smaller size, a lower number of parameters has to be estimated. The data used for estimation may be experimental data found in the literature, or pseudo-experimental data from dynamic simulations if part of the system has been kinetically characterized.

When abstracting a reaction subnetwork into one or more macro-reactions, it is important to consider the assumptions created by such abstraction. As in Michaelis–Menten kinetics, these simplifications result in a pseudo-steady-state assumption for the intermediate species that disappear. While this may not be a problem for flux balance models, it changes the transient behavior of dynamic models because the buffering effect of intermediates in a pathway is neglected. The selection of metabolites to be removed depends on the purpose of the reduction. The network may have different levels of granularity based on the availability of experimental data, topological properties, or simply in order to aggregate pathways according to biological function.

3.1 Basic definitions

The proposed method for model reduction uses several Petri net concepts from the literature. We will use the following definition of an unmarked continuous Petri net (adapted from [4]) for modeling a stoichiometric metabolic network:

$$Pn = < P, T, Pre, Post >$$
$$Pre : P \times T \rightarrow \mathbb{R}^+$$
$$Post : P \times T \rightarrow \mathbb{R}^+$$

where the set of places P represents the metabolites, the set of transitions T represents the reactions and $Pre, Post$ are, respectively, the substrate and product stoichiometries of the reactions. Note that for the representation of a stoichiometric network, a discrete Petri net usually suffices; however, because some models may contain non-integer stoichiometric coefficients, the continuous version was adopted. Moreover, we will assume that reversible reactions are split into irreversible reaction pairs. We will also use the following definitions:

$$loc(x) = \{x\} \cup {}^\bullet x \cup x^\bullet$$
$$In(p) = \sum_{t \in {}^\bullet p} Post[p,t] \cdot v(t)$$
$$Out(p) = \sum_{t \in p^\bullet} Pre[p,t] \cdot v(t)$$

where ${}^\bullet x, x^\bullet$ are sets representing the input and output nodes of a node x, the set $loc(x) \subseteq P \cup T$ is called the locality of x, function $v : T \rightarrow \mathbb{R}_0^+$ is a given flux distribution (or the so-called instantaneous firing rate), and $In, Out : P \rightarrow \mathbb{R}_0^+$ are, respectively, the feeding and draining rates of the metabolites.

The method for network reduction consists of eliminating a set of selected metabolites from the network. For each removed metabolite its surrounding reactions are lumped in order to maintain the fluxes through the pathways. This reduction assumes a steady-state condition for the metabolite, *i.e.* $In(p) = Out(p)$.

3.2 Model reduction: Conjunctive fusion

There are two options for lumping the reactions depending on the transformation method applied. The first approach is based on a transformation called *conjunctive transition fusion* [8] and it results in an abstraction that replaces the transition-bordered subnet $loc(p)$ by a single macro-reaction. The drawback of this method is that the flux ratios between the internal reactions are lost. If a known steady-state flux distribution (v) is given, then the stoichiometric coefficients can be adjusted to preserve the ratios for that distribution; however, the space of solutions of the flux balance formulation becomes restricted to a particular solution. In the limiting case, if all the internal metabolites are removed, the cell is represented by one single macro-reaction connecting extracellular substrates and products with the stoichiometric yields inferred from the

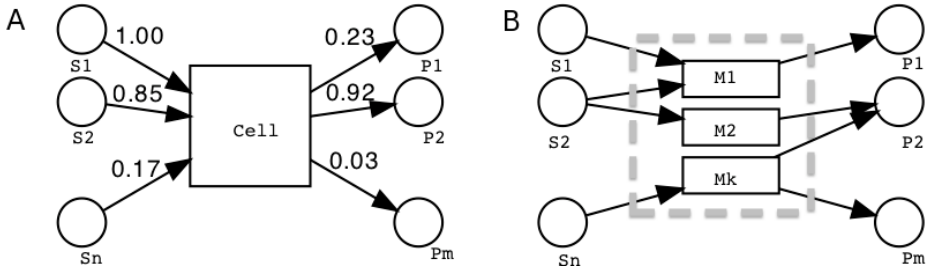

Fig. 2. Exemplification of limit scenarios where all the internal metabolites are removed. (A) In the conjunctive reduction case the result is one single macro-reaction converting substrates into products with the respective yields specified in the stoichiometry. (B) In the disjunctive reduction method, all possible pathways connecting substrates and products are enumerated.

network topology for one particular steady-state (Fig 2A). The transformation method for removing metabolite p in Pn given a flux distribution v is described as follows:

$$
\begin{aligned}
Pn' &= < P', T', Pre', Post' > \\
P' &= P \setminus \{p\} \\
T' &= T \setminus ({}^\bullet p \cup p^\bullet) \cup \{t_p\} \\
Pre' &= \{(p_i, t_j) \mapsto Pre(p_i, t_j) \mid (p_i, t_j) \in dom(Pre) \setminus (P \times ({}^\bullet p \cup p^\bullet))\} \\
&\quad \cup \{(p_i, t_p) \mapsto f_{in}(p_i) \mid p_i \in {}^\bullet({}^\bullet p \cup p^\bullet), p_i \neq p, v'(t_p) \neq 0, In_{t_p}(p_i) \neq 0\} \\
Post' &= \{(p_i, t_j) \mapsto Post(p_i, t_j) \mid (p_i, t_j) \in dom(Post) \setminus (P \times ({}^\bullet p \cup p^\bullet))\} \\
&\quad \cup \{(p_i, t_p) \mapsto f_{out}(p_i) \mid p_i \in ({}^\bullet p \cup p^\bullet)^\bullet, p_i \neq p, v'(t_p) \neq 0, Out_{t_p}(p_i) \neq 0\} \\
v' &= \{t \mapsto v(t) \mid t \in T \setminus ({}^\bullet p \cup p^\bullet)\} \cup \{t_p \mapsto In(p)\}.
\end{aligned}
$$

where

$$
\begin{aligned}
f_{in}(p_i) &= \frac{\sum_{t \in p_i^\bullet \cap ({}^\bullet p \cup p^\bullet)} Pre(p_i, t) \cdot v(t)}{v'(t_p)} \\
f_{out}(p_i) &= \frac{\sum_{t \in {}^\bullet p_i \cap ({}^\bullet p \cup p^\bullet)} Post(p_i, t) \cdot v(t)}{v'(t_p)}
\end{aligned}
$$

The stoichiometric coefficients of the new reaction may be very high or low, depending on $v'(t_p)$ and so, optionally, one may also normalize them with some scalar λ, such that $Pre''(p_i, t_p) = \frac{1}{\lambda} \cdot Pre'(p_i, t_p)$, $Post''(p_i, t_p) = \frac{1}{\lambda} \cdot Post'(p_i, t_p)$ and $v''(t_p) = \lambda \cdot v'(t_p)$. This will also make the final result independent of the order of the metabolites removed. A good choice for λ is:

$$
\lambda = \max\left(\{Pre(p_i, t_p) \mid p_i \in {}^\bullet t_p\} \cup \{Post(p_i, t_p) \mid p_i \in t_p{}^\bullet\}\right)
$$

3.3 Model reduction: Disjunctive fusion

The second approach is based on a transformation called *disjunctive transition fusion* [8], where every combination of input and output reaction pairs connected by the removed metabolite is replaced by one macro-reaction. Although this approach does not constrain the steady-state solution space of the flux distribution, it has the drawback of increasing the number of transitions, if the metabolite is highly connected, due to the combinatorial procedure. Note that applying this reduction step to metabolite p_i is equivalent to performing one iteration of the *t-invariant* calculation algorithm to remove column i of the transposed incidence matrix. Therefore, in the limiting case where all internal metabolites are removed, the cell is represented by the set of all possible pathways connecting extracellular substrates and products (Fig. 2B), as was done in [20]. The definition, similar to the previous one, is as follows:

$$
\begin{aligned}
Pn' &= < P', T', Pre', Post' > \\
P' &= P \setminus \{p\} \\
T' &= T \setminus ({}^\bullet p \cup p^\bullet) \cup \{t_{xy} \mid (x,y) \in ({}^\bullet p \times p^\bullet)\} \\
Pre' &= \{(p_i,t) \mapsto Pre(p_i,t) \mid (p_i,t) \in dom(Pre) \setminus (P \times ({}^\bullet p \cup p^\bullet)\} \\
&\quad \cup \{(p_i,t_{xy}) \mapsto Pre_0(p_i,x) \cdot Pre(p,y) + Pre_0(p_i,y) \cdot Post(p,x) \\
&\qquad \mid (x,y) \in ({}^\bullet p \times p^\bullet), p_i \in {}^\bullet\{x,y\}\} \\
Post' &= \{(p_i,t) \mapsto Post(p_i,t) \mid (p_i,t) \in dom(Post) \setminus (P \times ({}^\bullet p \cup p^\bullet)\} \\
&\quad \cup \{(p_i,t_{xy}) \mapsto Post_0(p_i,x) \cdot Pre(p,y) + Post_0(p_i,y) \cdot Post(p,x) \\
&\qquad \mid (x,y) \in ({}^\bullet p \times p^\bullet), p_i \in \{x,y\}^\bullet\}
\end{aligned}
$$

where

$$
Pre_0(p,t) = \begin{cases} Pre(p,t) & \text{if } (p,t) \in dom(Pre) \\ 0 & \text{if } (p,t) \notin dom(Pre) \end{cases}
$$

$$
Post_0(p,t) = \begin{cases} Post(p,t) & \text{if } (p,t) \in dom(Post) \\ 0 & \text{if } (p,t) \notin dom(Post) \end{cases}
$$

Whenever there are pathways with the same net stoichiometry, these can be removed by checking the columns of the incidence (stoichiometric) matrix and eliminating repeats. It should also be noted that in both methods, if a metabolite acts both as substrate and product in a lumped reaction, it will create a redundant cycle that is not reflected in the incidence matrix. If these cycles are not removed, they propagate through the reduction steps; therefore, they should be replaced by a single arc containing the overall stoichiometry. The procedure

works as follows:

$$\begin{aligned} Pre' =& \{(p,t) \mapsto Pre(p,t) \mid (p,t) \in dom(Pre) \setminus dom(Post)\} \\ & \cup \{(p,t) \mapsto Pre(p,t) - Post(p,t) \\ & \quad \mid (p,t) \in dom(Pre) \cap dom(Post), Pre(p,t) > Post(p,t)\} \\ Post' =& \{(p,t) \mapsto Post(p,t) \mid (p,t) \in dom(Post) \setminus dom(Pre)\} \\ & \cup \{(p,t) \mapsto Post(p,t) - Pre(p,t) \\ & \quad \mid (p,t) \in dom(Pre) \cap dom(Post), Post(p,t) > Pre(p,t)\} \end{aligned}$$

The previous arc removing procedure may cause isolation of some nodes when $Pre(p,t) = Post(p,t)$; therefore, the isolated nodes should be removed:

$$\begin{aligned} P' &= \{p \mid p \in P, loc(p) \neq \{p\}\} \\ T' &= \{t \mid t \in T, loc(t) \neq \{t\}\} \end{aligned}$$

3.4 Kinetics inference

Given a stoichiometric model, if metabolomic or fluxomic data are available for parameter estimation, one may try to build a dynamic model by inferring appropriate kinetics for the reactions. In [25] the authors propose that this is performed by assuming linlog kinetics for all reactions using an FBA solution as the reference state and the stoichiometries as elasticity parameters. An integration of Biochemical Systems Theory (BST) with Hybrid Functional Petri Nets (HFPN) is presented in [29], where general mass action (GMA) kinetics is assumed for each transition. The review of kinetic rate formulations is out of the scope of this work and may be found elsewhere [10].

Assuming that all metabolites with unknown concentration were removed, we will extend our definition to a marked continuous Petri net:

$$Pn =< P, T, Pre, Post, m_0 >$$

where $m_0 : P \to \mathbb{R}_0^+$ denotes the initial marking (concentration) of the metabolites. The kinetics inference process consists on defining a firing rate $v : T \to \mathbb{R}_0^+$, which will be dependent on the current marking (m) and the specific kinetic parameters (see [7] for an introduction on marking-dependent firing rates). As we assumed irreversible reactions, each rate will only vary with substrate concentration. The rates can be easily derived from the net topology. In case of GMA kinetics v is given by:

$$v(t) = k_t \prod_{p \in {}^\bullet t} m(p)^{a_{p,t}}$$

where k_t is the kinetic rate of t and $a_{p,t}$ is the kinetic order of metabolite p in reaction t. A usual first approximation for $a_{p,t}$ is $Pre(p,t)$.

Linlog kinetics are formulated based on a reference rate v_0, and defined by:

$$v(t) = v_0(t) \left(1 + \sum_{p \in {}^\bullet t} \varepsilon_{p,t}^0 \ln \left(\frac{m(p)}{m_0(p)} \right) \right)$$

where $\varepsilon^0_{p,t}$ is called the elasticity of metabolite p in reaction t, reflecting the influence of the concentration change of the metabolite in the reference reaction rate. As in the previous case, $Pre(p,t)$ can be chosen as an initial approximation for $\varepsilon^0_{p,t}$. The relative enzyme activity term (e/e_0) commonly present in linlog rate laws to account for regulatory effects at larger time scales will not be considered.

4 Results and Discussion

The proposed methods were tested using the dynamic central carbon metabolism model of *E. coli* [3], where the stoichiometric part was used for the application of the reduction methods, and the dynamic profile was used to generate pseudo-experimental data sets for parameter estimation and validation of the kinetics inference method. A Petri net representation of this model (Fig. 3) was built using the Snoopy tool [21]. All reversible reactions were split into irreversible pairs. The net contains a total of 18 places, 44 transitions and is covered by 95 *semipositive t-invariants*, computed with the Integrated Net Analyzer [27].

In the application of the conjunctive method (Fig 4A), the metabolites were classified as in [17] based on their timescale (Table 1), by calculating their turnover time ($\tau : P \rightarrow \mathbb{R}^+_0$) using the reference steady-state of the dynamic model, where:

$$\tau(p) = \frac{m_0(p)}{In(p)}$$

Metabolites with small turnover time are considered fast. In this case, all metabolites except the slowest 5 (*glcex, pep, g6p, pyr, g1p*) were removed.

For the application of the disjunctive method (Fig 4B), the metabolites were classified based on their topology (Table 1). We conveniently opted to remove the metabolites with lower connectivity to avoid the combinatorial explosion problem. All metabolites except 5 (*g6p, pyr, f6p, gap, xyl5p*) were removed. This reduction assumes steady-state for the removed metabolites. However, it makes no assumptions on the ratios between the fluxes, therefore preserving the flux-balance solution space.

Because we are assuming that the reference steady-state is known, the conjunctive reduced model was chosen for the application of the kinetics inference method assuming linlog kinetics at the reference state. The elasticity parameters were estimated using COPASI [13]. The pseudo-experimental data was generated from simulation with the original model after a 1 mM extracellular glucose pulse with the addition of Gaussian noise ($std = 0.05$ mM) (Fig. 5A). The fitted model was then validated using pseudo-experimental data from a 2 mM pulse (Fig. 5B). It is possible to observe an instantaneous increase in *pyr* (from 2.67 to 3.93) and an instantaneous decrease *pep* (from 2.69 to 1.26) which the model is unable to reproduce. The poor fitting in some of the intracellular metabolites is expected given the significant reduction to the model. However, the extracellular glucose consumption profile is remarkably good, both in the fitting and validation cases.

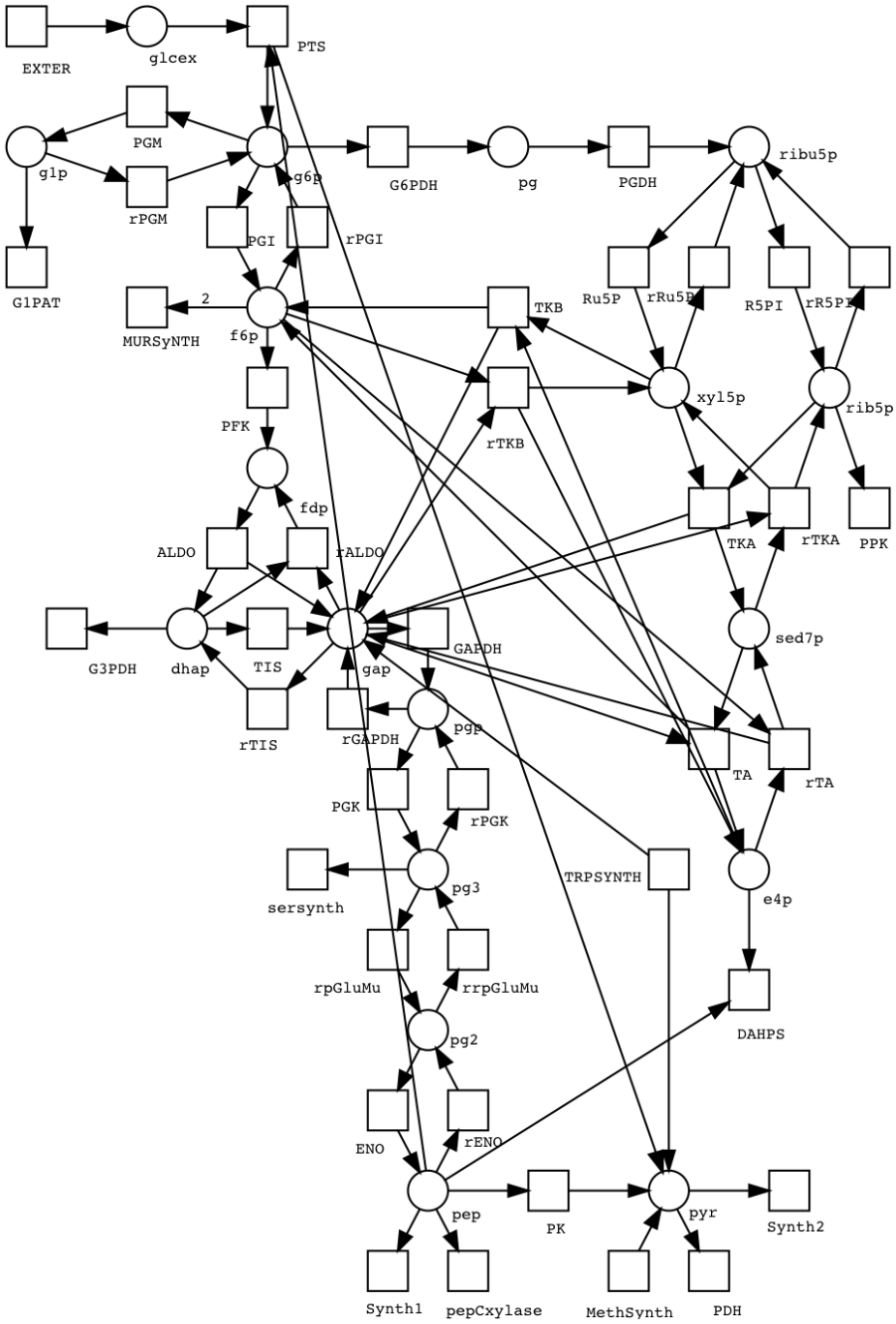

Fig. 3. Petri net model of the dynamic central carbon metabolism model of *E. coli* with reversible reactions split into irreversible pairs.

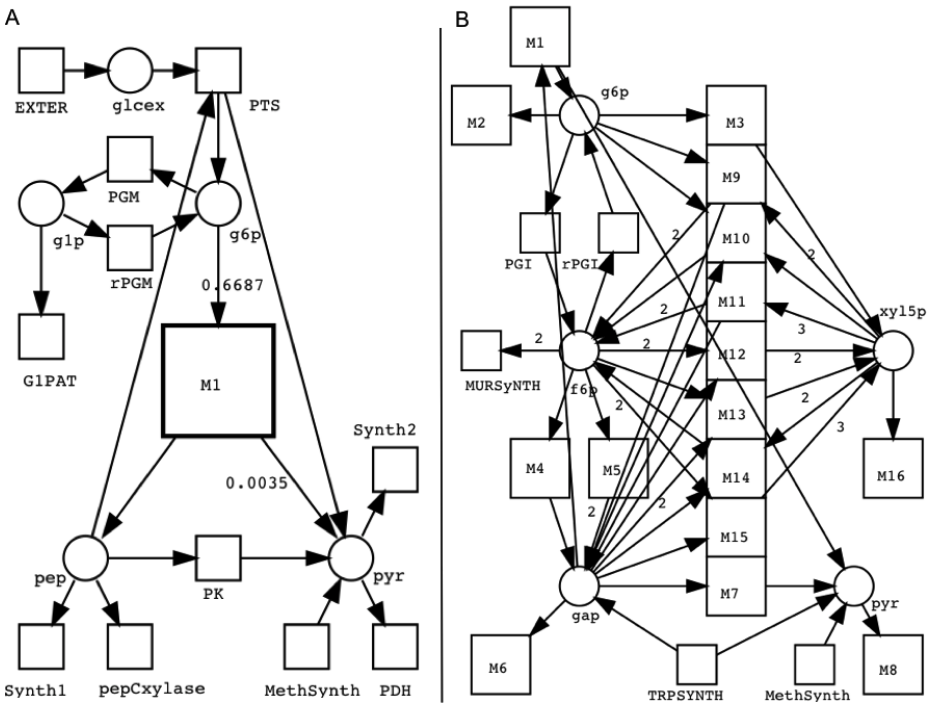

Fig. 4. Reduced versions of the original network. (A) Conjunctive reduction method. (B) Disjunctive reduction method.

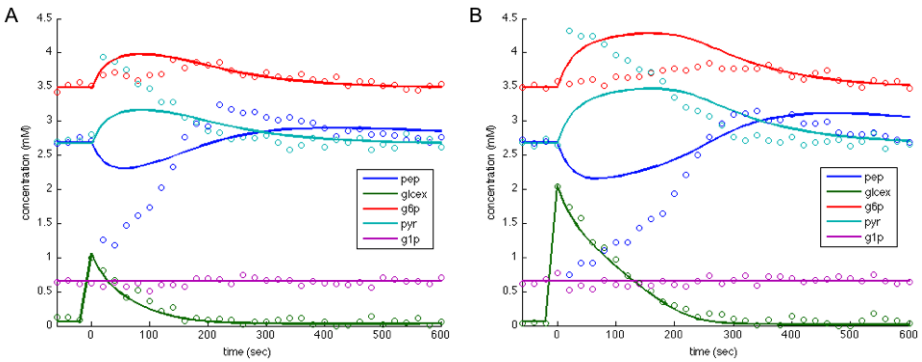

Fig. 5. (A) Results of parameter estimation with pseudo-experimental data with 1 mM extracellular glucose pulse. (B) Validation of the model with a 2 mM extracellular glucose pulse. In both cases, the circles represent the experimental data and the lines represent time-course simulations generated by the reduced model.

Table 1. Metabolite topological properties (input reactions, output reactions, connectivity) and dynamic properties (concentration, flux, turnover time) at the reference steady-state.

Metabolite	$\#({}^\bullet p)$	$\#(p^\bullet)$	$\#({}^\bullet p \times p^\bullet)$	m_0 (mM)	In (mM/s)	τ (s)
glcex	1	1	1	0.0558	0.0031	**18.099**
pep	1	6	6	2.6859	0.3031	**8.8603**
g6p	3	3	**9**	3.4882	0.2004	**17.406**
pyr	4	2	**8**	2.6710	0.2418	**11.044**
f6p	3	5	**15**	0.6014	0.1423	4.2266
g1p	1	2	2	0.6539	0.0023	**278.62**
pg	1	1	1	0.8092	0.1397	5.7929
fdp	2	1	2	0.2757	0.1414	1.9495
sed7p	2	2	4	0.2761	0.0454	6.0757
gap	7	6	**42**	0.2196	0.3661	0.5997
e4p	2	3	6	0.0986	0.0454	2.1684
xyl5p	3	3	**9**	0.1385	0.0839	1.6503
rib5p	2	3	6	0.3994	0.0558	7.1626
dhap	2	3	6	0.1682	0.1414	1.1892
pgp	2	2	4	0.0080	0.3207	0.0251
pg3	2	3	6	2.1437	0.3207	6.6851
pg2	2	2	4	0.4014	0.3031	1.3241
ribu5p	3	2	6	0.1114	0.1397	0.7974

Although both reducing methods can be combined with kinetics inference, the conjunctive version seems more suitable if a steady-state distribution is known, because it generates smaller models, hence less parameters. The disjunctive version is appropriate for analyzing all elementary pathways between a set of metabolites without the burden of calculating the set of EFMs of the whole model. For instance, the macro-reactions *M4* ($ALDO + G3PDH$) and *M5* ($ALDO + TIS$), with net stoichiometries of, respectively, [$fdp \rightarrow gap$] and [$fdp \rightarrow 2\ gap$], are two unique pathways between these two metabolites.

5 Conclusions

This work presents strategies for model reduction of metabolic networks based on a Petri net framework. Two approaches, conjunctive and disjunctive reduction are presented. The conjunctive approach allows the abstraction of a subnetwork into one lumped macro-reaction, however limited to one particular flux distribution of the subnetwork. The disjunctive approach on the other hand, makes no assumptions on the flux distribution by replacing the removed subnetwork with macro-reactions for all possible pathways through the subnetwork, therefore not constraining the steady-state solution space. In both cases, the reduced model may be transformed into a dynamic model using kinetics inference and parameter estimation if experimental data is available. Using the reduced model,

instead of the original, facilitates this process because it significantly decreases the number of parameters to be estimated.

In future work, we intend to build a dynamic genome-scale model of *E. coli* by using the already available central carbon dynamic model [3], complemented with lumped versions of the surrounding pathways in the genome-scale network [5]. Note that some of the reactions on the central carbon model already represent lumped versions of some biosynthetic pathways (*e.g. mursynth, trpsynth, methsynth, sersynth*). However they were not deduced from the genome-scale network and may not be accurate abstractions of these pathways.

Among the extensions available to Petri nets are the addition of different types of arcs, such as read-arcs and inhibitor-arcs, which could be use to represent activation and inhibition in biochemical reactions. They could also be used to integrate metabolic and regulatory networks. Optimization in metabolic processes is usually based on knockout simulations in metabolic networks. However, these simulations do not take into consideration the possible regulatory effects caused by the knockouts. In our transformation methods we removed the arcs with the same stoichiometry in both directions, because these are not reflected in the stoichiometric matrix. In the Michaelis–Menten example this results in removing the enzyme from the network. The proposed methods can be extended to consider read-arcs for these situations, which should be preserved during the reduction steps, therefore establishing connection places to the integration of a regulatory network (Fig 6).

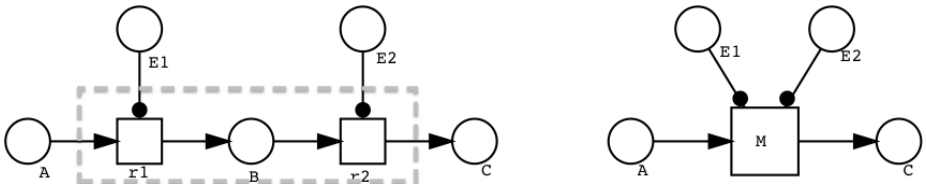

Fig. 6. Reduction step conserving the read-arcs associated with the enzymes of the original reactions.

An alternative to the reduction of the models would be to consider their representation using hierarchical Petri nets. In this case, each macro-reaction would be connected to its detailed subnetwork. Although this would not reduce the number of kinetic parameters in the case of kinetics inference, it would be extremely useful for facilitated modeling and visualization of large-scale networks without compromising detail. It could also be the solution for genome-scale pathway analysis, if it is performed independently at each hierarchical level. The hierarchical model composition proposed for SBML [6] may facilitate the implementation of this alternative. See [11] for an automatic network coarsening algorithm based on hierarchical petri nets applied to different kinds of biological networks.

Acknowledgments. Research supported by PhD grants SFRH/BD/35215/2007 and SFRH/BD/25506/2005 from the Fundação para a Ciência e a Tecnologia (FCT) and the MIT–Portugal Program through the project "Bridging Systems and Synthetic Biology for the development of improved microbial cell factories" (MIT-Pt/BS-BB/0082/2008).

References

1. S.A. Becker, A.M. Feist, M.L. Mo, G. Hannum, B.Ø. Palsson, and M.J. Herrgard. Quantitative prediction of cellular metabolism with constraint-based models: the COBRA Toolbox. *Nature Protocols*, 2(3):727–738, 2007.
2. A.P. Burgard, P. Pharkya, and C.D. Maranas. Optknock: A bilevel programming framework for identifying gene knockout strategies for microbial strain optimization. *Biotechnology and Bioengineering*, 84(6):647–657, 2003.
3. C. Chassagnole, N. Noisommit-Rizzi, J.W. Schmid, K. Mauch, and M. Reuss. Dynamic modeling of the central carbon metabolism of Escherichia coli. *Biotechnology and Bioengineering*, 79(1):53–73, 2002.
4. R. David and H. Alla. *Discrete, continuous, and hybrid Petri nets*. Springer Verlag, 2005.
5. A.M. Feist, C.S. Henry, J.L. Reed, M. Krummenacker, A.R. Joyce, P.D. Karp, L.J. Broadbelt, V. Hatzimanikatis, and B.Ø. Palsson. A genome-scale metabolic reconstruction for Escherichia coli K-12 MG1655 that accounts for 1260 ORFs and thermodynamic information. *Molecular systems biology*, 3(1), 2007.
6. A. Finney. Developing SBML beyond level 2: proposals for development. In *Computational Methods in Systems Biology*, pages 242–247. Springer, 2005.
7. D. Gilbert and M. Heiner. From Petri nets to differential equations-an integrative approach for biochemical network analysis. *Petri Nets and Other Models of Concurrency-ICATPN 2006*, pages 181–200, 2006.
8. C. Girault and R. Valk. *Petri Nets for System Engineering: A Guide to Modeling, Verification, and Applications*. Springer-Verlag New York, Inc., Secaucus, NJ, USA, 2001.
9. E. Grafahrend-Belau, F. Schreiber, M. Heiner, A. Sackmann, B.H. Junker, S. Grunwald, A. Speer, K. Winder, and I. Koch. Modularization of biochemical networks based on classification of Petri net t-invariants. *BMC bioinformatics*, 9(1):90, 2008.
10. J.J. Heijnen. Approximative kinetic formats used in metabolic network modeling. *Biotechnology and bioengineering*, 91(5):534–545, 2005.
11. M. Heiner. Understanding Network Behavior by Structured Representations of Transition Invariants. *Algorithmic Bioprocesses*, page 367, 2009.
12. M. Heiner and K. Sriram. Structural analysis to determine the core of hypoxia response network. *PloS one*, 5(1):e8600, 2010.
13. S. Hoops, S. Sahle, R. Gauges, C. Lee, J. Pahle, N. Simus, M. Singhal, L. Xu, P. Mendes, and U. Kummer. COPASI—a COmplex PAthway SImulator. *Bioinformatics*, 22(24):3067–3074, 2006.
14. N. Jamshidi and B.Ø. Palsson. Mass action stoichiometric simulation models: Incorporating kinetics and regulation into stoichiometric models. *Biophysical Journal*, 98:175–185, 2010.
15. D. Machado, R.S. Costa, M. Rocha, I. Rocha, B. Tidor, and E.C. Ferreira. A critical review on modelling formalisms and simulation tools in computational biosystems. In *Distributed Computing, Artificial Intelligence, Bioinformatics, Soft Computing, and Ambient Assisted Living*, pages 1063–1070. Springer, 2009.

16. R. Mahadevan, J.S. Edwards, and F.J. Doyle. Dynamic flux balance analysis of diauxic growth in Escherichia coli. *Biophysical journal*, 83(3):1331–1340, 2002.
17. I.E. Nikerel, W.A. van Winden, P.J.T. Verheijen, and J.J. Heijnen. Model reduction and a priori kinetic parameter identifiability analysis using metabolome time series for metabolic reaction networks with linlog kinetics. *Metabolic Engineering*, 11(1):20–30, 2009.
18. D. Noble. The rise of computational biology. *Nature Reviews Molecular Cell Biology*, 3(6):459–463, 2002.
19. G.M. Oddone, D.A. Mills, and D.E. Block. A dynamic, genome-scale flux model of Lactococcus lactis to increase specific recombinant protein expression. *Metabolic Engineering*, 2009.
20. A. Provost and G. Bastin. Dynamic metabolic modelling under the balanced growth condition. *Journal of Process Control*, 14(7):717–728, 2004.
21. C. Rohr, W. Marwan, and M. Heiner. Snoopy-a unifying Petri net framework to investigate biomolecular networks. *Bioinformatics*, 2010.
22. A. Sackmann, M. Heiner, and I. Koch. Application of Petri net based analysis techniques to signal transduction pathways. *BMC bioinformatics*, 7(1):482, 2006.
23. C.H. Schilling and B.Ø. Palsson. Assessment of the metabolic capabilities of Haemophilus influenzae Rd through a genome-scale pathway analysis. *Journal of Theoretical Biology*, 203(3):249–283, 2000.
24. S. Schuster, T. Pfeiffer, F. Moldenhauer, I. Koch, and T. Dandekar. Exploring the pathway structure of metabolism: decomposition into subnetworks and application to Mycoplasma pneumoniae, 2002.
25. K. Smallbone, E. Simeonidis, D.S. Broomhead, and D.B. Kell. Something from nothing-bridging the gap between constraint-based and kinetic modelling. *FEBS Journal*, 274(21):5576–5585, 2007.
26. K. Smallbone, E. Simeonidis, N. Swainston, and P. Mendes. Towards a genome-scale kinetic model of cellular metabolism. *BMC Systems Biology*, 4(1):6, 2010.
27. P.H. Starke. INA: Integrated Net Analyzer. *Reference Manual*, 1992.
28. G. Stephanopoulos. Metabolic engineering. *Biotechnology and Bioengineering*, 58, 1998.
29. J. Wu and E. Voit. Hybrid modeling in biochemical systems theory by means of functional Petri nets. *Journal of bioinformatics and computational biology*, 7(1):107, 2009.

Applying Petri nets for the analysis of the GSH-ASC cycle in chloroplasts *

Hermenegilda Macià*, M. Isabel González-Sánchez**, Valentín Valero***, and Edelmira Valero**

* Department of Mathematics, Escuela Superior de Ingeniería Informática. Albacete. University of Castilla-La Mancha. Spain
** Department of Physical Chemistry, Escuela de Ingenieros Industriales. Albacete. University of Castilla-La Mancha. Spain
***Department of Computer Science, Escuela Superior de Ingeniería Informática. Albacete. University of Castilla-La Mancha. Spain
{Hermenegilda.Macia, MIsabel.Gonzalez, Valentin.Valero, Edelmira.Valero}@uclm.es

Keywords: Petri nets, metabolic pathways, biological systems.

Abstract. Petri nets are a useful framework for the analysis of biological systems in various complementary ways, integrating both qualitative and quantitative studies. We apply this formalism to the Glutathione Ascorbate Redox cycle (GSH-ASC) in chloroplasts case study, considering structural Petri net techniques from standard Petri nets to validate the model and to infer new properties, as well as continuous Petri nets in order to have a behavior prediction. In this way, from the continuous Petri net representation we can analyze its behavior under oxidative stress conditions, and from the standard Petri net we can identify some state-conserving or mass-conserving properties.

1 Introduction

Petri nets [8, 10] are a well-known mathematical formalism for the modeling and analysis of concurrent systems. They were introduced by Carl A. Petri [11] in the early 60's. Since this time, they have been extended and applied to several areas [4] such as manufacturing systems, workflow management, telecommunications, communication protocols, etc. Some reasons for using Petri nets are the following: it is easy to describe concurrency and they have a rigorous formal semantics, i.e., their behavior is defined in a precise and unambiguous manner. Additionally, one of the main features of Petri nets is that they have a graphical nature, i.e., you can early get a good knowledge of the system by simple inspection of the Petri net model that represents the system. But, most importantly, there are many tools [21] supporting the model, not only to provide the

* Supported by the Spanish government (cofinanced by FEDER founds) with the project TIN2009-14312-C02-02, and the JCCM regional projects PEII09-0232-7745, PAI-08-0175-8618 and POII10-0235-8597.

capability to create or edit Petri net models, but also to simulate the system evolution and even to analyze some properties of interest. Then, there has been an intensive research in the area of Petri nets in the last 40 years to extend the basic model by including some additional features that are of special interest in some specific application domains. Thus, timed and probabilistic extensions of the basic model have been defined [7, 20], as well as continuous and hybrid Petri nets [1]. The application of Petri nets to the description of chemical processes was already proposed by Carl A. Petri in the 70's [12]. In the 90's Reddy et al. [14] were the first who applied Petri nets to the modeling and analysis of metabolic pathways. Nowadays, there are several different extensions of Petri nets for modeling and simulating biological systems, depending on the specifities of the particular chemical processes described (see [9]). A rich framework for modeling and analyzing biochemical pathways which unifies the qualitative, stochastic and continuous paradigms using Petri nets can be found in [3].

In this paper we consider the GSH-ASC cycle in chloroplasts, which is described and analyzed by using continuous and standard Petri nets. There is a previous model for the GSH-ASC cycle in the literature, the Polle's model [13], which has some shortcomings that have been discussed and improved in [17], where the same ODEs that we use for the continuous Petri net representation were used to model the GSH-ASC cycle. Thus, the main goals of this paper can be summarized as follows:

(i) The application of continuous Petri nets to this specific biological process, which provides us with a graphical representation of this biochemical process, which becomes easier to modify and analyze than the corresponding (equivalent) ODEs, which can be found in [17].
(ii) The application of the classical theory and tools of Petri nets (in the discrete Petri net), and specifically in this paper the structural theory in order to get a better understanding of the biological model and conclude the relationship between the structural elements (invariants) of the underlying discrete Petri net with the chemical properties of this biological process.

The outline of the paper is as follows. Section 2 contains a brief description of the GSH-ASC cycle in chloroplasts. In Section 3 we study the dynamic behavior of this biological model by using continuous Petri nets. Then, the structural qualitative study is presented in Section 4, and finally, the conclusions and hints for future research are presented in section 5.

2 The Biological Model

The glutathione-ascorbate redox (GSH-ASC) pathway in chloroplasts is a complex network of spontaneous, photochemical, and enzymatic reactions for detoxifying hydrogen peroxide. In brief, superoxide dismutase (SOD) acts as the first line of defense, dismutating superoxide radical (O_2^-) to H_2O_2 and O_2. In chloroplasts, H_2O_2 thus generated is reduced to water by ascorbate (ASC) catalyzed with L-ascorbate peroxidase (APX). This is the first step of the GSH-ASC cycle,

producing monodehydroascorbate radicals (MDA), which spontaneously disproportionate to ASC and dehydroascorbate (DHA). The next step in the cycle is the regeneration of ASC by glutathione (GSH) either enzymatically catalyzed by glutathione dehydrogenase ($DHAR$) or chemically but a too slow rate to account for the observed photoreduction of DHA in chloroplasts. Lastly, the redox cycle is closed by the regeneration of GSH catalyzed by glutathione reductase (GR) at the expense of photoproduced $NADPH$. These steps are captured by the continuous Petri net model depicted in Figure 1, which provides us with a graphical representation of this metabolic pathway.

Tables 1-5 provide mathematical expressions for rate equations as well as the conditions (rate constants and initial concentrations) used for the mathematical modeling of the pathway. Due to the lack of space we omit a detailed description of this metabolic pathway, which can be found in [17], which contains a supplementary material section devoted to this description.

It is very difficult to validate numerical data here shown against real biological data. The metabolic pathway under study includes four enzymatic steps and a complex set of photochemical and spontaneous chemical reactions, which is not possible to implement under "in vitro" conditions so that data from Figures 2 and 3 can be tested in an experimental way in the laboratory. However, the values of the kinetic constants and initial conditions used to run the model (Tables 4 and 5) have been taken, when possible, from data reported in the scientific literature, obtained with real systems. APX does not appear in Table 3 because it has not been considered under steady-state conditions, since it is the most hydrogen peroxide sensitive enzyme in the pathway. Instead, we have introduced its catalytic mechanism including a stage of inactivation by excess of hydrogen peroxide and a step of *de novo* synthesis of the protein (Table 2), which gives the cell the opportunity to recover the amount of APX inactivated, which represents one of the main defense mechanisms of plants to mitigate oxidative stress.

Table 1. Chemical reactions involved in the cycle which have been introduced in the model and notation used for their respective apparent bimolecular rate constants.

Reaction	Notation Reaction
$MDA + MDA \rightarrow ASC + DHA$	k_1
$DHA + 2\ GSH \rightarrow ASC + GSSG$	k_4
$2\ O_2^- + 2\ H^+ \rightarrow O_2 + H_2O_2$	k_5
$O_2^- + ASC \rightarrow H_2O_2 + MDA$	k_6
$O_2^- + 2\ GSH \rightarrow H_2O_2 + GSSG$	k_7
$H_2O_2 + 2\ ASC \rightarrow 2\ H_2O + 2\ MDA$	k_8

Table 2. Reactions involved in the APX mechanism.

Reaction	Notation Reaction
$APX + H_2O_2 \rightarrow CoI + H_2O$	k_1^{APX}
$CoI + ASC \rightarrow CoII + MDA$	k_2^{APX}
$CoII + ASC \rightarrow APX + MDA$	k_3^{APX}
$CoI + H_2O_2 \rightarrow APX_i$	k_4^{APX}
synthesis *de novo* of APX	k_5^{APX}

Table 3. Steady-state rate equations used for the enzymes involved in the model.

Enzyme	Rate equation
SOD	$k_{SOD}[SOD]_0[O_2^-]$
$DHAR$	$\frac{k_{cat}^{DHAR}[DHAR]_0[DHA][GSH]}{K_i^{DHA}K_M^{GSH1} + K_M^{DHA}[GSH] + (K_M^{GSH1} + K_M^{GSH2})[DHA] + [DHA][GSH]}$
GR	$\frac{k_{cat}^{GR}[GR]_0[NADPH][GSSG]}{K_M^{NADPH}[GSSG] + K_M^{GSSG}[NADPH] + [NADPH][GSSG]}$

Table 4. List of kinetic constants values used to simulate the model under "standard" conditions (see [17]).

F	640	k_{cat}^{GR}	595	k_{cat}^{DHAR}	142	k_{SOD}	200	k_1^{APX}	12	k_2^{APX}	50
k_3^{APX}	2.1	k_4^{APX}	0.7	k_5^{APX}	0.01	k_1	0.5	k_4	0.1	k_5	0.2
k_6	0.2	k_7	0.7	k_8	$2E-6$	k_{12}	1.3	k_{13}	42.5	k_N	0.5
K_M^{NADPH}	3	K_M^{GSSG}	200	K_M^{GSH}	2500	K	$5E5$				

Table 5. List of (non-zero) initial concentrations used to simulate the model under "standard" conditions.

Enzymes	Initial concentration (μM)	Species	Initial concentration (μM)
GR	1.4	$NADPH$	150
$DHAR$	1.7	GSH	4000
SOD	50	ASC	10000
APX	70		

3 Continuous Petri Nets

We use continuous Petri nets [1], for which places no longer contain integer values, but positive real numbers, and transitions fire in a continuous way. Semantics

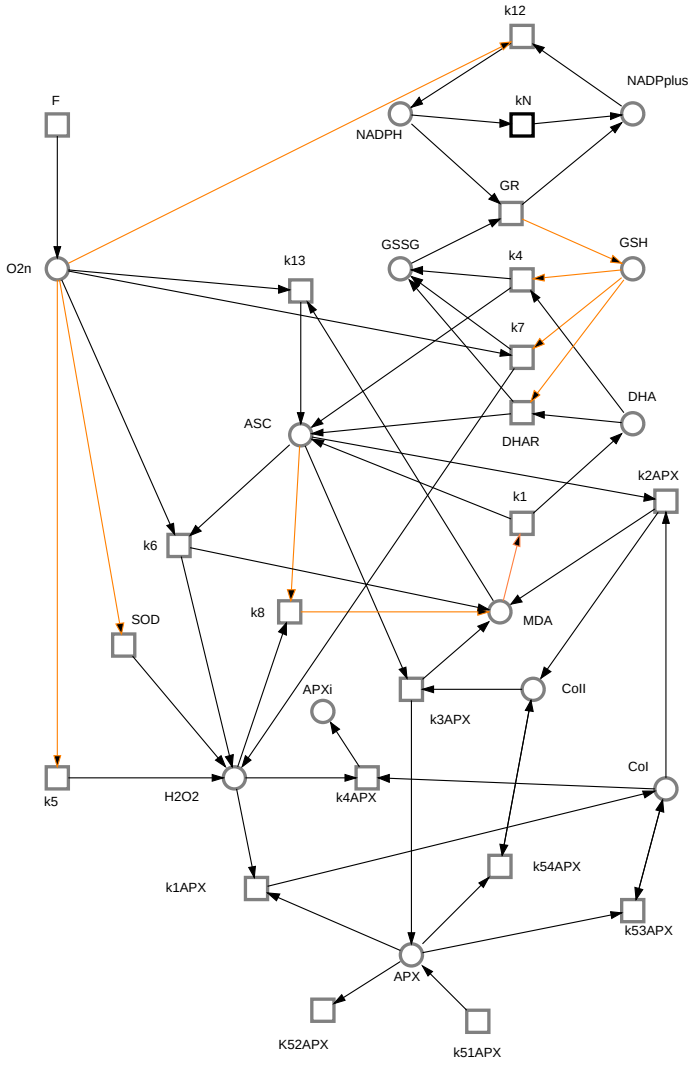

Fig. 1. Continuous Petri net model for the GSH-ASC cycle (orange arcs have weight 2)

of continuous Petri Nets is then defined by means of a system of Ordinary Differential Equations [2]. The continuous Petri net model for the GSH-ASC cycle is that shown in Figure 1 (obtained using the Snoopy tool [16]). This model has been obtained by adapting the biological process described in [17], according to the following considerations:

1. There is a constant electron source in the model, F, whose flux is divided among three competitive routes: the photoproduction of O_2^- (transition $k5$),

the photoreduction of $NADP^+$ (transition $k12$) and the photoreduction of MDA (transition $k13$).

2. The synthesis *de novo* of APX in [17] is considered as $k_5^{APX}([APX]_0 - [APX] - [CoI] - [CoII])$. Then, read arcs are used for CoI and $CoII$ places, since even if k_5^{APX} does not appear in their corresponding equations, it is included in the APX equation. We have then considered four new transitions in the continuous Petri net model, with the following associated kinetic constants: $k51APX$ with $k_5^{APX}[APX_0]$, and $k52APX$, $k53APX$ and $k54APX$ with k_5^{APX}.
3. $[CO_2]$ is considered constant, so that the flux of $NADPH$ consumption by the Calvin cycle (and other electron-consuming reactions) is $k_N = k'_N\ [CO_2]$.

The corresponding ODEs for this continuous Petri net model are those shown in Table 6, which consist of 13 molecular species and 21 reactions defining the equations. These are the same ODEs that we obtained in [17] (supplementary material).

Table 6. Differential equations system

$$\frac{d[NADPH]}{dt} = -v_{GR} - k'_N[CO_2][NADPH] + k_{12}[NADP^+] \quad (1)$$

$$\frac{d[NADP^+]}{dt} = v_{GR} + k'_N[CO_2][NADPH] - k_{12}[NADP^+] \quad (2)$$

$$\frac{d[GSH]}{dt} = 2\,(\,v_{GR} - v_{DHAR} - k_7[O2^-][GSH] - k_4[DHA][GSH]\,) \quad (3)$$

$$\frac{d[GSSG]}{dt} = -v_{GR} + v_{DHAR} + k_7[O2^-][GSH] + k_4[DHA][GSH] \quad (4)$$

$$\frac{d[ASC]}{dt} = v_{DHAR} + k_1[MDA]^2 + k_4[DHA][GSH] + k_{13}[MDA] - k_2^{APX}[ASC][CoI] - k_3^{APX}[ASC][CoII] - k_6[O2^-][ASC] - 2\,k_8[H_2O_2][ASC] \quad (5)$$

$$\frac{d[DHA]}{dt} = -v_{DHAR} + k_1[MDA]^2 - k_4[DHA][GSH] \quad (6)$$

$$\frac{d[MDA]}{dt} = k_2^{APX}[ASC][CoI] + k_3^{APX}[ASC][CoII] - 2\,k_1[MDA]^2 + k_6[O_2^-][ASC] + 2\,k_8[H_2O_2][ASC] - k_{13}[MDA] \quad (7)$$

$$\frac{d[H_2O_2]}{dt} = v_{SOD} - k_1^{APX}[H_2O_2][APX] - k_4^{APX}[H_2O_2][CoI] + k_5[O_2^-]^2 + k_6[O_2^-][ASC] + k_7[O2^-][GSH] - k_8[H_2O_2][ASC] \quad (8)$$

$$\frac{d[APX]}{dt} = -k_1^{APX}[H_2O_2][APX] + k_3^{APX}[ASC][CoII] + k_5^{APX}([APX]_0 - [APX] - [CoI] - [CoII]) \quad (9)$$

$$\frac{d[CoI]}{dt} = k_1^{APX}[H_2O_2][APX] - k_2^{APX}[ASC][CoI] - k_4^{APX}[H_2O_2][CoI] \quad (10)$$

$$\frac{d[CoII]}{dt} = k_2^{APX}[ASC][CoI] - k_3^{APX}[ASC][CoII] \quad (11)$$

$$\frac{d[APX_i]}{dt} = k_4^{APX}[H_2O_2][CoI] \quad (12)$$

$$\frac{d[O_2^-]}{dt} = -\,2\,v_{SOD} + F - 2\,k_{12}[NADP^+] - 2\,k_5[O_2^-]^2 - k_6[O_2^-][ASC] - k_7[O2^-][GSH] - k_{13}[MDA] \quad (13)$$

As a consequence of the electron source indicated above, the recovery of the reducing power is variable and dependent on the $NADP^+$ and MDA concentrations present in chloroplasts. This provides a great flexibility to the model and a greater ability to study stress conditions. The next values have been used for F:

(i) Unstressed chloroplasts, $F = 640\ \mu M s^{-1}$, giving a production rate of O_2^- of 222.2 $\mu M s^{-1}$, which is within the range previously mentioned in chloroplasts [13] (Figure 2); under these conditions, a steady state was rapidly achieved by the system, in which metabolite concentrations and fluxes remained constant.

(ii) Stressed chloroplasts, $F = 2400\ \mu M s^{-1}$ (intense light exposure), which gives rise to APX photoinactivation (Figure 3); under these conditions, the antioxidant concentration in the chloroplast gradually decreased, in the order $NADPH$, GSH and ASC, so that their respective oxidized species concentrations increased. The disappearance of ASC was followed by the rapid inactivation of APX, reflecting what occurs in reality, accompanied by a sharp increase in APX_i and H_2O_2.

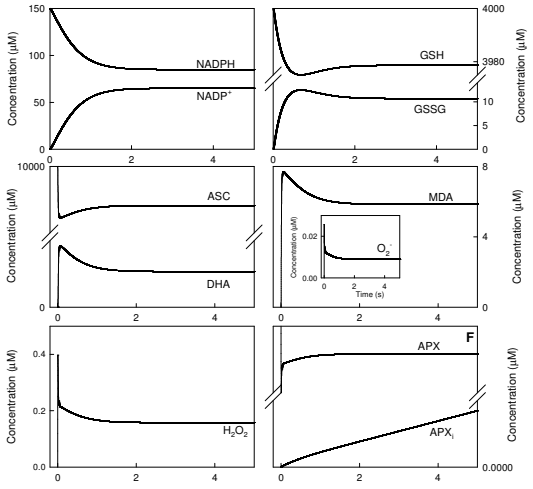

Fig. 2. Simulated progress curves corresponding to the species involved in the mechanism with $F = 640\ \mu M s^{-1}$.

4 Structural Analysis

In this section we apply the classical structural techniques on Petri nets [10] in order to verify and analyze the metabolic pathway. For that purpose we build a discrete Petri net model (see Figure 4) from the description of the cycle following the steps described in [2]. Furthermore, we need to adapt the Petri net for

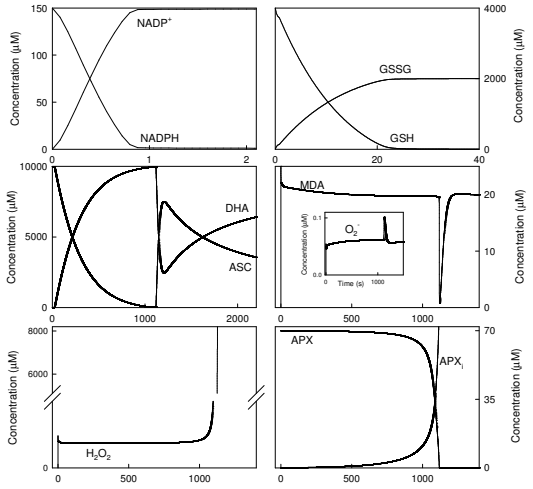

Fig. 3. Simulated progress curves corresponding to the species involved in the mechanism with $F = 2400\ \mu M s^{-1}$.

the discrete mode. We remove two edges leaving the place O_2^-, those reaching transitions k_{12} and k_{13}, since in the discrete model we do not require any tokens on O_2^- to fire these transitions. These edges are related to electron source. We can also remove the read arcs (also called test arcs) from the continuous Petri net of Figure 1, since they are irrelevant in the corresponding incidence matrix, and therefore in the structural analysis. We then join the transitions *k52APX*, *k53APX* and *k54APX* into a single output transition from *APX*, named *k5APXo*, and we also rename the input transition *k51APX* by *k5APXi*. On the other hand, in order to identify the I/O behavior we add a new place that represents the water generated by the reactions (transitions) *k4APX* and *k1APX*, and a new transition (*outwater*) that models the water self control of chloroplasts.

The obtained Petri net has been analyzed by using a well known Petri net tool, Charlie [15], which allows us to obtain the corresponding invariants for this Petri net.

4.1 P-invariants

A P-invariant defines a mass conservation law and has associated its corresponding biological interpretation. In this case we have obtained three P-invariants (Table 7). This means that the pathway under study consists of three moiety-conserved cycles coupled in series to attain a very high amplification capacity [18] against an increase in hydrogen peroxide concentration. In its evolution, since the appearance of oxygen in the atmosphere, the cell has developed a very efficient defense tool against oxygen toxicity, although it needs a continuous supply of *NADPH*.

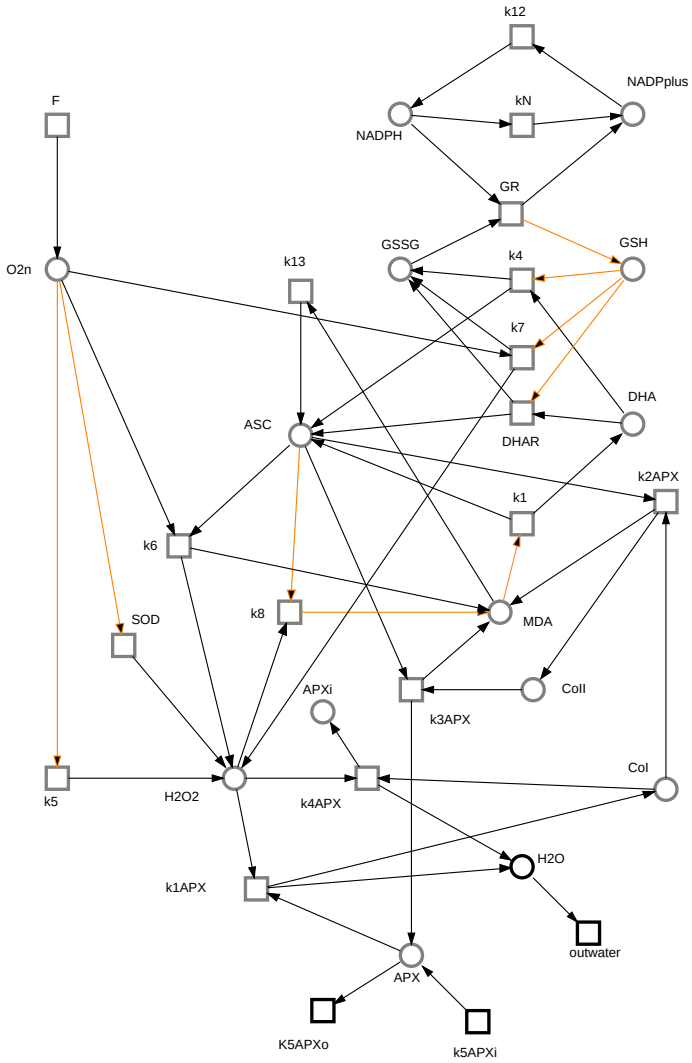

Fig. 4. Petri net model for the GSH-ASC cycle (orange arcs are of weight 2).

Table 7. P-invariants

$P-inv_1 = \{\ NADPH\ ,\ NADP^+\ \}$
$P-inv_2 = \quad \{\ 2\,GSSG\ ,\ GSH\ \}$
$P-inv_3 = \{\ ASC\ ,\ DHA\ ,\ MDA\ \}$

Observe that for each P-invariant there must be a non-zero initial concentration spread along its places, otherwise these places would remain unmarked forever.

(i) $P - inv_1$ captures the consumption of $NADPH$ by the Calvin cycle and GR, and its corresponding recovery in daylight.
(ii) $P - inv_2$ corresponds to the glutahione pool in chloroplasts involving the enzymes GR and $DHAR$. Spontaneous oxidation of GSH in the presence of DHA and O_2^- is also included.
(iii) $P - inv_3$ is related to the interconversion of ASC both spontaneously and catalyzed by $DHAR$ and APX.

4.2 T-invariants

A T-invariant defines a state-conserving subnetwork and has associated its corresponding biological interpretation. In our case (Table 8), using again the Charlie tool, there are 26 minimal semipositive transition invariants.

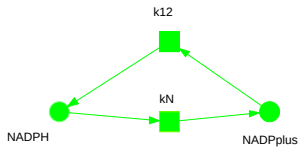

Fig. 5. $T - inv_2$.

Let us see a brief description of some of them:

(i) $T - inv_2$ (Fig. 5) is a trivial T-invariant. These transitions capture a reversible reaction, each one modeling a direction in this reaction. Biologically speaking, it corresponds to the consumption and regeneration of $NADPH$ in the two stages of the photosynthesis.
(ii) $T - inv_6$ (Fig. 6) represents in a very clear way the removal of O_2^- and H_2O_2 (reactive oxygen species) by reaction with the reducing agents GSH and ASC, at the expense of the reducing power of $NADPH$.
(iii) $T - inv_7$ (Fig. 6) refers to the catalytic cycle of APX.
(iv) $T - inv_{15}$ (Fig. 7) represents the removal of O_2^- by its spontaneous reduction to H_2O_2 in the presence of ASC, the subsequent removal of H_2O_2 by the catalytic cycle of APX, and the recovery of ASC through the substrate cyclying of GSH and $NADPH$.
(v) $T - inv_{24}$ (Fig. 7) is a reflection of the enzymatic steps involved in the pathway: SOD, GR, $DHAR$ and APX.

Another advantage of the Petri net representation is that it can be easily modified for modeling different situations. For instance, in order to consider the same cycle in dark conditions, we only have to remove in Figure 4 the transitions F, k_{12} and k_{13}. Then, if we now apply structural analysis we obtain the same three P-invariants, but we only obtain the first T-invariant, $T - inv_1$, which is the input (synthesis *de novo*) and output (inactive enzyme) of APX.

Table 8. T-invariants.

T-invariant	Transitions/Reactions (number of fires)
$T - inv_1$	k5APXo (1), k5APXi (1)
$T - inv_2$	kN (1), k12 (1)
$T - inv_3$	k13 (3),k6 (1), k8 (1), F (1)
$T - inv_4$	k13 (2), k8 (1), SOD (1), F (2)
$T - inv_5$	k13 (2), k8 (1), k5 (1), F (2)
$T - inv_6$	GR (1), k12 (1), k7 (1), k13 (2), k8 (1), F (1)
$T - inv_7$	k13 (3), k2APX (1), k3APX (1), k6(1), k1APX (1), F (1), outwater (1)
$T - inv_8$	k13 (2), k2APX (1), k3APX (1), SOD (1), k1APX (1), F (2), outwater (1)
$T - inv_9$	k13 (2), k2APX (1), k3APX (1),k5 (1), k1APX (1),F (2), outwater (1)
$T - inv_{10}$	GR (1), k12 (1), k7 (1), k13 (2), k2APX (1), k3APX(1), k1APX (1), F (1), outwater (1)
$T - inv_{11}$	GR (3), k12 (3), k4 (3), k1 (3), k6 (2), k8 (2), F (2)
$T - inv_{12}$	GR (1), k12 (1), k4 (1), k1 (1), k8 (1), SOD (1), F (2)
$T - inv_{13}$	GR (1), k12 (1), k4 (1), k1 (1), k8 (1), k5 (1), F (2)
$T - inv_{14}$	GR (2), k12 (2), k4 (1), k7 (1), k1 (1), k8 (1), F (1)
$T - inv_{15}$	GR (3), k12 (3), k4 (3), k1 (3), k2APX (2), k3APX (2), k6 (2), k1APX (2), F (2), outwater (2)
$T - inv_{16}$	GR (1), k12 (1), k4 (1), k1 (1), k2APX (1), k3APX (1), SOD (1), k1APX (1), F (2), outwater (1)
$T - inv_{17}$	GR (1), k12 (1), k4 (1), k1 (1), k2APX (1), k3APX (1), k5 (1), k1APX (1), F (2), outwater (1)
$T - inv_{18}$	GR (2), k12 (2), k4 (1), k7 (1), k1 (1), k2APX (1), k3APX (1), k1APX (1), F (1), outwater (1)
$T - inv_{19}$	GR (3), k12 (3), DHAR (3), k1 (3), k6 (2), k8 (2), F (2)
$T - inv_{20}$	GR (1), k12 (1), DHAR (1), k1 (1), k8 (1), SOD (1), F (2)
$T - inv_{21}$	GR (1), k12 (1), DHAR (1), k1 (1), k8 (1), k5 (1), F (2)
$T - inv_{22}$	GR (2), k12 (2), k7 (1), DHAR (1), k1 (1), k8 (1), F (1)
$T - inv_{23}$	GR (3), k12 (3), DHAR (3), k1 (3), k2APX (2), k3APX (2), k6 (2), k1APX (2), F (2), outwater (2)
$T - inv_{24}$	GR (1), k12 (1), DHAR (1), k1 (1), k2APX (1), k3APX (1), SOD (1), k1APX (1), F (2), outwater (1)
$T - inv_{25}$	GR (1), k12 (1), DHAR (1), k1 (1), k2APX (1), k3APX (1), k5 (1), k1APX (1), F (2), outwater (1)
$T - inv_{26}$	GR (2), k12 (2), k7 (1), DHAR (1), k1 (1), k2APX (1), k3APX (1), k1APX (1), F (1), outwater (1)

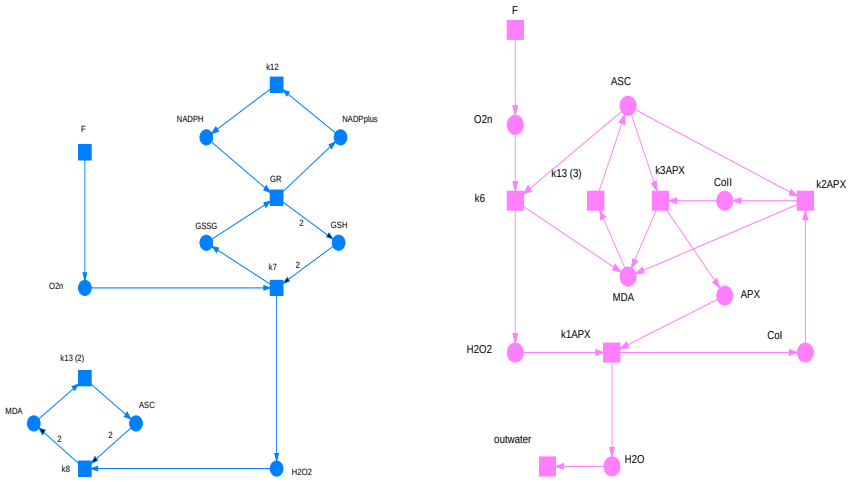

Fig. 6. $T - inv_6$ and $T - inv_7$.

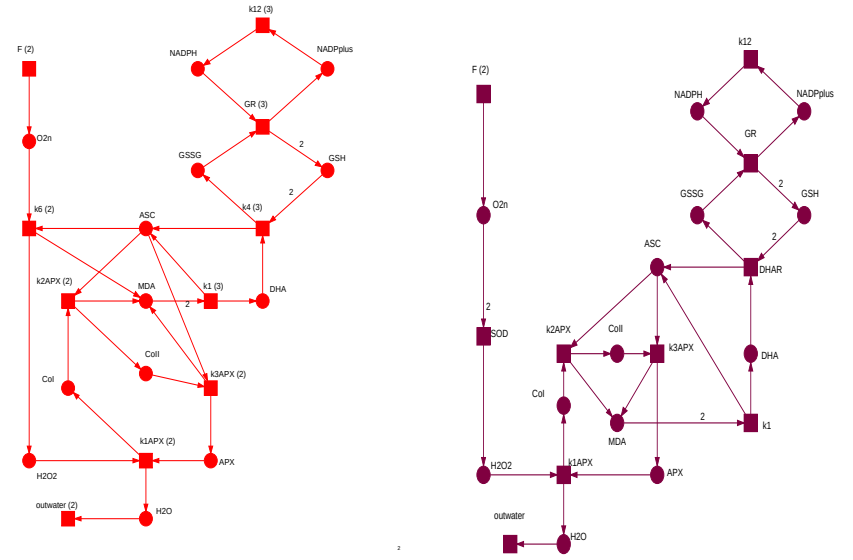

Fig. 7. $T - inv_{15}$ and $T - inv_{24}$.

4.3 Core network

We now apply the procedure proposed in [5] in order to identify the core net that represents the network's dynamics. Transition $k4APX$ does not belong to

any T-invariant, therefore, it can be removed at the steady-state, together with the place $APXi$, which becomes isolated upon the removal of $k4APX$. Furthermore, $T - inv_2$ is a trivial T-invariant, so that we can use a macro transition for these transitions. Next, we compute the maximal Abstract Dependent Transition (ADT) sets, considering that two transitions depend on each other if they occur always together in the set of T-invariants. In this case we obtain an only connected ADT set $\{k1APX, k2APX, k3APX\}$, which can also be collapsed in a single macro-transition (together with $T - inv_1$). This coarse network (Figure 8) gives us a reduced vision of the chemical process behavior, so it contributes to attain a better understanding of this process, also allowing us to test the robustness and the identification of the fragile nodes.

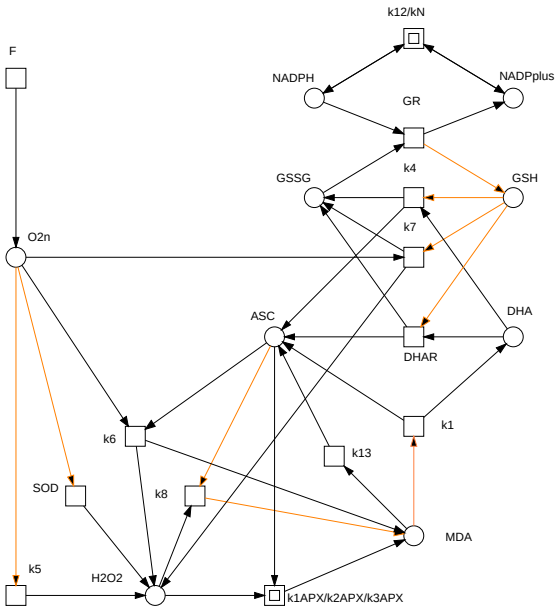

Fig. 8. Coarse Petri net structure of the GSH-ASC cycle.

Robustness is defined as the ability of the system to maintain its function against internal and external perturbations [6]. In the pathway under study, robustness is directly related to APX activity [17]. To maintain APX activity, the cell has developed a very efficient defense tool against oxygen toxicity, based on two coupled substrate cycles: *GSH-GSSG* ($P - inv_2$) and *ASC-MDA-DHA* ($P - inv_3$), although it needs a continuous supply of *NADPH* ($P - inv_1$). Substrate cycles are powerful metabolic tools involving two enzymes acting in opposite directions, whereby a target metabolite is reversibly interconverted into another chemical species without being consumed [19]. The physiological explanation proposed for this wasteful cycling is that is mainly a way of amplifying

a metabolic response to a change in a metabolic concentration, thus greatly improving the sensitivity of metabolic regulation. The waste of *NADPH* can then be understood as the cost that chloroplasts must pay to swiftly detoxify H_2O_2 and O_2^-.

It is also very important to analyze the redundancy of a pathway. It is the hallmark of biological networks where the very same function is carried out by different pathways, which provides robustness against perturbations like mutation. In the *GSH-ASC* cycle, if a mutation blocks *SOD*, there is a parallel spontaneous step for ${O_2}^-$ dismutation (k_5), as can been seen in Figure 8. The same holds for *DHAR* (k_4), in such a way that chloroplasts can recover the reducing power necessary to detoxify reactive oxygen species in the absence of these enzymes. Redundancy of the pathway under study is clearly revealed by comparison of $T - inv_{15}$ and $T - inv_{24}$, which represent the chemical and the enzymatic pathways, respectively, to eliminate H_2O_2.

Another information that is teased out from the coarse network is that *NADPH* is the shared node for two pathways: the *Calvin* cycle and the *GSH-ASC* cycle. If the recovery of *NADPH* is silenced, it results in a complete loss of function of both pathways in the core network indicating that it is indeed the fragile node in the network. The pathway under study is very interesting, since the same day-light that gives rise to O_2^- radicals also generates *NADPH* and *ASC* to detoxify H_2O_2 arising from O_2^- dismutation. Therefore it is very important to know the relative weight of each route in the growth conditions of plants.

5 Conclusions and Future Work

The GSH-ASC cycle in chloroplasts has been modelled using continuous and discrete Petri nets. For that purpose, we have defined the specific continuous Petri net model that corresponds to the network of chemical and enzymatic steps involved in the cycle, and we have studied it in two ways: the quantitative one, which helps us to make a prediction behavior; and the qualitative one, applying structural techniques, considering the core structure. We have obtained their corresponding biological interpretation that help us to understand this metabolic pathway.

As future work we intend to add some additional steps into the pathway, which would be helpful to have a better understanding of the biological behavior considering some new features, such as dark-light interactions. We also intend to apply other known formal techniques to the study of the GSH-ASC cycle in chloroplasts, for instance, we may apply model checking techniques in order to conclude whether a certain property is fulfilled or not by the biological system. Finally, it can also be of interest to derive probabilistic information from a metabolic pathway, i.e., we can use a probabilistic framework, like stochastic Petri nets (SPNs), for the modeling of the GSH-ASC cycle in chloroplasts, and derive the relevant stochastic information of the system.

References

1. R. David and H. Alla. *Discrete, Continuous and Hybrid Petri Nets*. Springer, 2005.
2. D. Gilbert and M. Heiner. *From Petri Nets to Differential Equations - an Integrative Approach for Biochemical Network Analysis*. Proc. ICATPN 2006, Turku, June, Springer LNCS 4024, pp. 181-200, 2006.
3. D. Gilbert, M. Heiner, and S. Lehrack. *A Unifying Framework for Modelling and Analysing Biochemical Pathways Using Petri Nets*. Proc. of Computational Methods in Systems Biology 2007, CMSB 2007, M. Calder and S. Gilmore (eds), Springer, LNCS/LNBI 4695, pp.200-216, 2007.
4. C. Girault and R. Valk. *Petri Nets for Systems Engineering. A Guide to Modelling, Verification, and Applications*. Springer, 2003.
5. M. Heiner and K. Sriram. *Structural Analysis to Determie the Core of Hypoxia Response Network*. PLoS ONE 5(1): e8600, doi:10.1371/journal.pone.0008600, 2010.
6. H. Kitano. *Biological robustness*. Nature Reviews Genetics, Vol. 5, pp. 826-837, 2004.
7. M. Kudlek. *Probability in Petri Nets*. Fundamenta Informaticae, vol 67,1-3, pp.121-130, 2005.
8. T. Murata. *Petri Nets: Properties, Analysis and Applications*. Poc. of IEEE, vol. 77, 4, pp.541-580, 1989.
9. M. Peleg, D. Rubin, and R.B. Altman. *Using Petri Net Tools to Study Properties and Dynamics of Biological Systems*. Journal of the American Medical, vol 12, 2, pp.181-199, 2005.
10. J.L. Peterson. *Petri Net Theory and the Modeling of Systems*. Prentice-Hall, 1981.
11. C.A. Petri. *Kommunication mit Automaten*. PhD thesis, Schriften des IMN, Institut für Instrumentelle Mathematic, Bonn, 1962.
12. C.A. Petri. *Interpretations of Net Theory*. GMD, Interner Bericht, 2nd improved edition, 1976.
13. A. Polle. *Dissesting the superoxide dismutase-ascorbate-glutathione-pathway in chloroplasts by metabolic modeling: computer simulations as a step towards flux analysis*. Plant Physiology, Vol. 126, pp. 445-461, 2001.
14. V.N. Reddy, M.L. Mavrovouniotis, and M.N. Liebman. *Petri Net Representation in Metabolic Pathways*. In Proc. First International Conference on Intelligent Systems for Molecular Biology, pp. 328û336, Menlo Park. AAI, 1993.
15. Data Structures University of Technology in Cottbus, Dep. of Computer Science and Software Dependability. *Charlie*. 2010. http://www-dssz.informatik.tu-cottbus.de/.
16. Data Structures University of Technology in Cottbus, Dep. of Computer Science and Software Dependability. *Snoopy*. 2009. http://www-dssz.informatik.tu-cottbus.de/.
17. E. Valero, M. I. González-Sánchez, H. Macià, and F. García-Carmona. *Computer Simulation of the Dynamic Behavior of the Glutathione-Ascorbate Redox Cycle in Chloroplasts*. Plant Physiology, Vol. 149, pp. 1958-1969, 2009.
18. E. Valero, R. Varón, and F. García-Carmona. *Kinetic analysis of a model for double substrate cycling: highly amplified ADP (and/or ATP) quantification*. Biophysical Journal, Vol. 86, pp. 3598-3606, 2004.
19. Valero, E. and Varón, R. and García-Carmona, F. *Kinetics of a self-amplifying substrate cycle: ADP-ATP cycling assay*. Biochem J 350, pp. 237-243, 2000.
20. J. Wang. *Timed Petri nets: theory and application*. Kluwer international series on discrete event dynamic systems, vol.9, 1998.
21. Petri Nets World. *http://www.informatik.uni-hamburg.de/TGI/PetriNets/*.

Petri Net Modeling via a Modular and Hierarchical Approach Applied to Nociception

Mary Ann Blätke[1], Sonja Meyer[1], Christoph Stein[2] and Wolfgang Marwan[1]

[1]Otto-von-Guericke Universität Magdeburg, Universitätsplatz 2, 39106 Magdeburg, Germany
[2]Dep. Anesthesiology, Charité - Freie Universität Berlin, Hindenburgdamm 30, 12200 Berlin, Germany
marwan@mpi-magdeburg.mpg.de

Abstract. We describe signal transduction of nociceptive mechanisms involved in chronic pain by a qualitative Petri net model. More precisely, we investigate signaling in the peripheral terminals of dorsal root ganglion (DRG) neurons. It is a first approach to integrate the current neurobiological and clinical knowledge about nociception on the molecular level from literature in a model describing all the interactions between the involved molecules.
Due to the large expected total size of the model under development, we employed a hierarchical and modular approach. In our entire nociceptive network, each biological entity like a receptor, enzyme, macromolecular complex etc. is represented by a self-contained and functional autonomous Petri net, a module.
Analysis of the Petri net modules and simulation studies ensure the fulfillment of criteria important for biological Petri nets and the ability to represent the modeled biological function.

Key words: Petri net, qualititative approach, module, pain, nociception, G-protein-coupled receptor, large biological systems

1 Introduction

Clinical pain is a very complex phenomenon with behavioural, peripheral and central nervous system components. Often, pain can not be successfully treated due to the lack of knowledge about the molecular basis on which pain killers take effect. A mechanism-based pain therapy is largely missing, rendering undertreated pain a serious public health issue (see [7] and references therein).
At the molecular level, many extracellular stimuli and substances in the peripheral tissue are known that provoke nociceptive signaling in DRG neurons and subsequent pain (a complex sensation resulting from integration of peripheral and central messages). A variety of membrane components and intracellular signaling molecules have been identified that play key roles in pain sensation. Examples are G-protein-coupled receptors (GPCR), ion channels, receptor tyrosine kinases, cytokine and hormone receptors, which in turn activate a plethora

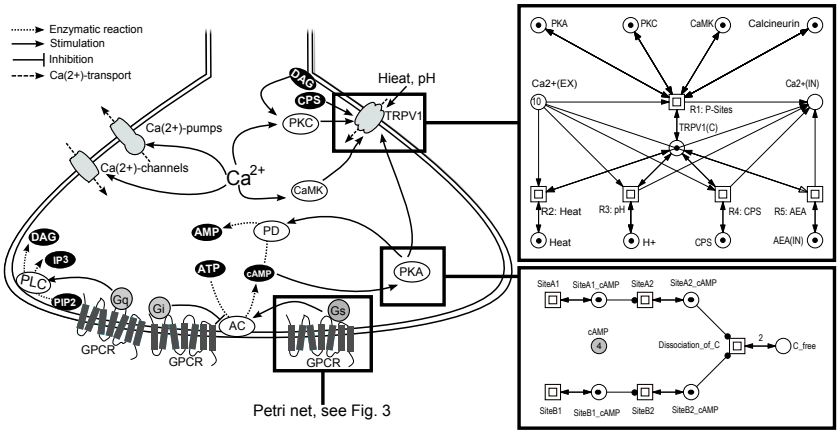

Fig. 1: *Left:* Signaling components in nociceptors. Nociception is triggered by a large number of extracellular signals acting through several receptor classes and initiating a plethora of intracellular signaling cascades. *Right:* Molecular entities like receptors, enzymes (and other biomolecules or macro-molecular complexes) are represented as functional units in the form of self-contained and functionally autonomous Petri nets. The subnets can be coupled by shared places representing identical, common components.

of signaling cascades like the cAMP pathway and calcium signaling [6, 7] (see Fig. 1). However, the quantitative and qualitative relationships between the different intracellular signaling mechanisms acting downstream of the receptor to which those substances bind are still poorly understood [7].

It seems straightforward to apply the Petri net framework to study pain signaling 'in silico', because Petri nets are designed for concurrent systems and also were shown to be ideally suited to model biological systems [9].

For the description of the nociceptive network we choose qualitative modeling as the preceding step for simulation studies which can be performed either stochastically or continuously. It has been shown that a continuous Petri net is equivalent to a structured description of ODEs [9]. However, it is known that many of the involved processes are inherently stochastic. Due to this reason, we prefer stochastic simulations studies to validate our model. The extension of the entire qualitative Petri net to a stochastic one with parameters from experimental data is not possible at the moment because kinetic information of nociceptive mechanisms is hitherto largely missing.

In our modular approach, a module represents a biological functional entity like a receptor, a channel, an enzyme or a macro-molecular complex in form of a self-contained and functional autonomous Petri net graph. The places of a module correspond to functional domains (binding domains, phosphorylation sites, autoinhibitoy domains etc.). These functional domains are regulated by other biological entities and second messengers or are responsible for the effector func-

tion. Thus, transitions stand for actions (dissociation, binding, phosphorylation etc.) occurring within a biological entity. There exist no input or output transitions (sources or sinks of a certain molecule). Due to mass conservation and the fact that a molecular entity is not used up by signaling, the corresponding Petri net graph must be covered with P-invariants [9]. Likewise, the Petri net graph of a module should be bounded to ensure that biological entities, second messengers, precursors, degradation products and energy equivalents do not accumulate. The coverage of T-Invariants of the whole module is not necessary due to the limitation of components which take part in the regulation of the module or which are substrates for the effector function. Therefore, the fulfillment of properties like liveness, reversibility and no dead states it is not mandatory. In contrast, substructures of the modules where reversible changes occur should be covered with T-invariants to assure that the initial state of the involved domains can be restored. Ideally, the computed T-invariants have to be covered by P-invariants [9]. Both, T- and P-invariants, correspond to important biological functions. The up and down regulation of molecular entities by others and second messengers should be reflected in the token flow of the module especially in the increase or decrease of its effector function.

2 Goal

Our goal is to represent nociceptive mechanisms in DRG neurons in a single, coherent Petri net and to establish relationships between signaling components. With the help of simulations we aim at reproducing effects of known nociceptive stimuli correctly and attempt to predict effects of specific perturbations (drugs for therapeutic interventions).
We also aim to establish a module repository. A major advantage is that the modules can be variably combined and reused in other systems according to the requirements of specific 'wet lab' or 'in silico' experiments.

3 Method

We collected literature about nociceptive signaling in DRG neurons, the most investigated cell type in pain-related studies at the molecular level. We extracted those nociceptive signaling components from the literature, whose molecular interaction with other pain-related components is well described and proven by experiments. Further, we searched in detail for the regulatory and effector functions of each of those molecules.
Subsequently, we translated each biological functional unit into a Petri net using the qualitative approach, see e.g. [1, 2, 9, 8]. We used time-free transitions and obtained a time-free Petri net accordingly [9]. Our nets were constructed with Snoopy, a tool to design and animate hierarchical graphs [13].
Each qualitative Petri net is finally subjected to a comprehensive analysis. Here, we apply all validation criteria for biochemical pathway models given in [9]. Therefore, we determine behavioural properties like liveness, reversibility and

boundness, as well as P- and T-invariants. The analyses have been performed using the software Charlie, a software tool to analyse place/transition nets [11]. Having successfully validated the qualitative model, we perform stochastic simulations by assigning stochastic rate functions to all reactions in the network to study the dynamic behaviour of the systems in terms of the flow of token in our model. In particular, we used the stochastic biomass action function, which is available in Snoopy, together with a simple test parameter sets. In these sets, the firing rates of transitions inactivating the effector function of a molecule are assumed to be lower compared to those of transitions activating the effector function (also see section 5).

4 Nociceptive Network

The entire nociceptive network is build by connection of the constructed modules. Here, places sharing the same molecules/molecular complexes (logical places) constitute the natural connections between the modules.
Currently, we have constructed approximately 40 modules on the basis of 251 scientific articles [8]. We expect that at least twice as many modules are required for a comprehensive description of the entire nociceptive network on the basis of the current knowledge.
This expected total size of the model under development precludes a flat representation. Thus, a modeling approach is applied, which yields immediately a hierarchically structured model. So far, the latest version of the entire network consists of 22 connected modules, the representation is distributed over 67 pages with a nesting depth up to 4, compare Fig. A.1 in the appendix. The model consists of about 300 places and 350 transitions.

5 Example for a Module : G-Protein-coupled Receptor

In this section, we representatively describe the construction and structural analysis of one functional unit of our entire net, the G-protein-coupled receptor (GPCR), a typical seven-helix-transmembrane receptor.
GPCRs relay external signals by activating heterotrimeric guanine-nucleotide-binding proteins (G-protein). Seven-helix receptors form the largest family of transmembrane receptors and are therefore crucial components in many signal cascades including nociceptive pathways. There are several GPCRs in nociception interacting specifically with endogenous and exogenous opioids, cannabinoids or substances released as a result of inflammation (e.g. bradykinin), thus having substantial modulating effects on pain sensation. A heterotrimeric G-protein consists of α[1], β and γ subunits (see also [3–5]). Fig. 2 shows the interaction of GPCR with coupled G-protein.

[1] The Gα subunit occurs in three main isoforms with distinct functions: Gα_s (stimulation of adenylyl cyclases), Gα_i (inhibition of adenylyl cyclases)and Gα_q (stimulation

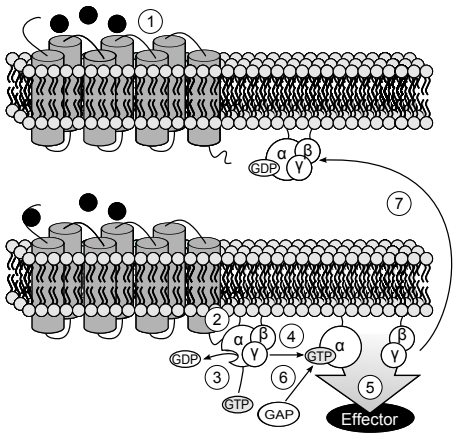

Fig. 2: Regulation of GPCR and its coupled G-protein (see also [3–5]): The activation of a GPCR occurs by binding of a specific ligand at the extracellular side *(step 1)* causing a conformational change *(step 2)*, which activates the recruited resting G-protein in its GDP-bound form. This causes the exchange of GDP by GTP in the specific binding pocket of the Gα subunit. *(step 3)*. Gα subunits with GTP bound dissociate from the G-protein complex *(step 4)* and act on further downstream signal molecules like adenylyl cyclase or phospholipase C β *(step 5)*. The remaining Gβ/γ subunit in addition causes multiple regulatory effects mostly on ion channels and on isoforms of adenylyl cyclases *(also step 5)*. The effector function of the Gα subunit is terminated by the binding of a GTPase activating protein (GAP) stimulating the intrinsic GTPase function of the Gα subunit. GTP is hydrolysed to GDP *(step 6)*. The GDP bound form of the Gα subunit then reassociates with the Gβ/γ subunit to assume its initial pre-stimulus state *(step 7)*.

The regulatory mechanisms and effector functions of GPCRs and the associated G-proteins are translated into a place/transition Petri net (see Fig. 3).
Places may either represent individual molecules or functional states of more complex molecules. Places that are connected by two opposite edges (in this example replaceable by read arcs) with a transition represent molecules or states, which are necessary for a signaling event to occur without being consumed by the reaction. Transitions describe biochemical reactions and molecular interactions.
To provide a neat arrangement of the Petri net, we used coarse transitions (double squares), integrated at the top level. The entire (flattened) place/transition Petri net of this submodel consists of 27 places and 17 transitions connected by 72 edges.
Computation of the invariants shows the coverage of the net by P- and partly by T-invariants (see Fig. 4). Furthermore, there are no invariants without biological

of phospholipase d β). GPCR are mostly associated with one particular G-protein isoform.

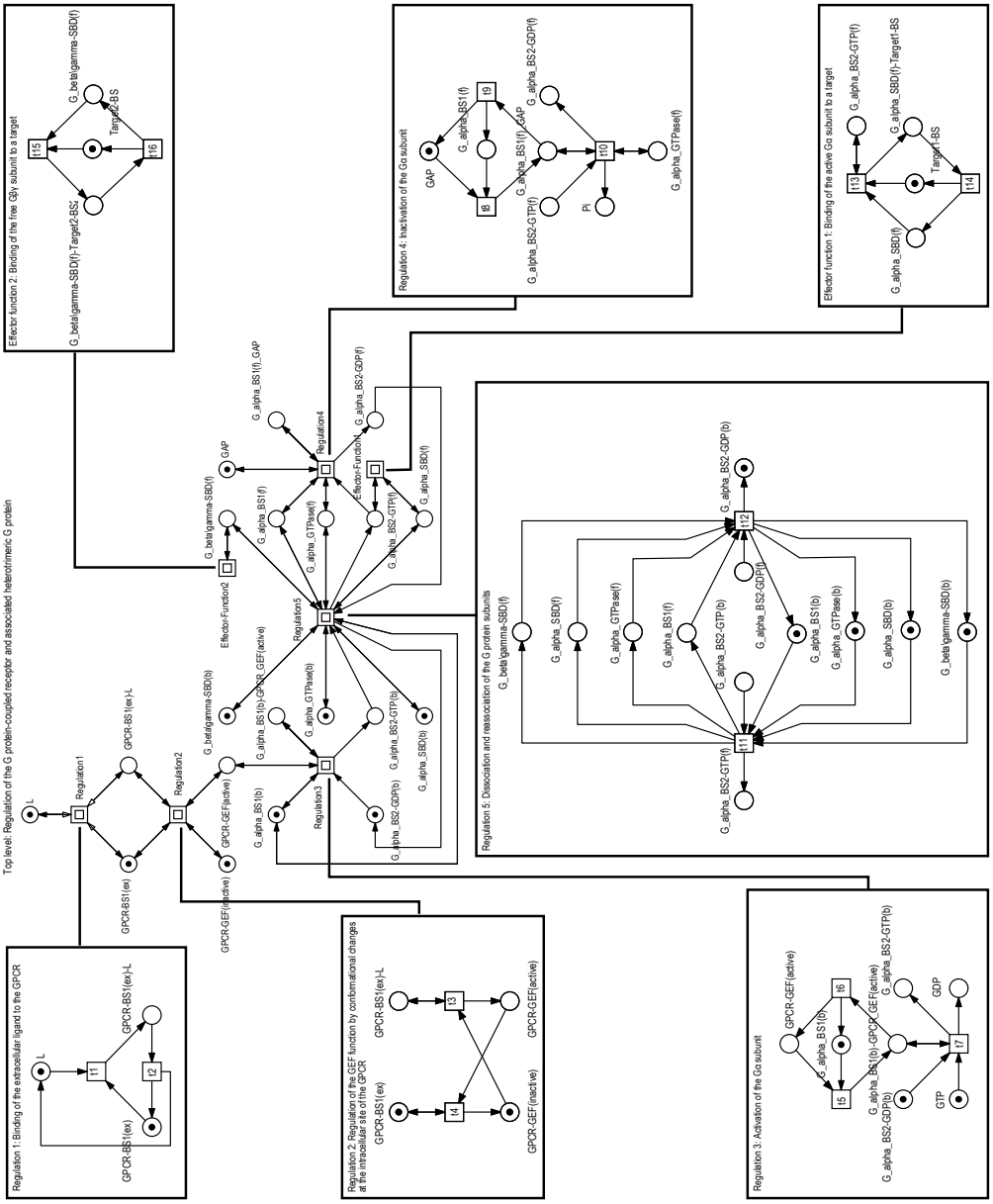

Fig. 3: Petri net module representing GPCR and G-protein regulation: The top level in the center represents all functional sites of GPCR and G-protein which take part in the regulation and effector function. The surroundig Petri nets show the respective coarse transitions in detail.

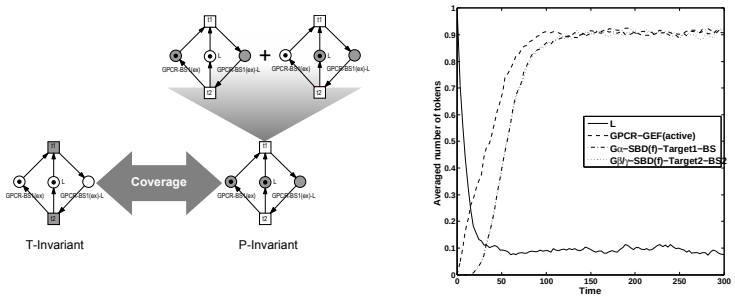

Fig. 4: *Left:* Result of the structural analysis. Shown are T-Invariant 1 (with transitions t1, t2) and P-Invariant 1 (with places GPCR-BS1(ex), GPCR-BS1(ex)-L), 2 (with places L, GPCR-BS1(ex)-L). For the biological meaning of these invariants and all others of the GPCR module see Tab. A.1 and Tab. A.2 in the appendix. *Right:* Result of a stochastic simulation run with test firing rates.

meaning (see Tab. A.1 and Tab. A.2 in the appendix). Thus, essential validation criteria for a Petri net model of a signal transduction network are fulfilled.
Stochastic simulations with test rates show the expected effector function of the module. The dissociation of the ligand from GPCR (t2) and the dissociation of the targets from the substrate binding sites of both G-protein subunits (t16, t18) are assumed to proceed slower *(BioMassAction(0.01))* than all other reactions *(BioMassAction(0.1))*. Upon ligand binding to the receptor (decrease of free ligand), we first observe an increase in the activated GPCR GEF function, followed by an increase of the dissociated G-protein subunits, which can subsequently trigger downstream signaling events.

6 Conclusion

Models allow to perform experiments 'in silico', to study the systems properties and behaviour, to make predictions and thus to contribute to a further understanding of the involved processes. As the body of biological data is steadily increasing, it becomes more and more important to find a way to integrate huge amounts of available information in the form of a model. We are currently working on a method consisting of a modular design principle that allows to check and validate each functional subunit thorougly due to its managable size. Step by step connection and combination of subunits (in the form of submodels) and validation of the connected parts ensures that the resulting composed net is coherent as well. Depending on specific 'wet lab' experiments, which are performed to validate the model in turn, different modules can be combined in order to study the behaviour of subsystems or of the entire system that has been modeled. As many biological functional units (like enzymes, receptors) play a role in different signaling pathways, the respective modules can be reused and recombined in different ways. The modules can be applied to other Petri net

classes; they can be easily converted into a colored Petri net [12], or a stochastic Petri net, see intoduction. In a next step we intend to color our low-level Petri net [12] in cooperation with the group of Prof. Heiner. This more compact description will enable us to depict and study the behavior of populations of nociceptive DRG neurons as well as multiple copies of biological entities.
As far as pain and the contribution of nociceptors is concerned, we hope to contribute with our net to a mechanism-based pain therapy by identifying possible targets for the development of new therapeutic intervention strategies.
The modular design together with the Petri net framework seems to be a promising tool to handle large biological systems even when exact quantitative parameter values are missing.

7 Acknowledgements

This work is supported by the Modeling Pain Switches (MOPS) program of Federal Ministry of Education and Research (Funding Number: 0315449F). We thank Prof. Heiner for the outstanding support and cooperation during this work.

References

1. Reisig, W.: Petri Nets; An Introduction. Springer (1982)
2. Murata, T.: Petri Nets: Properties, Analysis and Applications. Proc.of the IEEE. 4, 541-580 (1989)
3. Strader, C. et al.: Structure and Function of G-Protein-coupled Receptors. Annual Review of Biochemistry 63, 101-132 (1994)
4. Lambright, D. et al.: The 2.0 Crystal Structure of a Heterotrimeric G-Protein. Nature 379, 311 - 319 (1996)
5. Ross, E. and Wilkie T.: GTPase-activating G-Proteins for Heterotrimeric G-Proteins: Regulators of G-Protein Signaling (RGS) and RGS-like Proteins. Annual Review of Biochemistry 69, 795-827 (2000)
6. McMahon, S. and Koltzenburg, M.: Textbook of Pain. Churchill Livingstong (2005)
7. Hucho, T. and Levine, J.: Signaling Pathways in Sensitization: Toward a Nociceptor Cell Biology. Neuron 55, 365-376 (2007)
8. Blätke, MA.: Petri-Netz-Module eines Integrativen Nozizeptiven Neurons. Otto von Guericke University Magdeburg (2009)
9. Heiner, M., Gilbert, D., and Donaldson, R.: Petri Nets in Systems and Synthetic Biology. In Schools on Formal Methods (SFM), LNCS 5016 Springer. , 215-264 (2009)
10. Stein, C. and Lang, L.J.: Peripheral Mechanisms of Opioid Analgesia. Current Opinion in Pharmacology 9, 3-8(2009).
11. Franzke, A.: Charlie 2.0 - A Multithreaded Petri Net Analyzer. Brandenburg University of Technology Cottbus (2009)
12. Liu, F. and Heiner, M.: Using Colored Petri Nets to Model and Simulate Biological Systems. Same Issue (2010)
13. Rohr, C., Marwan, W. and Heiner, M.: Snoopy - A Unifying Petri Net Framework to Investigate Biomolecular Networks (2010)

Appendix

Tab. A.1: List of T-invariants and their interpretation

Number	Transition	Interpretation
1	t1 t2	Binding of the ligand to GPCR and dissociation
2	t3 t4	Activation and inactivation of the GEF function of GPCR due to conformational changes
3	t5 t6	Binding of the G-Protein to the GEF domain of GPCR and dissoziation
4	t8 t9	Binding of the GAP to the G-Protein and dissoziation
5	t13 t14	Binding of the Gα subunit from the target and dissociation
6	t15 t16	Binding of the Gβ/γ subunit from the target and dissociation

Tab. A.2: List of P-invariants and their interpretation

Number	Place	Interpretation
1	GPCR-BS1(ex) GPCR-BS1(ex)-L	Extracellular binding site of the GPCR is unbound or bound to the ligand.
2	GPCR-BS1(ex)-L L	The ligand is free in the extracellular space or bound to the GPCR.
3	GPCR-GEF(active) GPCR-GEF(inactive) Gα-BS1(b)-GPCR-GEF(active)	GEF part of the GPCR can be inactive or active or active and bound to the G-protein.
4	GAP *G*α-BS1(f)-GAP	GAP is free in cytoplasma or bound to the G-Protein.
5	Gα-SBD(f)-Target1-BS Target1-BS	The target for the Gα subunit is free or bound to Gα substrate binding domain.
6	Gβ/γ-SBD-Target2-BS2 Target2-BS	The target for the Gβ/γ subunit is free or bound to Gβ/γ substrate binding domain.
7	Gα-GTPase(b) Gα-GTPase(f)	The confromation of the GTPase domain corresponds to that of the whole Gα subunit .
8	Gα-BS2-GDP(b) Gα-BS2-GDP(f) Gα-BS2-GTP(b) Gα-BS2-GTP(f)	The same as above goes for binding site 2 of the Gα subunit. In both cases GTP or GDP is bound.
9	Gα-BS1(b) Gα-BS1(b)-GPCR-GEF(active) Gα-BS1(f) Gα-BS1(f)-GAP	The same as above goes for binding site 1 of the Gα subunit. In both cases it can be unbound or bound to GAP respectively the GEF part of the GPCR.
10	Gβ/γ-SBD(b) Gβ/γ-SBD(f) Gβ/γ-SBD(f)-Target2-BS2	The Gβ/γ subunit can be associated to the G-protein complex (no substrate binding) or free (substrate binding possible).
11	Gα-BS1(b) Gα-BS1(b)-GPCR-GEF(active) Gα-SBD(f) Gα-SBD(f)-Target1-BS	If one domain is in the conformation where the Gα subunit is associated to the G-protein complex another domain can not be in the comformation where the Gα subunit is free (vice versa).
12	Gα-BS1(f) Gα-BS1(f)-GAP Gα-BS2-GDP(b) Gα-BS2-GTP(b)	see no. 11
13	Gα-BS2-GDP(b) Gα-BS2-GTP(b) Gα-SBD(f) Gα-SBD(f)-Target1-BS	see no. 11
14	Gα-SBD(b) Gα-GTPase(f)	see no. 11
15	Gα-BS1(f) Gα-BS1(f)-GAP	see no. 11

	Gα-SBD(b)	
16	Gα-BS2-GDP(f) Gα-BS2-GTP(f) Gα-SBD(b)	see no. 11
17	Gα-SBD(b) Gα-SBD(f) Gα-SBD(f)-Target1-BS	see no. 11
18	Gα-BS1(f) Gα-BS1(f)-GAP Gα-GTPase(b)	see no. 11
19	Gα-BS2-GDP(f) Gα-BS2-GTP(f) Gα-GTPase(b)	see no. 11
20	Gα-SBD(f) Gα-SBD(f)-Target1-BS Gα-GTPase(b)	see no. 11
21	Gα-BS1(b) Gα-BS1(b)-GPCR-GEF(active) Gα-GTPase(f)	see no. 11
22	Gα-BS2-GDP(b) Gα-BS2-GTP(b) Gα-GTPase(f)	see no. 11
23	Gα-BS1(b) Gα-BS1(b)-GPCR-GEF(active) Gα-BS2-GDP(f) Gα-BS2-GTP(f)	see no. 11
24	Gα-BS1(b) Gα-BS1(b)-GPCR-GEF(active) Gβ/γ-SBD(f) Gβ/γ-SBD-Target2-BS2	If the substrate binding domain is in the conformation where the Gβ/γ subunit is associated to the G-protein complex, another domain can not be in the comformation where Gα subunit is free (vice versa).
25	Gα-SBD(f) Gα-SBD(f)-Target1-BS Gβ/γ-SBD(b)	see no. 24
26	Gα-BS1(f) Gα-BS1(f)-GAP Gβ/γ-SBD(b)	see no. 24
27	Gα-BS2-GDP(f) Gα-BS2-GTP(f) Gβ/γ-SBD(b)	see no. 24
28	Gα-BS2-GDP(b) Gα-BS2-GTP(b) Gβ/γ-SBD(f) Gβ/γ-SBD-Target2-BS2	see no. 24
29	Gα-GTPase(f) Gβ/γ-SBD(b)	see no. 24
30	Gα-GTPase(b) Gβ/γ-SBD(f)	see no. 24

	Gβ/γ-SBD(f)-Target2-BS2	
31	Gα-SBD(b) Gβ/γ-SBD(f) Gβ/γ-SBD-Target2-BS2	see no. 24
32	GDP GTP	Free GTP can just be in a high or low engergy state
33	GTP Gα-BS2-GTP(b) Gα-BS2-GTP(f) Pi	The high energy state of GTP can just be free, bound at the free Gα subunit or at Gα subunit in the G Protein complex. If GTP is in one of those states there cannot be free Pi (vice versa)

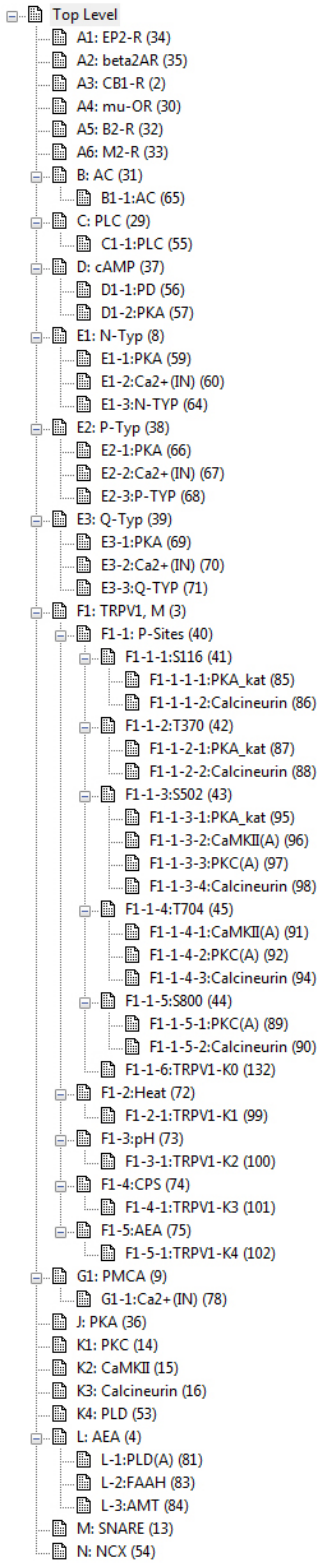

Fig. A.1: Hierarchy graph of the entire nociceptive network.

Author index